5   Cosmogenic Be-10 and the Solid Earth: Studies in Geomagnetism, Subduction Zone Processes, and Active Tectonics

Julie D. Morris

Department of Earth and Planetary Sciences, One Brookings Drive, CB 1169
Washington University, St. Louis, Missouri 63130
jmorris@levee.wustl.edu

John Gosse

Department of Geology, 120 Lindley Hall
University of Kansas, Lawrence, Kansas 66045

Now at: Dept. Earth Sciences, Dalhousie University
3006 LSC, Halifax, Nova Scotia, Canada B3H 3J5

Stefanie Brachfeld

Institute for Rock Magnetism, University of Minnesota
310 Pillsbury Drive, Minneapolis, Minneapolis 55455

Now at: Byrd Polar Research Center, Ohio State University
1090 Carmack Road, Columbus, Ohio 43210

Fouad Tera

Department of Terrestrial Magnetism
Carnegie Institution of Washington
5241 Broad Branch Road
Washington, DC 20015

INTRODUCTION

Since the mid-1980s, cosmogenic [10]Be, with a 1.5 Myr half-life, has proven to be an extremely useful tool for studies of the solid Earth and surface processes. Measured at very low concentrations using a particle accelerator, [10]Be reveals tantalizing clues to the behavior of the Earth's geodynamo, permits "geochemical imaging" of physical and magmatic processes in subduction zones, and provides ages and uplift and incision rates essential for understanding active tectonic processes. This paper emphasizes the utility of atmospheric and *in situ*-produced [10]Be in understanding these solid Earth processes, using igneous and sedimentary rocks, deep-sea and lacustrine sediment, and ice cores as archives.

One focus of this contribution is on studies of the geodynamo and subduction zone processes that utilize [10]Be produced by galactic cosmic radiation (GCR) in the atmosphere and subsequently adsorbed onto marine sediments. Following the extensive treatment of geomagnetic effects on cosmic radiation by Størmer (1955), Elsasser et al. (1956) recognized that variations in cosmogenic nuclide production rates could be used as proxies for changes in intensity of the Earth's magnetic field. A year earlier, Peters (1955) had also proposed that [10]Be may be favorable for recording Cenozoic marine sedimentation rates and other geophysical variations. High-resolution [10]Be-depth profiles in marine sediments have the potential to evaluate the suggestion of asymmetric sawtooth variation in the geomagnetic field paleointensity and to assess the speculation that Milankovitch variations in Earth's orbital parameters may influence the geodynamo. Globally coherent and systematic co-variations in paleointensity and [10]Be concentrations

in marine sediments and ice cores offer promise as a tool for correlating and dating marine sediments unsuited to other methods. The use of geomagnetic field paleointensity variations, derived magnetically and from cosmogenic nuclides, shows promise as an interhemispheric correlation tool at sub-Milankovitch time scales.

Coupled studies of ^{10}Be in sediments supplied to subduction trenches, archived in any accreted sediments, and erupting in volcanic arcs allows "geochemical imaging" of sediment accretion, underplating, subduction, and recycling at convergent margins. Flux balances for ^{10}Be on the incoming plate vs. that erupted from the volcanic arc constrain the volumes of sediment subducted to the depths of magma generation. High ^{10}Be concentrations in lavas erupting behind the volcanic front, as well as at it, map the path of slab-derived elements through the mantle. Combined U-series and ^{10}Be studies constrain time scales of magmatic processes.

Studies of late Cenozoic tectonics use ^{10}Be (and other cosmogenic nuclides) produced *in situ* through cosmic ray bombardment of rocks and minerals exposed at Earth's surface. Secondary nucleons produced in the atmosphere have sufficient energy to produce ^{10}Be through spallation and nuclear capture interactions. The concentration of ^{10}Be produced *in situ* in a rock is proportional to the time the surface has been exposed and decreases with decay during burial or with surface erosion. However, due to erosion on Earth's surface, the *in situ* ^{10}Be clock is useful only for the last few million years, unlike its atmospheric counterpart. Exposure ages for tuffs and lavas have been used to assess geologic hazards, while exposure histories for bedrock and faulted alluvial fans constrain Quaternary paleoseismicity and slip rates. ^{10}Be dating of otherwise undatable raised shorelines holds great promise for improving boundary conditions for mantle rheology and lithospheric flexure models. Bedrock incision rates and paleoaltitudes determined from cosmogenic radionuclides are central to studies of mountain evolution.

Following a brief discussion of analytical methods, this paper is divided into three major subsections, focusing on geomagnetism, subduction zone processes, and recent tectonic processes. Each section provides pertinent background, a review of published literature, and discussion of work in progress. Each also proposes future directions and any technical developments necessary. The reader is referred to Bierman et al. (this volume) for applications of ^{10}Be to studies of climate and Earth surface processes. Other articles reviewing the application of ^{10}Be to the Earth sciences include McHargue and Damon (1991), Morris (1991), Cerling and Craig (1994), Bierman (1994), Gillespie and Bierman (1995), Lal (1996) and Gosse and Phillips (2001).

BACKGROUND

This section provides an overview of ^{10}Be systematics as they relate to laboratory measurements and field applications. First is a brief discussion of laboratory methods, detection limits and analytical uncertainties. This is followed by a short section on the behavior of atmospherically produced ^{10}Be in the oceans and during sedimentation. A review of the principles for applying ^{10}Be produced *in situ*, with a focus on recent progress and aspects of the systematics that remain poorly known, concludes this section.

^{10}Be measurements

^{10}Be concentrations are determined by isotope dilution measurements using a tandem accelerator configured as a mass spectrometer (Finkel and Suter 1993). Stable ^{9}Be is added as a spike/carrier, equilibrated with the sample, and extracted for measurement as BeO. Sample preparation techniques vary widely depending on application. Leaching or total dissolution methods are typically used to extract ^{10}Be and ^{9}Be from 0.1-1 g of marine sediments. Volcanic rocks for subduction studies are prepared by total digestion

of 5-g samples, followed by selective precipitation or column extraction of Be. Studies of *in situ* [10]Be typically use selective dissolution to isolate ~30-50 g of quartz, which is then completely digested for analysis. BeO is selectively precipitated following ion chromatography.

Measurable [10]Be concentrations range from 10^4 atoms g^{-1} to 10^9 atoms g^{-1}, with the lower concentrations at, or very near, blank-determined detection limits. Expressed more conventionally, these concentrations correspond to sub-femtogram to picogram levels. Spiked samples presented to the accelerator generally have [10]Be/[9]Be ratios in the range 10^{-10} to 10^{-15}. Such low ratios are measurable by Accelerator Mass Spectrometry (AMS) because [10]BeO acceleration allows highly sensitive energy separation to be combined with mass separation to identify and count [10]Be. Recent results show that spiked samples with atom ratios $>10^{-15}$ can be measured to ±2-5% (1 σ) at the AMS facility at Lawrence Livermore National Laboratory. These uncertainties are large relative to those routinely achieved by thermal ionization mass spectrometry or multi-collector inductively coupled plasma mass spectrometry, which are used for isotope systems with larger ratios (typically $>10^{-6}$). The uncertainties in AMS [10]Be measurements are small, however, relative to the range observed in nature. Every study should be closely scrutinized for blank levels and sample reproducibility relative to the range reported for the samples of interest. In the following, [10]Be ages or dates are expressed as 'ka' or 'Ma', while 'kyr' and 'Myr' refer to the duration of an event or period.

Atmospheric [10]Be in marine sediments and glacial ice

[10]Be in marine sediments, measured by beta counting, was the focus of some of the earliest published works in this field (e.g., Somyajulu 1977; Tanaka and Inouye 1979). More recently, studies of geomagnetism and subduction zone processes, discussed below, use the atmospherically produced [10]Be as a proxy or tracer. Atmospheric cosmogenic nuclides accumulate in natural archives such as lacustrine and marine sediment, ice sheets, and loess sequences. This paper will focus on cosmogenic nuclide time series data obtained from water-lain sediment and ice cores. Discussions regarding cosmogenic nuclides as paleoclimate tracers in marine sediment and in loess-soil sequences can be found in Aldahan et al. (1997), Chengde et al. (1992), Beer et al. (1992), Ning et al. (1994), and Gu et al. (1996).

Atmospherically produced [10]Be is made by spallation (high energy fission) reactions on O and N, at a production rate second only to that of [14]C. Monaghan et al. (1985/86) estimated the globally averaged [10]Be atmospheric production rate at 1.2 million atoms cm^{-2} a^{-1}. The bulk of the [10]Be (~75%) is produced in the troposphere (Lal and Peters 1967), where a 1-year residence time allows the latitudinal variation in production rate to be largely mixed out (Raisbeck et al. 1981a).

The concentration of a cosmogenic nuclide in sediment or ice depends in part on production and in part on the subsequent transport of the nuclide to the site of deposition. The transfer of cosmogenic isotopes to the Earth's surface is controlled by mixing in the stratosphere and troposphere, with the maximum deposition of cosmogenic isotopes predicted to occur at approximately 40° latitude (Lal and Peters 1967). [10]Be (and [36]Cl) and ^{14}C are subject to different processes after production. [14]C is oxidized to [14]CO$_2$, which becomes homogenized in the atmosphere with a residence time of 6-7 years. [14]CO$_2$ then exchanges between the atmosphere, biosphere, and ocean (Siegenthaler et al. 1980). The movement of ^{14}C through the global carbon sample dampens short period variations in the production rate.

[10]Be does not form gaseous compounds at atmospheric conditions. [10]Be atoms in the atmosphere become attached to aerosols, micron- and sub-micron-sized solid and liquid

particles, which are carried to the Earth's surface by wet and dry precipitation (McHargue and Damon 1991). ^{10}Be does not participate in the global carbon cycle. Since the residence time of ^{10}Be in the atmosphere is only 1-2 years (Raisbeck et al. 1981a) it is better suited to monitor short period variations in production.

The short residence time in the atmosphere means that ^{10}Be deposition at a given site is strongly dependent on the local precipitation rate. This is critically important for ice core records, in which the source of moisture, transport path, and precipitation rate at the sample site will all affect the concentration of cosmogenic nuclides in the ice. A 30,000 year record of ^{10}Be accumulation from Dome C, Antarctica, indicated that ^{10}Be concentrations in late Pleistocene ice were a factor of 2 to 3 higher than in Holocene ice (Raisbeck et al.1981b). This was attributed to lower precipitation during the late Pleistocene. Similar correlations between ^{10}Be concentration and precipitation have been observed in ice cores from Vostok and Dome C, Antarctica (Raisbeck et al.1987) and in modern firn cores from Renland, East Greenland and Droning Maud Land, Antarctica (Aldahan et al. 1998).

In addition, ^{10}Be accumulating on ice sheets may have multiple sources. When used as a tracer in ice core records, ^{10}Be is assumed to have come directly from production in the atmosphere. However, wind-borne dust particles may bring inherited ^{10}Be to the ice (McHargue and Damon 1991; Baumgartner et al. 1997a). Dust particles generated at the Earth's surface carry old ^{10}Be from atmospheric rain out or ^{10}Be produced *in situ*. Inherited ^{10}Be can potentially be several million years old when it is deposited on the ice sheet. Once in the ice, it is not known if ^{10}Be is mobile. Inherited ^{10}Be on dust may desorb into the ice, or dust particles trapped in the ice may scavenge the freshly produced atmospheric ^{10}Be. The inherited ^{10}Be contribution of terrestrial dust in polar ice cores is often neglected since the dust content itself is very small in polar ice, particularly during the Holocene (Thompson et al. 1994). However, low latitude ice cores have a very high dust content (e.g., Thompson et al. 2000a,b). Efforts to use ^{10}Be as a geophysical tracer in these records will require a means of separating fresh atmospheric ^{10}Be from inherited ^{10}Be in terrestrial dust; Baumgartner et al. (1997a) give a very thorough discussion of this matter, and address potential methods of quantifying inherited versus fresh ^{10}Be in ice.

Once introduced to the ocean ^{10}Be does not re-exchange with the atmosphere. Dissolved ^{10}Be is removed from the ocean by scavenging to particles and burial in sediments. If ^{10}Be deposition to the seafloor were globally uniform, the steady-state ^{10}Be inventory (total ^{10}Be in the sediment column, calculated for a column 1 cm^2, from the seawater-sediment interface to basement) everywhere would be ~ 2.6×10^{12} atoms cm^{-2}. However, dissolved ^{10}Be is laterally transported in the ocean by different water masses and preferentially deposited in regions of high particle flux (boundary scavenging) (Anderson et al. 1990). ^{10}Be in sediment is redistributed by bottom currents, which cause sediment focusing or winnowing. These processes can cause apparent ^{10}Be accumulation rates in excess of global production (e.g., Anderson et al. 1990; Lao et al. 1992; 1993; Frank et al. 1994, 1995, 1999, 2000; Chase et al. in press). Continental margin localities typically have higher deposition rates (1.5 to 6 times the globally averaged value), with much lower rates observed in open ocean locations (as low as 0.2 times the globally averaged value). Because boundary scavenging is important in ^{10}Be transport to the sea floor, large variations are observed in the amount of ^{10}Be supplied to different subduction trenches.

^{10}Be concentrations in very young marine sediments also vary as a function of lithology, grain size, and secular variation in production rate. The magnitude of atmospheric production rate variations over the last 800 kyr is discussed below. The effect of particle lithology on ^{10}Be concentrations in the sediment column can be

dramatic. For example, Henken-Mellies et al. (1990) reported that ^{10}Be concentrations in zero age *Globigerina* oozes are 10% of ^{10}Be concentrations in associated pelagic clays. Volcaniclastic arc turbidite sediments can have 20-50% as much ^{10}Be as nearby pelagic sediments (Zheng et al. 1994, Morris et al. 2002; Valentine and Morris, submitted a). The study of ^{10}Be as a proxy for geomagnetic variation faces the challenge of isolating a geomagnetic signature from those caused by changing lithology or sedimentation rate.

The goal of obtaining high-resolution records of paleoclimatic and paleoceanographic processes has led programs such as the Ocean Drilling Program, IMAGES, and the Antarctic programs of several countries to select sites in high sedimentation rate areas. These include continental margins and inner shelf basins where the particle flux is high, and sediment drifts and contourite deposits created by bottom currents that focus sedimentation. These are precisely the settings where boundary scavenging and sediment redistribution are maximized and the accumulation history is the most complicated.

Isolation of the ^{10}Be production signal in marine sediment may be possible by using ^{230}Th to correct for sediment redistribution (Bacon and Rosholt 1982; Bacon 1984). ^{230}Th is introduced into the water column by decay of ^{234}U, which is the only source of ^{230}Th in the ocean. ^{230}Th is insoluble and highly particle reactive, being scavenged on timescales of 10 to 50 years, much shorter than its half life of 75,200 years (Anderson et al.1983a,b; Chase et al. in press). The rain rate of ^{230}Th to the seafloor is nearly independent of the particle flux, and approximately equal to its rate of production by decay of ^{234}U in the water column. In contrast, ^{10}Be is less particle-reactive. Its residence time in the ocean is 500 to 1000 years (Anderson et al. 1990), making it much more susceptible to lateral redistribution. Therefore, ^{230}Th may serve as a reference when examining the accumulation rates of other components of the sediment assemblage. Frank et al. (1994, 1995, 1997, 1999, 2000) recommend the use of the ^{10}Be/^{230}Th$_{ex}$ ratio in deep-sea sediment profiles to remove the sediment redistribution effects before interpreting a ^{10}Be record in terms of paleoproductivity or geomagnetic field variations.

The sediment supply to subduction zones is integrated over the last 12 Myr, such that the net effect of secular variation in production rate is probably less than 15% (Tanaka and Inouye 1979; Gosse and Phillips 2001). The challenge for subduction zone studies is that variations in lithology or sedimentation rate can change the ^{10}Be inventory in the subducting sediment over time, leading to a departure from the steady-state conditions assumed in quantitative models.

In situ cosmogenic ^{10}Be

Previous reviews of geological applications of ^{10}Be produced *in situ* include Lal (1988, 1991, 1996, 2000a,b), Bierman (1994), Bierman and Steig (1996), Gillespie and Bierman (1995), Gosse and Phillips (2001), and Granger and Muzikar (2001). This section provides the rudimentary principles for the use of *in situ* cosmogenic nuclides, in order to acquaint the reader with basic approaches and limits to using ^{10}Be for tectonic studies. The use of *in situ* ^{10}Be in studies of other surficial processes is described by Bierman et al. (this volume). The production of *in situ* terrestrial cosmogenic nuclides (TCN) is similar in many respects to the production of extra-terrestrial cosmogenic isotopes in meteorites. Extraterrestrial cosmogenic nuclides and those produced in Earth's atmosphere (described in the preceding sections) are primarily produced from high-energy primary GCR. Interactions with atmospheric molecules produce neutrons, muons, and other particles that form a cascade of secondary radiation falling toward the Earth. It is this secondary radiation that produces on Earth's surface a variety of different nuclides and subatomic particles. The atmospheric cosmic ray flux attenuation causes the *in situ* production rate of ^{10}Be on a landform surface to be lower (by a factor of ~10^{-3}) than the integrated atmospheric production of ^{10}Be above the surface. Although a wide

variety of different isotopes and subatomic particles can be produced during cosmic-ray interactions, relatively few *in situ* isotopes are useful for tectonic studies over time-scales of 10^3 to 10^7 years. Besides ^{10}Be, only five other *in situ* cosmogenic nuclides (^{3}He, ^{14}C, ^{21}Ne, ^{26}Al, and ^{36}Cl) have been used for Late Cenozoic landform studies because their half-lives are suitably long (or they are stable), the sample preparation and analysis is reproducible, and non-cosmogenic sources of the nuclides are negligible or can be determined.

Tectonic studies have relied on the measurement of *in situ* ^{10}Be produced at and below a landform surface. The cosmogenic isotope concentration in a rock at earth's surface, N (atoms g^{-1}), can be used to calculate the duration of exposure, T (annum, a) to cosmic radiation if the total rate of the nuclide production at the surface, P_o (atoms g^{-1} a^{-1}), from all possible interactions, is known. As discussed below, at any given time P_o will vary as a function of latitude, elevation, and depth below the rock surface. If the nuclide is stable,

$$T = \frac{N}{P_o} \tag{1}$$

at the rock surface. If the isotope is radioactive with a decay constant, λ:

$$T = -\ln\left(1 - \frac{N\lambda}{P_o}\right) \Big/ \lambda \tag{2}$$

Some studies of tectonic geology have required the measurements of ^{10}Be below the surface of the Earth (for instance, when dealing with the exposure of a bedrock fault scarp or when dating alluvial fan and terrace sediments). For subsurface exposures in rock, the production rate decreases by a factor of 1/e approximately every 56 cm (the production of ^{10}Be in shallow rock is dominated by fast neutrons, with Λ_n in rock similar to that in air, ~160±20 g cm^{-2}, and a rock density ρ = 2.7 g cm^{-3}). Currently the community tends to ignore the possibility of a small deviation from a simple exponential for fast neutron attenuation due to boundary effects at the atmosphere-rock surface. Recent work by Heisinger et al. (1997) and J. Stone (Stone 1999, 2000; Gosse and Stone 2001) has shown that only about 2.2% of ^{10}Be production (on a rock surface at sea level) is produced through muon capture. Compared to fast neutrons, the attenuation length of muons is much longer (Λ_μ = 247 g cm^{-2} in air, longer in rocks), so the relative muonic contribution of ^{10}Be production increases with depth. Burial by rock, sediment, snow, ice, water, or other materials likewise needs to be considered in using *in situ* ^{10}Be to date a surface because all shield the surface. The subsurface production rate (P_z) due to fast neutrons and muons at depth Z (cm) is given by:

$$P_o^Z = P_n e^{\left(-Z\rho/\Lambda_n\right)} + P_\mu e^{\left(-Z\rho/\Lambda_\mu\right)} \tag{3}$$

which sums the fast neutron (n) and muon (μ) contributions. Derivations of these equations and expressions for natural exposure scenarios can be found in Bierman (1994), Cerling and Craig (1994), Gosse and Phillips (2001), and Lal (1988, 1991). Radioactive ^{10}Be (λ = 4.62×10^{-7} a^{-1}) can be produced from any exposed targets with atomic masses > 10. Quartz is the mineral of choice for most ^{10}Be exposure studies because of its crustal abundance, resistance to weathering, and simple chemical formula that makes production systematics relatively straightforward. Production rates of ^{10}Be in other minerals such as magnetite (D. Lal, pers. comm.) and olivine (Nishiizumi et al. 1990; Kong et al. 1999) are currently being determined. In quartz, ^{10}Be is produced primarily from spallation interactions between the fast (>10 MeV) secondary neutrons and Si and O nuclei. There are no significant radiogenic or nucleogenic sources of ^{10}Be,

unlike the other five commonly used TCN.

Applications of ¹⁰Be exposure dating require some assumptions about the surface system that is being dated. As warned by D. Lal (1996; 2000a) and others, it is important to realize that in most natural settings the sampled surface was not always at the surface of the landform during the exposure history. With rare exception (indicated by the presence of surface preservation indicators such as striae or growth fibers on a fault scarp), *in situ* ¹⁰Be abundances measured in a surface or subsurface mineral must be interpreted to represent some dynamic record of exposure history that involves surface processes as well as time. Typically, we simplify the interpretation by assuming an uncomplicated exposure history for the landform we wish to date. That is, during exposure, we assume that the rock was never shielded from cosmic radiation by snow, ice, or sediment, the rock was not eroded, and the rock was continually exposed at its present position (i.e., there was no rolling, isostatic uplift, or tilting). If any of these assumptions are known to be invalid, estimates of the effects of the condition must be taken into account. Finally, it is assumed that the system is closed (both geologically and isotopically), in the sense that there are no additions or depletions of the ¹⁰Be concentration other than by cosmogenic production and radioactive decay, and that there are no significant nucleogenic sources of ¹⁰Be. Also implied is that any atmospheric ¹⁰Be adhered to the quartz was removed during sample preparation.

As the exposure age equations above reveal, the precision and accuracy of the chronometer will also depend on the certainty in the time-integrated production rates at a given geomagnetic latitude, altitude, and rock depth. On Earth's surface, the production rate of ¹⁰Be in quartz ranges between 3 and 150 atoms g⁻¹ a⁻¹ (corresponding respectively to production on the equator at sea level and on a mountain peak at the poles). The spatial variation of *in situ* production is due to two factors. First, the production rate increases with elevation because of the corresponding decrease in atmospheric attenuation of the cosmic ray flux. Secondly, the geomagnetic field interacts with the primary and perhaps secondary cosmic ray flux. At low geomagnetic latitudes, where the field lines are approximately parallel to the earth, the lower energy spectrum of the cosmic radiation tends to be strongly deflected. In this sense, the cosmic ray flux above the equator is said to be 'harder.' Contrarily, at the poles where the field lines tend to converge, lower energy cosmic rays can make it to the atmosphere (discussed in next section). Therefore, sea level cosmogenic production rates are highest above about 58° latitude because there is no deflection of the component of the cosmic ray flux with sufficient energy to produce the secondary cascades and ultimately *in situ* ¹⁰Be.

Time-integrated production rates of the most commonly utilized TCN are believed to be known to within 15% (Gosse and Phillips 2001) and some nuclides (¹⁰Be and ³He) may be known within 5% (Stone 1999, 2000; Gosse and Stone 2001; Liccardi et al. 1999). An important resolution in ¹⁰Be production rates was accomplished when J. Stone (1999, 2000) recognized that the disparity in published production rate estimates (4.7 to 6.1 atoms g⁻¹ yr⁻¹) appears only to be an artifact of how the production rates from different sites were scaled (normalized) to high latitude sea level. Brown et al. (1995) and Heisinger et al. (1997) independently showed that muon interactions account for a smaller proportion of the total production of ¹⁰Be at the Earth's surface. Using a 2.2% muon contribution to normalize the site production rates (Lal 1991; Table 1 assumed 15.6%), all of the production rates converged on one rate: 5.1 atoms ¹⁰Be g⁻¹ quartz a⁻¹.

Table 1. ^{10}Be flux calculations.

	Aleutian	Guatemala-Nicaragua	Costa Rica	Honshu, Japan	Mariana
DSDP/ODP SITE	183	495	1039	436	777B
Subducting ^{10}Be					
^{10}Be inventory, 10^{13} atoms cm^{-2}	0.97	1.35	1.42	1.3	0.11
^{10}Be Depth in Sediment*	>210	203	192	246	25
Convergence Rate, cm yr^{-1}	7.9	8.1	8.7	10.5	9
Subduction time, Myr	2.6	2.5	2.2	2.6	2
^{10}Be Flux to Trench, 10^{24} atoms/km-arc-Myr	7.7	10.9	12.5	13.9	0.99
^{10}Be Flux to arc, decay corrected	2.3	3.2	4.5	4.2	0.39
Erupting ^{10}Be					
Avg. basaltic ^{10}Be, million atoms g^{-1}	3	10	1	<1	0.33
Magma Prod. Rate, km^3/km-arc-Myr	28	40	40	25	30
Volcanic ^{10}Be Flux, 10^{24} atoms/km-arc-Myr	0.22	1	<0.1	<0.07	0.03
^{10}Be Flux out/Flux in	0.096	0.31	0.02	<0.017	0.077
References for sediment data	1, 2	1, 3	3, 4	1, 4	1, 5

Sediment depth above which ^{10}Be > 10^7 a cm^{-3}
Magma production rates from Reymer and Schubert (1984)
References: (1) Zheng et al. (1994); (2) George et al. (submitted); (3) Valentine and Morris (submitted a); (4) Morris et al. (2002); (5) Valentine and Morris (submitted b)

The flux of cosmic radiation over the exposure duration must be known or considered constant to use ^{10}Be for exposure dating. The integrated GCR flux to Earth is probably constant over the time scales of interest (10^4 to 10^7 a) even considering the effects of solar modulation and supernovae (Gosse and Phillips 2001). This is probably not true for the secondary cosmic radiation flux. The secondary flux is influenced by temporal variations in the geomagnetic field strength, secular variations of the position of the geomagnetic dipole axis, influences of persistent non-dipolar field attributes, and variations in atmospheric shielding due to climatic or isostatic changes. The effects of variation in geomagnetic paleointensity and dipole axis position on production rates over shorter intervals are still uncertain, and may have caused variations in integrated production rates as high as 20% if we use the relationship between geomagnetic field and cosmic ray flux estimated by Elsasser et al. (1956). Fortunately, the axis position variation influences only Holocene ages because the integrated *in situ* production rate is less variable over longer exposure periods. Despite these uncertainties, ^{10}Be ages on boulders are found to be concordant with calibrated radiocarbon ages (e.g., Gosse et al. 1995c) and other cosmogenic nuclide ages (Ivy-Ochs et al. 1998; Phillips et al. 1997). There is also reasonable consistency of ^{3}He, ^{10}Be, and ^{36}Cl production rates over different exposure durations (Liccardi et al. 1999; Phillips et al. 1996; Gosse and Phillips 2001; Gosse and Stone 2001). This consistency in production rates suggests that the effect of geomagnetic field fluctuations at the base of the atmosphere may be considerably less than predicted by the widely used approximation of the paleointensity effect on atmospheric production (Elsasser et al. 1956). Relying on transport codes to simulate cosmic ray particle interactions in the atmosphere, Masarik et al. (2001) also found that

the geomagnetic field appears to have a smaller influence on production rates than Elsasser et al. suggested. With levels of precision of multiple exposure ages on a single landform approaching 3% and the persistent need for high accuracy in the ages, it is necessary to re-evaluate the influence of dipole and non-dipole variations and reconsider using the Elsasser et al. equation, which was never meant for this purpose.

The cosmogenic ^{10}Be dating method is capable of dating exposure durations ranging between 5 ka and 5 Ma. This range overlaps and bridges the gaps between the practical ranges of other radiometric dating methods commonly used in Cenozoic tectonic investigations, such as radiocarbon dating (currently calibrated to 22 ka), optically stimulated luminescence, U-series, and ^{40}Ar/^{39}Ar. The analytical limit on the resolution of the ^{10}Be technique is about 500 years at mountain elevations; however, uncertainties in the geomagnetic field secular variation effects may become important for exposures of such short (less than 6000 year) duration. Unlike the atmospheric cosmogenic radiocarbon chronometry, which is sensitive to high frequency variations in geomagnetic paleointensity, *in situ* ^{10}Be chronometry improves with age as the geomagnetic field influences are integrated over longer exposure durations. Sample preparation and analytical techniques have improved to the point that ^{10}Be concentrations in deep (>20 m) and young (<1000-yr-old) quartz targets can be measured (Gosse and Phillips 2001). The upper limit of the dating method is controlled by geologic factors and by the achievement of radioactive secular equilibrium (> 5 half-lives). For example, with the exception of unique climatic environments such as the Antarctic dry valleys (where Pliocene surfaces have been dated (Brook et al. 1995a,b) erosion will significantly alter landform surfaces beyond a few million years. Erosion will have several effects on the ^{10}Be system:

(1) The concentration (Eqn. 3) on an eroded surface will be less than a surface on that same landform that was not eroded (and therefore the eroded surface age will need to be interpreted as a minimum bracketing age).

(2) Differential erosion will increase variability among multiple ages from the same landform.

(3) Secular equilibrium of ^{10}Be concentration due to decay will be attained more rapidly.

(4) Older surfaces will be more sensitive to the influence of erosion (more time means more rock mass removed).

Fortunately, this sensitivity of ^{10}Be (and other TCN) to erosion provides a unique means of directly determining erosion rates on landforms (see below, and Bierman et al., this volume). The chronometric technique is thus optimum for dating tectonic events in the 10^4 to 10^5 year span.

^{10}BE AND GEOMAGNETISM

Introduction

The ability of rocks and sediment to act like tape recorders of the geomagnetic field has made key contributions in the earth sciences. Magnetic recording in oceanic crust and continental rocks was a key element in the development of the theory of plate tectonics. Paleomagnetic recording enables the tracking of continental motions through time, and the geomagnetic polarity timescale (GPTS) provides a global chronological tool covering the past ~160 million years (Myr).

Observation and study of the geomagnetic field for its own sake has a long history, due to in part to its use as a navigational aid to sailors. Presently, direct measurements of the Earth's magnetic field are made at geomagnetic observatories and during aircraft and satellite surveys. These systematic measurements of the full geomagnetic field vector exist in a select few areas, covering only the past several centuries.

Efforts to extend the record of geomagnetic field observations back in time is motivated by a desire to understand the origin and evolution of the geodynamo. Observations of the geomagnetic field made at and above the Earth's surface provide a means of remotely observing the Earth's outer core where the field originates. Paleomagnetic recording in rocks and sediments provides a means of extending geomagnetic field records back through time. In this respect paleomagnetism is unique among geophysics disciplines, as it provides a means to observe past states of the Earth's interior. Geological materials have revealed a wide range of geomagnetic field behaviors, from century-scale secular variation to complete reversals of the geomagnetic dipole to long periods of field stability known as superchrons (see Merrill et al. 1996 for full discussion).

Both igneous rocks and sediments are capable of producing high fidelity records of the orientation of the geomagnetic field vector. It is more challenging to extract the intensity of the ancient field from rocks and sediment because the intensity of the signal is dependent on the properties of the recorder. Absolute paleointensity data, the intensity of the ambient field at the time of remanence acquisition, can only be obtained from volcanic rocks and archeological baked clays (pottery, bricks). These materials have been heated above the Curie temperature of the constituent magnetic minerals and cooled rapidly in the presence of the geomagnetic field, a solid-state process that imparts a thermoremanent magnetization (TRM). TRM represent an instantaneous spot reading of the geomagnetic field. Unfortunately, volcanic samples and baked clays are unequally distributed temporally and spatially. There are several sites from volcanic islands that have yielded high resolution volcanic sequences (Tric et al. 1992, 1994; Raïs et al. 1996; Brassart et al. 1997; Valet et al. 1998; Laj et al. 1997; Laj and Kissel 1999; Laj et al. 2002), but even these records are less continuous and of lower resolution than sediment sequences.

Sediments are attractive geomagnetic field recorders due to their continuity, high temporal resolution, and global availability. However, sediments can only provide relative variations in the geomagnetic field strength. The intensity of the natural remanent magnetization (NRM) recorded in sediments is strongly affected by mineralogical content and physical properties of the sediment, which are unrelated to the geomagnetic field at the time of deposition. Extracting accurate paleointensity data from sediment requires a means of removing these non-field effects.

Advances in instrumentation enabling the rapid measurement of continuous u-channel sub-samples (Tauxe et al. 1983; Nagy and Valet 1993; Weeks et al. 1993) has led to a large increase in the number of long, continuous, sedimentary records analyzed for geomagnetic paleointensity variations. The emerging database of globally distributed records has revealed the global nature of certain geomagnetic field features, as well as some unexpected behaviors. Many of the current controversies in geomagnetism center on sedimentary records of geomagnetic field behavior, mainly due to the non-field effects that enter into the recording process. Therefore, alternate tracers of geomagnetic field behavior have been sought in order to verify the geomagnetic origin of the observed records.

^{14}C, ^{36}Cl, and ^{10}Be are widely used as chronological tools in the geosciences, requiring knowledge of their production rates back through time and hence a knowledge of solar activity and geomagnetic field variations that modulate production rates. Conversely, cosmogenic nuclide production rates can be used to track solar variability and geomagnetic field variations back through time. The possibility of using radionuclide production rates as proxy indicators of these processes has stimulated measurements of ^{10}Be profiles in deep-sea sediment, lacustrine sediment, and ice cores. The results of

some of these studies have been ambiguous or even contradictory, owing to the many variables that influence [10]Be accumulation in sediments and the magnetic recording process in sediments. However, there are many current controversies in geomagnetism whose study would benefit from the combined application of paleomagnetic and cosmogenic isotope analyses. This approach has been undertaken by several groups that focused on geomagnetic paleointensity reconstructions for the last ~100 to 200 kyr, for which there are a relatively large number of globally-distributed sediment cores and ice cores possessing their own independent chronologies (e.g., Henken-Mellies et al. 1990; Mazaud et al. 1994; Robinson et al. 1995; Guyodo and Valet 1996, 1999; Frank et al. 1997; Baumgartner et al. 1998; Frank 2000; McHargue et al. 2000; Stoner et al. 2000, 2002; Wagner et al. 2000a). It is our purpose in the following sections to address the potential of [10]Be to contribute to building time-series data of geomagnetic field variations, and to contribute to several current debates in geomagnetism. We will review advances on the subject, limitations, and discuss future directions for this approach.

Magnetic modulation of the primary galactic cosmic ray flux

The production rates of radionuclides such as [10]Be, ^{14}C, and [36]Cl are modulated by magnetic fields from two main sources. The primary galactic cosmic ray flux (GCR) is comprised of charged particles such as protons (in addition to lesser amounts of alpha particles and other stellar-synthesized elements) that have been accelerated to high energies (up to 10^{20} eV) by astrophysical phenomena. The GCR itself may have varied over time as a consequence of supernovae (Sonett et al. 1987). However, the flux on a timescale of $>10^6$ years appears to have been constant within ±20% (Vogt et al. 1990).

Any charged particle traveling through a magnetic field will experience a force that acts at right angles to both the magnetic field direction and the direction of motion of the particle, as occurs inside an accelerator mass spectrometer. The simplest description of this force is given by:

$$\mathbf{F} = q\mathbf{v} \times \mathbf{B} \tag{4}$$

where q is the electrical charge of the particle, $\mathbf{v}$ is the particle's velocity vector, and $\mathbf{B}$ is the geomagnetic field vector. Consequently, the paths of charged particles are altered by magnetic fields, with the amplitude of the deflection dependent on the field strength, the particle's electrical charge, the energy of the particle, and the angle between the particle's trajectory and the ambient magnetic field vector.

The GCR first encounters the solar wind as the particles travel towards the Earth. On timescales of years to hundreds of years the GCR is "filtered" by solar activity. Solar wind is a plasma with very high electrical conductivity. The very high conductivity (very low diffusivity) results in the "freezing" of magnetic field lines into the plasma, which literally carries the solar magnetic field out into space far past the orbit of Pluto. Magnetic fields carried by the solar wind interact with the energetic particles, causing deflections, diffusion, scattering and energy loss (Lal 1988). Some of the particles are swept out of the solar system. Consequently, radionuclide production rates are inversely correlated with solar activity. Carbon-14 activity ($\Delta^{14}C = ^{14}C/^{12}C$) records obtained from tree rings and [10]Be records from polar ice cores (Stuiver 1961; Eddy 1976; Stuiver and Quay 1980; Raisbeck et al. 1981b; Beer et al. 1988; Damon and Sonnett 1991; Stuiver and Braziunas 1993; Bard et al. 1997) indicate that high production rates correspond to periods of low sunspot activity. In addition, periodicities of 11, 22, 200, 400, and ~2400 years have been observed in these records (Beer et al. 1983, 1988, 1990; Sonnett and Seuss 1984; Damon et al. 1989; Stuiver and Braziunas 1989, 1993; Suess and Linick 1990; Haubold and Beer, 1992; Steig et al. 1996, 1998; Finkel and Nishiizumi 1997; Aldahan et al.,1998; Bard 1998; Cini Castagnoli et al. 1998; Wagner et al. 2001).

The charged particles comprising the solar wind itself consist of energetic protons and heavier nuclei. These particles are typically of lower energy (1 to 100 MeV) than the GCR. Therefore, these particles only contribute to nuclear reactions at the very top of the Earth's atmosphere at high geomagnetic latitudes (>60°) where the amplitude of deflection is extremely low (Masarik and Beer 1999). Solar particles are not expected to make a significant contribution to radionuclide production, except in instances of extreme solar events that create higher than average proton fluxes (Lal 1988; Shea and Smart 1992).

The GCR next encounters the Earth's magnetosphere, in which the geomagnetic field alters the trajectories of charged particles and "shields" the Earth by preventing low-energy cosmic particles from entering and interacting with the atmosphere. The latitudinal dependence of this shielding can be visualized by considering the case of a charged particle that is vertically-incident at the geomagnetic equator, and another charged particle that is vertically incident at the geomagnetic pole. In a dipolar field, field lines are horizontal at the geomagnetic equator. The angle between the incident particle's trajectory and the geomagnetic field is 90° , and the force $F = qV\sin\theta$ is a maximum. The geomagnetic field orientation is vertical at the magnetic poles. At the magnetic pole, the angle between the incident particle's trajectory and the geomagnetic field is zero, and the force $F = qV\sin\theta$ is mathematically zero. Therefore, the shielding effect is greatest at low latitudes, even though the intensity of the geomagnetic field is only half as strong as at the poles. Consequently, the energy spectrum of particles penetrating the atmosphere varies with latitude. Again using the simplest conceptual model, strong shielding at the equator deflects the low energy particles, and the particle flux that penetrates the atmosphere at the geomagnetic equator has a higher average energy. The high geomagnetic latitudes receive a wider spectrum of energies.

The latitudinal effect of geomagnetic shielding results in a latitudinal dependence of cosmogenic nuclide production rates, with higher production rates at the poles and lower production rates at the equator (Lal and Peters 1967; O'Brien 1979; Castagnoli and Lal 1980; Lal 1988; Masarik and Beer 1999 and references therein). A first-order relationship between the geomagnetic field dipole moment (M) and the global average cosmogenic nuclide production rate (Q) was estimated by Elsasser et al. (1956) as:

$$Q/Q_O = (M/M_O)^{-1/2} \tag{5}$$

where M_O and Q_O are the present-day geomagnetic dipole moment and present-day production rate, respectively. This equation unsuccessfully predicted Q for very small values of M. However, there appeared to be a good correspondence between the available records of geomagnetic field paleointensity and ^{14}C activity in tree rings.

The geomagnetic field is not a pure dipole. Approximately 80% of the present day geomagnetic field can be explained with a dipole axis inclined 11° to the Earth's rotation axis. Approximately 20% of the field at the Earth's surface remains after the best fitting geocentric axial dipole (GAD) field is subtracted from the actual mapped field (Merrill et al.1996). This remaining part of the field is the non-dipole field, which consists of continent sized features where inclination and intensity are both higher than predicted for a GAD field (as over North America) and lower than expected for a GAD field (as over central Africa) (see Merrill et al. 1996).

Both the dipole and non-dipole parts of the geomagnetic field vary with time. However, the non-dipole components of the geomagnetic field are often ignored in cosmogenic nuclide studies for a number of reasons. First, the time-averaged field is assumed to be a geocentric axial dipole. This means that over a sufficiently long observation time, on the order of 10^4 years, the average vector orientation at any given

location should be that of a geocentric axial dipole. Second, the GCR encounters the Earth's magnetosphere long before it encounters the atmosphere. Charged particles begin to experience geomagnetic deflections when they are still several Earth radii away from the surface of the Earth. Given that the intensity of the geomagnetic field falls off as $1/R^3$, it is typically assumed that the weaker non-dipole features of the geomagnetic field are attenuated and the field seen by the GCR can be represented as dipolar.

The validity of both assumptions is a matter of serious debate. High resolution archives such as sediments and ice cores have millennial-scale down to annual-scale resolution, and therefore a single sample does not span the requisite 10^4 years needed to average out the non-dipole field effects. Further, the non-dipole field features become much more significant near the Earth's surface where the secondary particles generate *in situ* radionuclides. The strategy for working with or without these assumptions and simplifications depends in part on the goal.

The "forward problem" is defined here as using geomagnetic field models to calculate cosmogenic nuclide production rates. Størmer (1955) used a geocentric axial dipole model to calculate the cosmic ray "cutoff rigidity" as a function of position on Earth. Rigidity is defined as:

$$R = p\,c\,/\,Ze \tag{6}$$

where p is momentum, c is the velocity of light, and Ze is the charge of the particle. The magnetic rigidity, a particle's momentum per unit charge, is the quantity used to describe the particle's ability to penetrate the geomagnetic field. Depending on geomagnetic latitude and the particle's angle of incidence, there is a critical energy below which the particle cannot penetrate into the Earth's atmosphere. Simulations of cosmogenic nuclide production have used variations of Størmer's formula for cutoff rigidity to determine the latitudinal energy spectrum of GCR particles allowed into the simulation to produce cosmogenic nuclides (see Bhattacharyya and Mitra 1997; Masarik and Beer 1999 and references therein). However, Størmer's formula was shown to be invalid at low geomagnetic latitudes (see Bhattacharyya and Mitra 1997 for full discussion). Subsequent models based on a dipole field (e.g., Lal 1988; Masarik and Beer 1999; Wagner et al. 2000a) have refined the Elsasser et al., (1956) relationship. The physical models of Masarik and Beer 1999, and Wagner et al. (2000a) predict slightly higher production rates for very low field intensities, and predict a smaller modulation effect for very strong field intensities.

A more accurate way of determining cutoff rigidity is to start with a particle at the Earth's surface, for which the geomagnetic field has been mapped, and trace the trajectory as the particle spirals upward through the magnetic field. The drawback of this method is the large amount of computer time needed to calculate cutoff rigidities at enough locations on Earth to develop a global picture. Further, an enormous amount of computer time is needed to consider all possible angles of incidence. For this reason, modelers use the vertical cutoff rigidity (rigidity for a vertically-incident particle) as a representative value for a given location on Earth. Bhattacharyya and Mitra (1997) presented a method for calculating vertical cutoff rigidities using an "eccentric dipole," a spherical harmonics representation of the geomagnetic field including a quadrupole term. Isorigidity contours were calculated for four time periods. From 1835 up to 1985 the authors observed a westward drift in the location of maximum in vertical cutoff rigidity, and a decrease in the amplitude of the vertical cutoff rigidity. This suggests that effects of the non-dipole component of the geomagnetic field on cosmogenic isotope radionuclide production rates are non-negligible and need to be studied.

The inverse problem involves using a natural archive of cosmogenic nuclide production rates to extract geomagnetic field paleointensity. The inverse problem involves a single geological record from a single location on Earth, which is not sufficient to determine the global structure of the geomagnetic field. Therefore, the default assumption is that these archives are recording variations in the geomagnetic dipole moment. The similarity of geomagnetic paleointensity features with wavelengths longer than 10^3 years, collected from widely distributed sites, appears to confirm the global nature of the signal in these records (e.g., Guyodo and Valet 1996, 1999; Laj et al. 2000; Stoner et al. 2002).

Relative paleointensity recording in sediment

The potential to use sediments as geomagnetic field paleointensity recorders was convincingly demonstrated by Kent (1973). A slurry of marine sediment was repeatedly mixed and then allowed to settle in the presence of a laboratory field of varying strengths. When an invariant sediment assemblage was repeatedly re-deposited, a clear linear relation was observed between the ambient field and the intensity of remanence recorded in the sediment.

In nature, the intensity of the magnetization measured in sediments is related to the ambient field at the time of deposition, but not necessarily in a simple or linear manner. This is caused by variations in the sediment assemblage. The intensity of natural remanent magnetization (NRM) measured in sediments depends on the concentration of the magnetic material present, the composition of the magnetic material, and the grain size of the magnetic material, in addition to other influences related to the non-magnetic sediment matrix (see Tauxe 1993 for full discussion). These parameters are often influenced by environmental processes, and therefore the measured NRM does not solely reflect the ambient geomagnetic field at the time of deposition.

Relative paleointensity is obtained from sediments through "normalization," which entails dividing the intensity of the measured NRM by a parameter that tracks the concentration, composition, and grain size of those magnetic grains that carry the NRM. The most common normalization parameters in use are the anhysteretic remanent magnetization (ARM) and isothermal remanent magnetization (IRM) (see Tauxe 1993 for full discussion). The normalization parameter used in any given sedimentary record depends on the magnetic characteristics of that particular sediment. Unfortunately, the amplitude of normalized intensity features can be quite different depending on which normalization method is used (Schwartz et al. 1996; Brachfeld and Banerjee 2000). Further, normalization may not completely remove the environmental effects (e.g., Schwartz et al. 1996; Kok 1999; Lund and Schwartz 1999). Consequently, there are several debates concerning whether certain features observed in relative paleointensity records represent true field behavior or artifacts resulting from either the magnetic recording or an incomplete normalization process.

The accumulation of cosmogenic isotopes in geological archives has the potential to yield independent records of geomagnetic field behavior over time, and therefore to help to resolve controversies in geomagnetism. Records of cosmogenic isotope production rates are not influenced by the same complications involved with magnetic recording. However, as discussed earlier, isolating a geomagnetic field signal from a record of ^{10}Be accumulation in sediment or ice is a difficult task. ^{10}Be accumulation in marine sediment and ice is influenced by oceanographic, biogeochemical, and atmospheric processes that complicate, or even obscure the record of production rates. Although both proxies have their complications, a combined approach may ultimately lead to more accurate time-series data of geomagnetic field behavior.

Paleointensity as a correlation tool

The dipole component of the geomagnetic field exhibits temporal variations in its intensity on timescales of 10^2 to 10^6 years. Variations in the geomagnetic dipole are synchronously experienced everywhere on the globe. Therefore, a specific geomagnetic field paleointensity feature represents the same "instant" in time everywhere on Earth. High-resolution sedimentary records of geomagnetic field paleointensity from the Mediterranean Sea (Tric et al. 1992), the Somali Basin (Meynadier et al. 1992), Lake Baikal, Russia (Peck et al. 1996), Lac de Bouchet, France (Williams et al. 1998), the North Atlantic Ocean (Channell et al. 1997; Channell and Kleiven 2000; Laj et al. 2000), the Labrador Sea (Stoner et al. 1998, 2000), the South Atlantic Ocean (Channell et al. 2000; Stoner et al. 2002), and the Southern Ocean (Guyodo et al. 2001; Sagnotti et al. 2001) demonstrate the global coherence of features with wavelength of 10^4 to 10^5 years.

A common characteristic of these records is the presence of several intervals of very low intensity during the past 800 kyr. These are interpreted as geomagnetic excursions, which involve large but short-lived directional changes (>45° deviation of the virtual geomagnetic pole from its time-averaged position) followed by a return of the vector to its previous state. Several of the sedimentary records listed above suggest that excursions are associated with a reduction in field strength to less than 50% of its present day value.

The potential to use excursions as chronostratigraphic markers has been long been recognized. Given that excursions are associated with intervals of weak paleointensity, these features are also manifested as abrupt increases in radionuclide production rates. ¹⁰Be concentration peaks observed in ice cores from Vostok and Dome C were seen as possible marker horizons that could be used to synchronize records from the Northern and Southern hemispheres, particularly in cases where low snow accumulation rates precluded the identification of annual layers (e.g., Mazaud et al. 1994). The Vostok record displays a peak in ¹⁰Be concentration at 60,000 years B.P. with a duration of 1000 to 2000 years, and a second peak at 35,000 years B.P. (Fig. 1) (Yiou et al. 1985; Raisbeck et al. 1987). The 35-ka peak is also seen in the Dome C, Byrd, and Camp Century ice
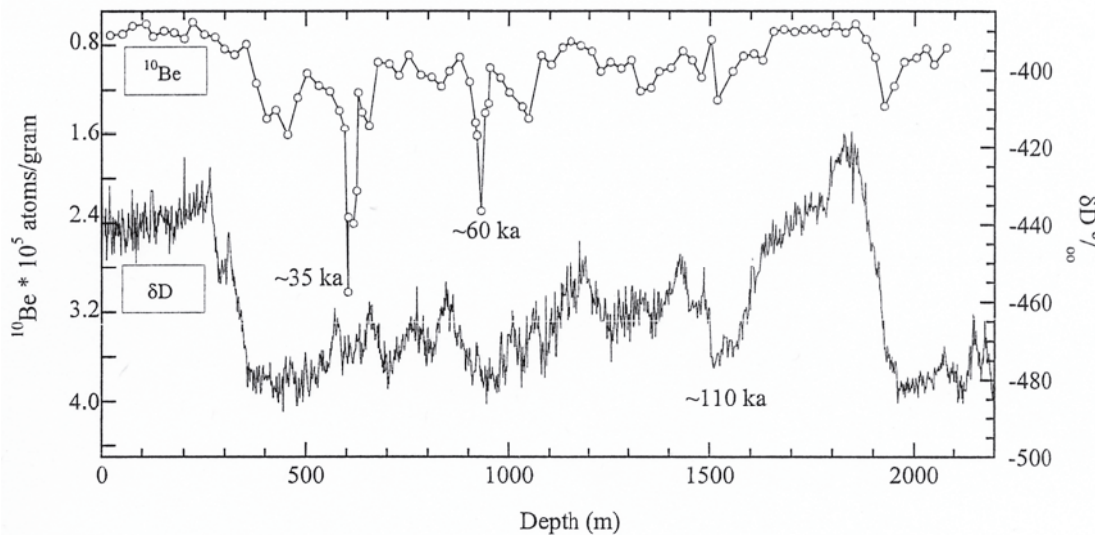
Figure 1. ¹⁰Be concentration from the Vostok ice core showing 2 peaks at ~35ka and 60 ka. The δD record, a proxy of local temperature change, is shown for comparison (Raisbeck et al. 1987; Petit et al. 1999). There are no climate features that coincide with the abrupt, narrow ¹⁰Be spikes. Mazaud et al. (1994) suggested a geomagnetic field origin for these features, and demonstrated the potential to use geomagnetic field paleointensity variations as a means of constraining the ages of these features.

cores (Beer et al. 1984, 1988, 1992). A peak in [10]Be concentration is observed in the Summit GRIP ice core at ~40 ka (Yiou et al. 1997). Two peaks in [36]Cl concentration at 32 ka and ~35-39 ka are seen in the Summit GRIP ice core (Baumgartner et al. 1997b, 1998; Wagner et al. 2000b). Enhanced [10]Be concentrations have also been observed in sedimentary records from Lake Baikal at 40 ka (Aldahan et al. 1999), the Caribbean Sea at 35-40 ka (Aldahan and Possnert 1998), the Gulf of California at 32 and 43 ka (McHargue et al. 1995), and the Mediterranean Sea at 34±3 ka (Cini Castagnoli et al. 1995).

Other hypotheses independent of the geomagnetic field have been proposed to explain these features including a long interval of low solar activity (Raisbeck et al. 1987), and cosmic ray shock way (Sonett et al. 1987), or a supernova explosion (Kocharov 1990). A climatic origin for some the features in the ice cores was ruled out by examining $\delta^{18}O$ and sulfate ion concentrations, which showed no evidence of a change in precipitation or atmospheric transport of aerosols coinciding with the [10]Be spikes (Beer et al. 1992). In a series of papers, Aldahan and coworkers (Aldahan et al. 1994, 1999; Aldahan and Possnert 1998) demonstrated that variations in sediment lithology and sediment grain size can also lead to enhancement of [10]Be content in sediments, and thus far only the ~32 ka feature and ~39 ka feature appear to have a robust, global signal.

While these individual [10]Be spikes provide chronostratigraphic tie points, a more powerful correlation and dating tool involves using a time series of geomagnetic paleointensity variations and cosmogenic nuclide production variations. Mazaud et al. (1994) observed that the [10]Be flux versus age in the Vostok ice core largely co-varied with a synthetic curve generated by assuming that ~75% of [10]Be production was modulated by geomagnetic field intensity. Starting with the geomagnetic paleointensity records of Meynadier et al. (1992) and Tric et al. (1992), the authors calculated the expected [10]Be production rate according to Lal (1988). The authors used this curve as a reference for tuning the ice paleoaccumulation rates. The resulting Vostok chronology improved the correlation between climatic signals in the Vostok ice core and in marine sediment records. Since geomagnetic modulation is minimal at the poles, this study implies that aerosols carrying [10]Be are transported from low latitudes to the Antarctic ice sheet (Mazaud et al. 1994).

One single record of geomagnetic field variability is not an ideal reference curve. Any single record may contain subtle flaws in its chronology or remanent magnetization. Guyodo and Valet (1996) proposed using a "stack," a weighted -average of several time-correlative records, to enhance the signal to noise ratio, average out any flaws present in the individual records, and extract the broad-scale, yet true global features of the geomagnetic field. Guyodo and Valet (1996) confirmed that a distinctive pattern of geomagnetic field paleointensity was observable in deep-sea sedimentary records from around the globe (Fig. 2). They produced a 200-kyr global stack of 19 paleointensity records, named Sint-200, which they suggested could be used as a millennial-scale correlation and dating tool. Each of the 19 constituent records in Sint-200 had its own oxygen-isotope stratigraphy. By correlating paleointensity variations in an undated core with the Sint-200 target curve, one could import the oxygen isotope stratigraphy to one's core site. For example, Stoner et al. (1998) successfully developed a geomagnetic paleo-intensity-based chronology for the Labrador Sea by correlating distinct intensity highs and lows in Labrador Sea sediment cores with Sint-200.

The constituent records of Sint-200, and its subsequent extension to the 800-kyr Sint-800 (Guyodo and Valet 1999) were all deep-sea sediment cores with relatively low sedimentation rates. A newer stack with higher temporal resolution, the 75-kyr North Atlantic Paleointensity Stack (NAPIS-75), was constructed from high sedimentation
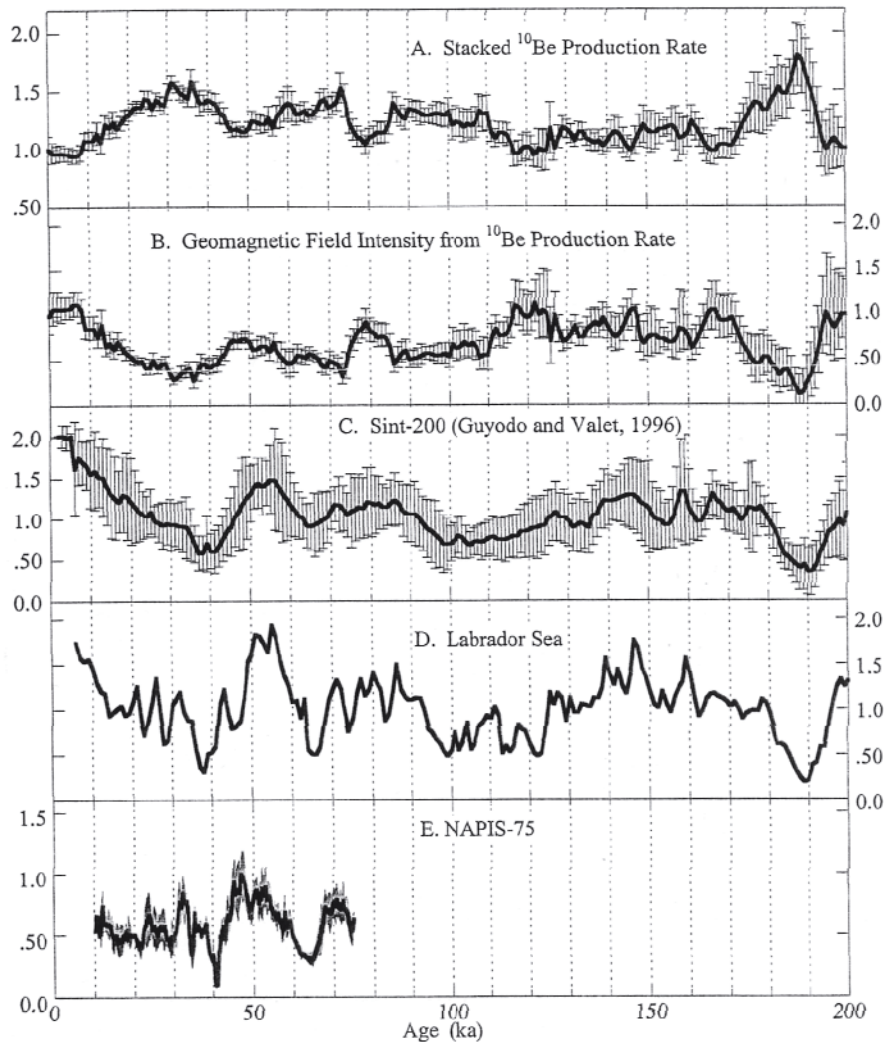
Figure 2. (a) Global stacked ${}^{10}Be$ production rate (Frank et al. 1997) (b) geomagnetic paleointensity derived from ${}^{10}Be$ production rates (Frank et al. 1997) (c) global stacked record of geomagnetic field paleointensity derived from paleomagnetic data (Guyodo and Valet 1996) (d) Labrador Sea relative paleointensity record for the past 200 kyr (Stoner et al. 1998) (e) NAPIS-75 geomagnetic paleointensity stack (Laj et al. 2000). Paleointensity is given in dimensionless, relative units. Geomagnetic field variations derived from paleomagnetic data and ${}^{10}Be$ production rates appear to be globally coherent over the past 200 kyr, which can be exploited as a correlation and dating tool. The higher resolution NAPIS-75 record suggests that the Laschamp Event at 40 to 41 ka is only 1000 years in duration.

rate cores from sediment drifts in the North Atlantic Ocean (Laj et al. 2000). NAPIS-75 is a stack of six individual high-resolution records (sedimentation rates = 20 to 30 cm/kyr) from cores recovered from the Nordic seas and the North Atlantic. The stack covers the time interval 10-75 ka, providing partial overlap with the radiocarbon timescale. NAPIS-75 was placed on the GISP2 age model by correlating the planktonic foraminifera $\delta^{18}O$ record in one of the sediment cores with the $\delta^{18}O$ record in the GISP2 ice core (Voelker et al. 1998; Kissel et al. 1999).

There are striking similarities between NAPIS-75 and the synthetic geomagnetic field record calculated from ${}^{36}Cl$ and ${}^{10}Be$ data obtained from the GRIP/GISP2 ice cores (Baumgartner et al. 1997, 1998; Finkel and Nishiizumi 1997; Yiou et al. 1997; Wagner et al. 2000a,b), which suggests a geomagnetic origin for the variations seen in NAPIS-75.

Features with a 1000 to 2000-year wavelength can be recognized in both records. The millennial scale features of NAPIS-75, coupled to the precise GISP2 time-scale, constitutes a highly efficient tool for correlating and dating cores in different oceans basins around the world (Stoner et al. 2000, 2002), particularly in the Arctic Ocean and Southern Ocean where $\delta^{18}O$ stratigraphy is not available. The extension of NAPIS-75 to NAPIS-300, a 300,000 year stack, is now in progress (C. Laj and C. Kissel, pers. comm.).

Frank et al. (1997) used similar methods to generate a 200-kyr global stack record of ^{10}Be production rates (named Sint-Be). This stack applied ^{230}Th-normalization of the ^{10}Be fluxes in order to correct for sediment redistribution effects. The ^{230}Th-normalized ^{10}Be deposition rates were then normalized to their mean value in each core and averaged in 1000-year increments to account for changes in boundary scavenging over time resulting from climatically-induced changes in particle flux and composition. The resulting record was then translated into geomagnetic field paleointensity according to Lal (1988).

Several paleointensity stacks and the ^{10}Be stack are shown in Figure 2. There are several interesting features to note. First, the peak-to-trough amplitudes of the geomagnetic records are very similar. This is encouraging and suggests that relative paleointensity normalization has been successful. Sint-200 and Sint-Be are in particularly good agreement over the past 20 kyr, one of the intervals of greatest discrepancies amongst sedimentary records using relative intensities. Second, all of the records show decreased geomagnetic field intensity over the intervals 30-42 ka, 60-75 ka, 85-110 ka, and 180-192 ka, which are all interpreted as geomagnetic excursions. Third, variations with wavelengths of ~10 kyr persist in both records. As has been noted previously, even shorter period features are correlative in the higher resolution NAPIS-75 and the GRIP/GISP2 ice cores The latter point is the basis for proposing that geomagnetic paleointensity has potential as a millennial-scale global correlation and dating tool (Guyodo and Valet 1996, 1999; Frank et al. 1997; Stoner et al. 2002).

In some cases the paleomagnetic record of deep-sea sediment may be compromised by post-depositional diagenesis or sediment disturbance. Iron-sulfur diagenesis (e.g., Karlin 1990; Leslie et al. 1990) may result in the dissolution of the magnetic grains that carry the NRM. Alternatively, magnetite authigenesis may result in the acquisition of a chemical overprint that obscures the primary NRM (e.g., Tarduno and Wilkison 1996). In rare cases, weakly magnetized sediments have been completely overprinted by a remanence acquired during the coring process (Fuller et al. 1998; Acton et al. 2002). In these cases the paleomagnetic-derived paleointensity record cannot be trusted, but paleointensity variations could be determined through ^{10}Be production rates, enabling the importation of the SPECMAP or GISP2 chronology to one's study area.

The asymmetric sawtooth

The asymmetric sawtooth pattern observed in deep sea sediments (Ninkovich et al. 1966; Kobayashi et al. 1971; Opdyke et al. 1973; Valet and Meynadier 1993; Meynadier et al. 1992; Yamazaki et al. 1995; Verosub et al. 1996) consists of an apparent rapid rise in relative paleointensity immediately after a geomagnetic field reversal, followed by a slow decay until the next reversal (Fig. 3). However, this pattern is absent in several records (e.g., Laj et al. 1996; Kok and Tauxe 1999), leading to uncertainties in its origins.

If the sawtooth represents true geomagnetic field behavior then it has strong implications for our understanding of the geodynamo (McFadden and Merrill 1997). Whether or not a relationship exists between dipole intensity and reversal frequency, or core processes in general, has long been a topic of debate in geomagnetism (see Merrill et al. 1996 for a full discussion). The sawtooth pattern displays a positive correlation between the magnitude of the post-reversal intensity recovery and the duration of the
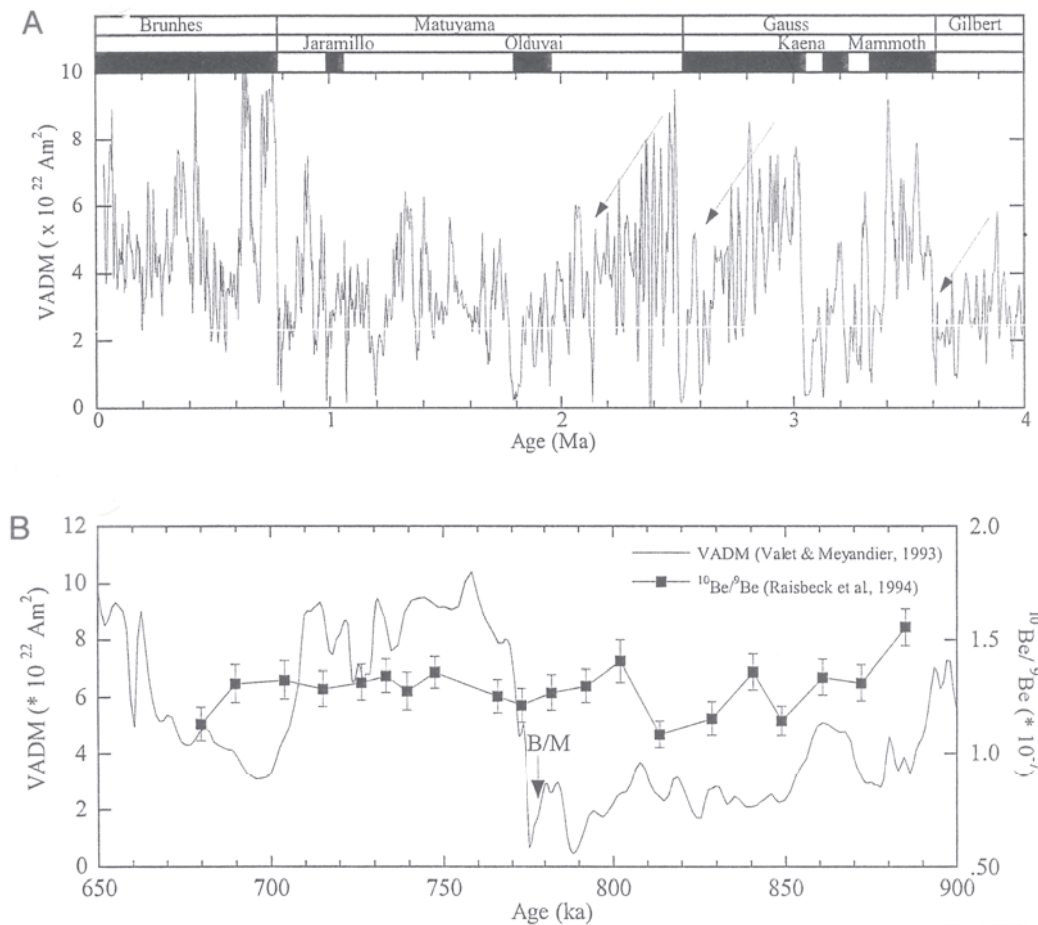
Figure 3 (A) Composite relative paleointensity variations from Ocean Drilling Program (ODP) Leg 138 Sites 848, 851, and 852, equatorial Pacific Ocean. The virtual apparent dipole moment (VADM) appears to gradually decay over time (arrows), then rebound immediately following a geomagnetic field reversal (Valet and Meynadier 1993). (B) ¹⁰Be variations from Leg 138 cores 851C and 851E (Raisbeck et al. 1994) are incompatible with the paleomagnetic data. The ¹⁰Be/⁹Be ratio *decreases* leading up to the Brunhes-Matuyama reversal at ~778 ka. Further, the production-rate change at the reversal itself is substantially smaller than predicted by the paleomagnetic data. The apparent discrepancies may be due in part to lithological differences between the cores.

subsequent interval of constant polarity. This suggests that a strong field inhibits a future reversal and requires the geodynamo to have a memory of when the previous reversal occurred. From this we might suspect that geomagnetic field intensity is unusually high during superchrons. However, this suggestion is not supported by the available, and very limited, absolute paleointensity data from the Cretaceous Normal Superchron (Juárez et al. 1998).

McFadden and Merrill (1993, 1997) examined the frequency of reversals and duration of constant polarity intervals (chrons) in the Cenozoic and compared these statistics with models of inhibition in the reversal process. These studies found that a reversal at time t_1 can inhibit the next reversal at time t_2 for, at most, 50,000 years after time t_1. The sawtooth requires inhibition on timescales of 10^5 to 10^6 years. While the observational data and model results disagree in this particular instance, the sawtooth pattern presented by Valet and Meynadier (1993) represents a continuous well-dated paleointensity time series that can provide important input and "ground-truthing" for

theoretical, numerical, and statistical geomagnetic field models. Therefore, it is critical that the observational data represents true geomagnetic field behavior.

Other mechanisms have been proposed to explain the sawtooth pattern, all of which invoke magnetic recording artifacts in sediments. These include intensity decay as resulting from the vector sum of oppositely aligned (normal and reversed) magnetization in the sediment (Ninkovich et al. 1966; Opdyke et al. 1973; Kobayashi et al. 1971; Mazaud 1996), "chemical lock-in" of a magnetiza tion carried by authigenic magnetite (Tarduno and Wilkison 1996), or thermoviscous overprinting of a magnetization with a secondary component acquired in a field of opposite polarity (Kok and Tauxe 1996a,b). All of these arguments have their own complications, requiring magnetic grains to remain mobile and reorient several meters below the sediment-water interface or requiring an unrealistically narrow distribution of magnetic grain sizes (Meynadier and Valet 1996; Meynadier et al. 1998). There are presently more arguments and mechanisms for an artifact origin of the sawtooth, but debate continues over its origins (e.g., Valet and Meynadier 2001; Kok and Ynsen 2002).

^{10}Be has the potential to provide corroborating or repudiating evidence of the sawtooth pattern. Henken-Mellies et al. (1990) investigated ^{10}Be/^{9}Be ratios across the BM reversal and the Matuyama-Gauss (MG) reversal. In contrast to the predictions of the sawtooth paleointensity model, the ^{10}Be/^{9}Be ratio decreased leading up to the BM reversal and remained roughly constant prior to the MG reversal. However, the ^{10}Be/^{9}Be ratio gradually increased following the MG reversal, which is in agreement with the sawtooth pattern.

Raisbeck et al. (1994) measured the ^{10}Be/^{9}Be ratio at the same site as Valet and Meynadier (1993) spanning the interval 650 to 900 ka. They observed that the ^{10}Be/^{9}Be variations at the Brunhes-Matuyama (BM) reversal were far smaller than those expected on the basis of relative paleointensity estimates (Fig. 3). Further, the ^{10}Be/^{9}Be ratio decreased leading up to the BM reversal, in direct opposition to the paleomagnetic record.

Aldahan and Possnert (2000) constructed a 3.5-Myr record of ^{10}Be flux in deep-sea sediment from the Caribbean Sea. This is one of the longest sedimentary records of ^{10}Be flux back through time, and spans several geomagnetic polarity chrons. The site was chosen for its uniform sedimentation rate and apparent lack of climatic overprinting. This record consists of 90 samples, with the highest density of samples taken from the Brunhes chron (0 to 780 Ma). The ^{10}Be flux was elevated during geomagnetic reversals and excursions (Aldahan and Possnert 2000). However, the record does not match the pattern predicted by asymmetric sawtooth behavior of the geomagnetic field. The ^{10}Be flux appears to decrease leading up to each reversal. However, the sample density is very low, particularly prior to the Brunhes chron, making evaluation of sawtooth pattern difficult in those intervals.

Sawtooth opponents point to the absence of the pattern during the Brunhes chron, arguing that Brunhes age sediments have not yet seen an oppositely oriented field that could cause either the mechanical, chemical, or viscous realignment of the magnetization. Therefore, the Brunhes-Matuyama reversal and the Brunhes Chron may not be the ideal place to confirm or deny the sawtooth. Sub-chrons within the Matuyama Chron would be ideal intervals for investigation using ^{10}Be. It is critical that any such paired paleomagnetic and ^{10}Be study be done on the same core. Raisbeck et al. (1994) suggested that the discrepancies between the Valet and Meynadier (1993) paleomagnetic data and ^{10}Be data may have resulted from the fact that the data were gathered from two different cores with different sediment textures. The paleomagnetic data were collected from a laminated core and the ^{10}Be data gathered from a heavily bioturbated core. Assuming that

the complicating influences of lithology can be minimized by careful core selection, a paired paleomagnetic and ¹⁰Be study across entire sub-chrons, including but not limited to the bounding reversals, should aid in investigation the origin of the sawtooth pattern.

Milankovitch periodicities in geomagnetic paleointensity records

The cause and significance of Milankovitch periodicities in geomagnetic field timeseries data has been debated for more than 30 years. The question of whether variations in Earth's orbital parameters perturb fluid motions in the outer core (e.g., Malkus 1968; Rochester et al. 1975) appeared to be answered affirmatively when Kent and Opdyke (1977) observed a 43-kyr periodicity in a geomagnetic field paleointensity record from a Pacific Ocean sediment core. Subsequently, other records suggest the presence of 100-kyr and 41-kyr periodicities in geomagnetic paleointensity timeseries (e.g., Tauxe and Wu 1990; Tauxe 1993; Channell et al. 1998; Yamazaki 1999; Channell and Kleiven 2000; Yamazaki and Oda 2002) within different intervals within the Brunhes and Matuyama chrons. This has led to speculation that variations in earth's orbital parameters may indeed influence the geodynamo.

Tauxe (1993) tested the coherence of normalized intensity with the various normalization parameters. It was observed that periodicities in normalized intensity were also present in the normalization parameters, and the two time-series were coherent at Milankovitch frequencies. Tauxe (1993) proposed that the presence of Milankovitch periodicities in paleointensity records were due to "contamination" of the paleointensity record by climate-induced variations in the concentration and grain size of the magnetic minerals in the sediment. In this instance, normalization was not completely efficient. Subsequent studies of sediment cores from the North Atlantic (Channell et al. 1998; Channell and Kleiven 2000) and North Pacific (Yamazaki 1999) conducted the same analyses and demonstrated the presence of Milankovitch periodicities (41 kyr and 100 kyr, respectively) in the paleointensity records but not in the bulk magnetic parameters. In both cases, the authors suggested that the paleointensity records were therefore free of contamination, and represented orbital modulation of the geomagnetic field.

The paleointensity records presented by Channell et al. (1998) and Channell and Kleiven (2000), were particularly intriguing. These records were generated from Ocean Drilling Program Site 983, the Gardar Drift in the North Atlantic. This site has the benefit of high temporal resolution and superior age control from a high density of oxygen isotope measurements. The power spectra of these paleointensity records contained significant peaks at 100 kyr and 41 kyr. A similar analysis was performed on magnetic parameters such as IRM and magnetic susceptibility, which track the concentration of magnetic material. The 100-kyr cycles were present in the bulk magnetic properties, leading the authors to interpret the 100-kyr paleointensity features as a lithologic contamination. However, the 41-kyr cycles were *not* observed in the bulk magnetic parameters, leading the authors to conclude that the 41-kyr paleointensity cycles were due to true geomagnetic field behavior. Guyodo et al. (2000), re-examined these records using wavelet analysis. Wavelet analysis enables the detection of non-stationarity in a signal and identifies the specific time intervals when a given frequency is present in a record. Guyodo et al. (2000) identified the presence of periodic, though non-stationary, signals at 100 kyr and 41 kyr. Whereas global Fourier analysis failed to detect the 41-kyr signal in the bulk magnetic parameters, wavelet analysis of a magnetic grain size proxy revealed the 41-kyr signal in three discrete time intervals. These authors concluded that a lithologic overprint remained in the normalized intensity record, creating the 41-kyr variations in the paleointensity record. The authors then filtered these wavelet components from the paleointensity record, demonstrating that the secondary overprint had a minor effect on the overall paleointensity profile.

Presently, there is no known mechanism that conclusively couples earth's orbital parameters with the geodynamo. However, this particular problem and the case study from ODP Site 983 raises the issue of how to confidently identify any real geomagnetic field periodicities that might be similar or identical to any real periodicities associated with other forcing mechanisms. Guyodo and Valet (1999) investigated this question using Sint-800, the global stack record of 33 geomagnetic field paleointensity variations for the past 800 kyr. The majority of the constituent records were dated by correlating their oxygen isotope (δ^{18}O) stratigraphies to those of the reference curve termed SPECMAP (Martinson et al. 1987; Bassinot et al. 1994). Stacking the 33 records together should average out any non-field effects in a given constituent record, while preserving the broad scale features of the geomagnetic field. The authors tested the validity of this assumption by re-calculating the stack 33 times, each time leaving out one of the constituent records. In each case the deviation between Sint-800 and the re-calculated stack was within the 2σ standard deviation of Sint-800, confirming the absence of significant outliers (Guyodo and Valet 1999).

Guyodo and Valet (1999) performed a spectral analysis of Sint-800 to look for periodic variations (Fig. 4). They first analyzed the entire signal, then they re-analyzed the signal in 400 kyr increments with a time step of 100 kyr (i.e., 0 to 400 kyr, 100 to 500 kyr, etc.). For comparison, the same analysis was performed with a stacked record of δ^{18}O values that was dated by orbital tuning (e.g., Imbrie et al. 1984; Martinson et al. 1987; Bassinot et al. 1994). The stacked δ^{18}O curve, named SPECMAP, is a proxy for global ice volume, which in turn is controlled by the Earth's orbital geometry (Milankovitch 1941). Orbital tuning involves synchronizing the proxy of global ice volume, typically δ^{18}O or $CaCO_3$ content in sediment, with the known history of orbital forcing, i.e., the calculated time series of summer solar irradiance at 65°N latitude, or a model of the climate response signal (e.g., Imbrie and Imbrie 1980) (see Martinson et al. 1987 for full discussion).

The spectral content of successive 400-kyr intervals of Sint-800 are very different from one another, confirming the absence of any stable periodicity (Fig. 4). In contrast, significant peaks in spectral power at the Milankovitch periodicities (23, 41, and 100 kyr) are seen in each increment of SPECMAP. Given that the SPECMAP chronology is derived from orbital tuning, it may seem circular to perform a spectral analysis, as the forcing function periodicities are guaranteed to be present. However, the purpose here is to illustrate the differences between the non-periodic Sint-800 signal and the periodic SPECMAP signal. While Sint-800 reveals large amplitude changes in geomagnetic field paleointensity, there is no evidence of a stable, dominant periodicity (Guyodo and Valet 1999).

Corroborating evidence could be obtained by performing the same analysis on a stack of ^{10}Be production. Unfortunately, neither the ^{230}Th-normalized 200-kyr Sint-Be record (Frank et al. 1997) nor the ~225-kyr Taylor Dome ^{10}Be record (Steig et al. 2000) is long enough to confidently identify the 100-kyr Milankovitch periodicity. An extension of Sint-Be would be ideal for investigation of the presence of Milankovitch cycles. The 3.5-Myr record of ^{10}Be flux in deep sea sediment from the Caribbean Sea of Aldahan and Possnert (2000) would also be well-suited to this purpose, given the site's uniform sedimentation rate and apparent lack of climatic overprinting. Another candidate is the ~400-kyr Vostok ice core (Petit et al. 1999). Both of these records would need to be enhanced with a higher sampling density in order to confidently identify Milankovitch periodicities.

Assuming that these existing records can be enhanced, or that new high resolution records will be generated, there is a good basis for expecting that geomagnetic
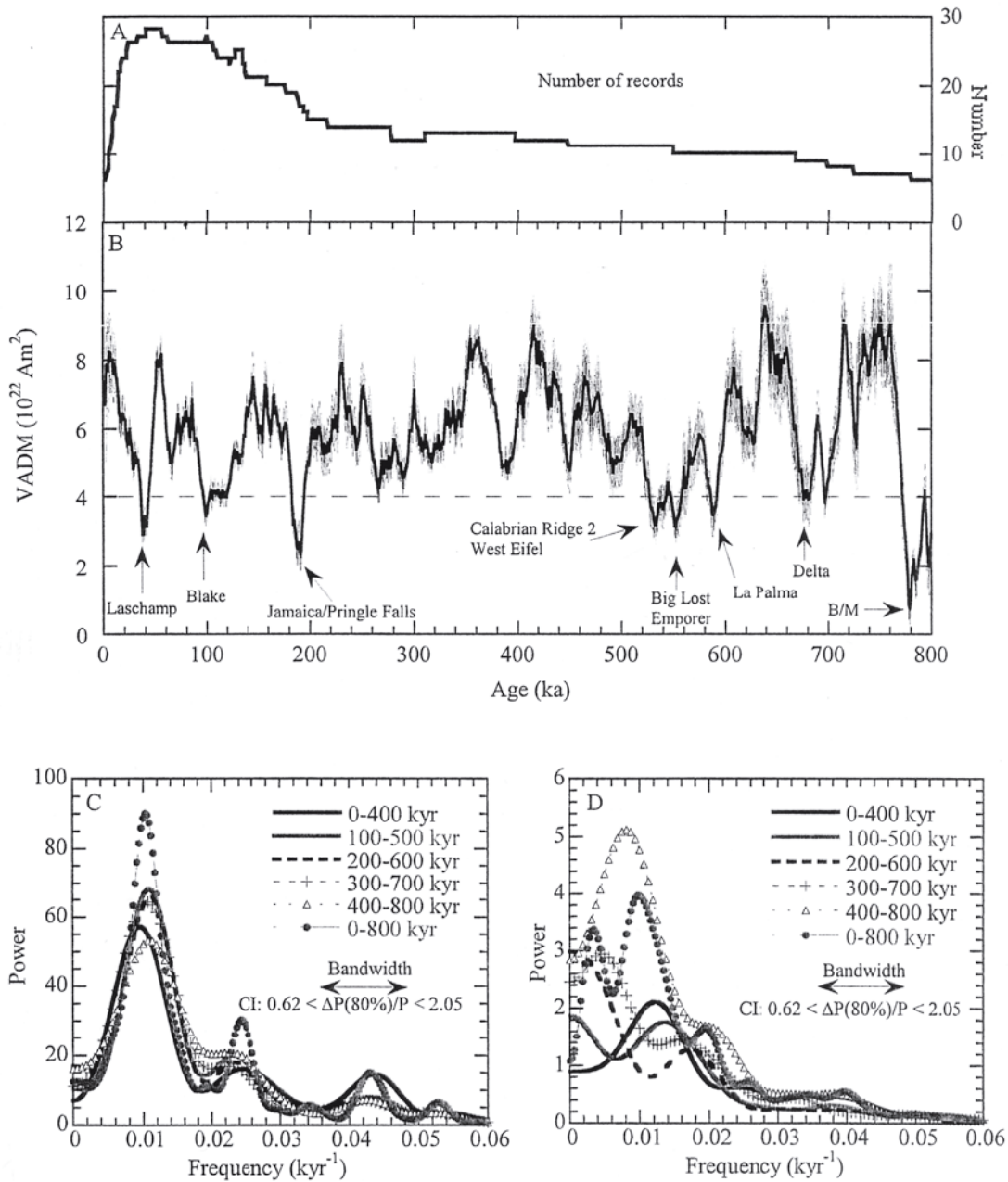
Figure 4. (a) Distribution of constituent records in Sint-800. (b) Sint-800 (Guyodo and Valet 1999) reveals 8 excursions during the Brunhes chron, each associated with a >50% reduction in the strength of the dipole moment. (c) Spectral analysis of Sint-800, and successive 400-kyr increments of Sint-800. There are no significant peaks in spectral power in the Sint-800 record. (d) In contrast, the 23-kyr, 41-kyr, and 100-kyr periodicities are present in each sub-set of the SPECMAP curve (redrawn after Guyodo and Valet 1999). Spectral analysis was performed using Analyseries software (Paillard et al., 1996).

modulation cycles can be identified in ¹⁰Be production rates. Radionuclide investigations using tree rings and ice cores have revealed century and decade scale variations in the production rates of ¹⁴C and ¹⁰Be (e.g., Beer et al. 1988; Stuiver and Braziunas 1989; Beer et al. 1990; Stuiver and Braziunas 1993; Steig et al. 1998; Wagner et al. 2001) which have been attributed to solar modulation of the primary cosmic ray flux. A similar approach in lithologically uniform, high-deposition rate sediments could potentially resolve long-period variations in the geomagnetic field.

Any such effort must remember that observed periodicities in ^{10}Be concentration in sediments need not be due to the geomagnetic field. Henken-Mellies et al. (1990) observed a strong anti-correlation between ^{10}Be concentration and $CaCO_3$ content. Further, Kok (1999) proposed that the excellent agreement between Sint-200 and Sint-Be is due to the paleoclimate contamination present in both records rather than true geomagnetic field behavior. Henken-Mellies et al. (1990) attempted to remove climatic influences by calculating the ^{10}Be concentration on a carbonate-free basis. The presence of periodicities in both a normalized relative intensity record and a ^{230}Th-normalized ^{10}Be record from the same core, while not conclusive evidence, would further the argument in favor of periodic variations in the geomagnetic dipole moment.

Summary

Variations in geomagnetic field paleointensity derived from ^{10}Be and ^{36}Cl production rates have the potential to contribute to the resolution of controversies in geomagnetism. ^{10}Be accumulation is not affected by sediment magnetic recording processes and normalization artifacts that are at the root of these controversies. The half-life of ^{10}Be (1.5 Myr) theoretically enables its application back to ~10 Ma, which would allow a study of the pattern of radionuclide production rates over several geomagnetic polarity intervals. Long records of ^{10}Be in sediments could potentially confirm or refute the asymmetric sawtooth pattern and the apparent 100-kyr periodicity in geomagnetic paleointensity variations. Using ^{10}Be and ^{36}Cl production rates obtained from glacial ice or sediment as proxies of geomagnetic field paleointensity requires the recognition and removal of complicating influences such as changing precipitation rates and moisture sources, boundary scavenging, sediment focusing and winnowing, and climatically-driven changes in ocean circulation and water mass distribution. Sedimentary profiles of ^{10}Be can be normalized to ^{230}Th to correct for sediment redistribution effects. However, the relatively short half-life of ^{230}Th (75 kyr) means that sedimentary records cannot be corrected for sediment redistribution effects beyond ~300 ka. The combined application of paleomagnetic and ^{10}Be methods has already enhanced the reconstruction of past geomagnetic field intensity variations over the past ~200 kyr. Comparison of ice core profiles of ^{10}Be and ^{36}Cl accumulation with high-resolution sediment sequences has confirmed the geomagnetic origin of high-frequency variations in the geomagnetic dipole moment, and revealed the very abrupt nature of the Laschamp geomagnetic excursion. These types of records are contributing to the development of geomagnetic paleointensity as a millennial-scale global correlation and dating tool.

SUBDUCTION AND MAGMATISM AT CONVERGENT MARGINS

Introduction

Cosmogenic ^{10}Be, with high concentrations in young marine sediments, is an outstanding tool for tracing sediment subduction and recycling at convergent margins. Decaying with a 1.5-Myr half-life (Yiou and Raisbeck 1972), high ^{10}Be concentrations are measured only in sediments younger than 12 Ma, and do not build up in the mantle over time. High ^{10}Be concentrations in arc lavas thus require the subduction to depth of the youngest part of the sedimentary veneer, and the transport of slab-derived elements to the mantle wedge and thence to the surface. As a result, ^{10}Be studies can constrain a wide variety of physical and magmatic processes operating at convergent margins, from the trench to the back-arc.

^{10}Be on the subducting plate

This section provides an overview of the ^{10}Be transport in subduction zones. It discusses the variations in ^{10}Be supplied to subduction trenches around the world, the

mineralogical hosts for [10]Be in the downgoing sediment column and evidence for and against [10]Be mobility in fluids leaving the slab at shallow levels.

The [10]Be cycle. Figure 5 illustrates a series of on-off switches in the subduction cycle, all of which must be in the "on" position for high [10]Be concentrations to be observed in arc lavas. [10]Be inventories in the incoming sediment column must be high enough that a small amount of young sediment mixed with large amounts of older sediment and mantle (or other diluents) can still produce a measurable [10]Be signal in the arc lava. Those uppermost [10]Be-rich sediments must largely escape frontal accretion and basal underplating as the plate subducts beneath the fore-arc. The convergence rate must be fast enough that the subducting [10]Be doesn't decay away during subduction (i.e., the [10]Be clock is still applicable). The [10]Be must be extracted from the downgoing slab and be transferred through the mantle and to the surface before the signal decays away (<2 Myr). The following section will discuss the global distribution of [10]Be in volcanic arcs in terms of these controlling factors.
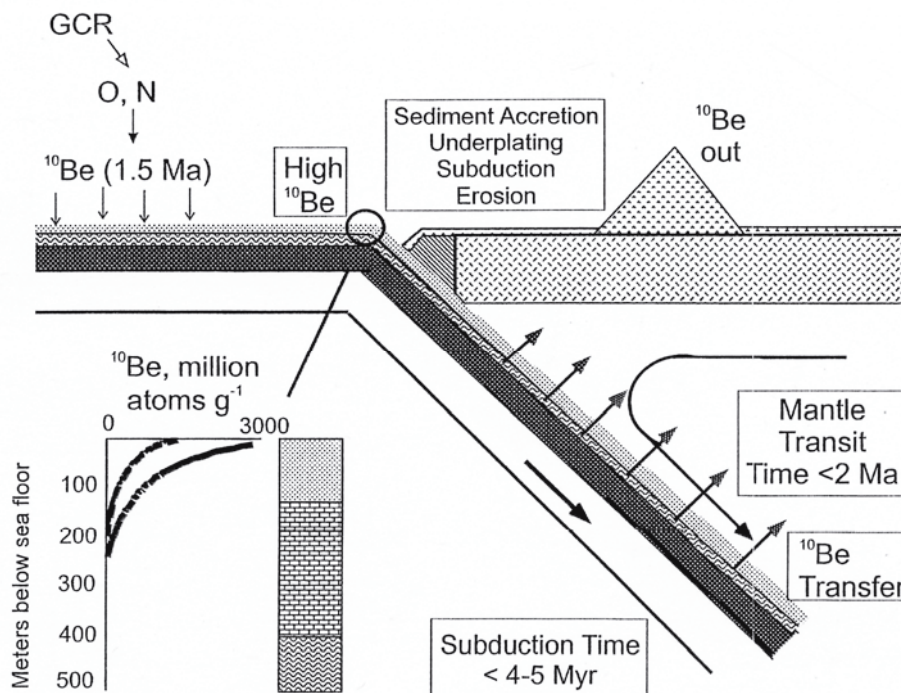
Figure 5. [10]Be cycle through subduction zone. [10]Be is created by spallation reactions on O and N in the atmosphere. It is strongly adsorbed onto settling sediment particles, and carried with the plate into the subduction zone. High [10]Be values in arc lavas require that (1) the incoming sediments have high [10]Be, (2) that most of the uppermost sediment column is not accreted but rather subducted to the depths of magma generation; (3) that the subduction time be less than 4-5 Myr, and that the [10]Be be extracted from the downgoing sediments and moved through the mantle within about a [10]Be half life. The lower left inset shows the distribution of [10]Be in DSDP Site 495, outboard of Guatemala. Higher values are those measured at the trench; the line displaced to lower concentrations is the calculated value for sediments subducted to a point beneath the volcanic arc and reflects the effect of [10]Be decay during subduction.

[10]Be in subducting sediments A quantitative comparison of the sediment hosted [10]Be flux into the trench with the [10]Be flux out of the volcanoes (the [10]Be flux balance) can be used to constrain the absolute volumes of sediments subducted to the depths of magma generation, if the necessary data are available and certain assumptions are met. A series of papers (Zheng et al 1994; Morris et al 2002; George et al., submitted; Valentine

and Morris, submitted a,b) show [10]Be inventories and/or [10]Be-depth profiles for sediments entering the Mariana, Aleutian, Japan, and Middle America (Guatemala and Costa Rica) trenches, using DSDP/ODP drill core. The data, summarized in the upper part of Table 1 (p. 214), show that the total amount of [10]Be in the sediment column (the inventory) supplied to different trenches can vary by an order of magnitude, e.g., the incoming sediment column off the Mariana trench has a [10]Be inventory close to the globally averaged [10]Be production rate (Monaghan et al. 1985/1986), while those for Japan and Central America are ten times greater. In general, margins studied to date have values comparable to or greater than that corresponding to the globally averaged [10]Be production rate, implying [10]Be deficits in much of the open Pacific Ocean. Table 1 also shows that the sediment layer tagged by high [10]Be can vary in thickness from ~25 m (Marianas) to 250 m (Japan) as a function of Plio-Pleistocene sedimentation rates; preliminary data for the Tonga section suggest all [10]Be will be within the upper 15 m (Morris, unpubl.). Sediment lithologies for the uppermost part of the cores reported here are pelagic to hemi-pelagic, often rich in volcanic detritus or with ash layers deposited as the incoming plate approaches the arc. Considering the heterogeneity in the total amount of [10]Be subducted and the thickness of the [10]Be-tagged sediment layer, [10]Be measurements in the arc and also in the specific sediment column entering the associated trench are necessary for detailed interpretations of sediment dynamics or flux balance (e.g., Plank and Langmuir 1993). The [10]Be inventory in Table 1 was converted to a [10]Be flux to the trench using published convergence rates (Jarrard 1986; Zhang and Schwartz 1992).

Quantitative [10]Be flux balances can be used to estimate the relative proportions of sediments accreted or underplated versus those subducted, with the assumption that the margin is in an approximately steady state. The lavas erupting today are sampling a plate that began subducting 1.8- to 4-Myr ago (for margins with high [10]Be). The sediment composition, supply rate and sediment dynamics need to be approximately constant over this duration in order to compare the amount of [10]Be subducted with that erupted from the arc. In some cases (e.g., Reagan et al. 1994; Plank et al., submitted) the sediment and arc data themselves argue strongly for steady state conditions. In other cases (see Von Huene and Scholl 1991; Rea and Ruff 1996) steady state conditions may not have applied due to recent changes in tectonic setting or sedimentological conditions. In such cases, flux balances for [10]Be (or any other tracer) must be evaluated carefully.

The bottom part of Table 1 shows the ratio of the [10]Be flux out of the arc, relative to the [10]Be flux to the depths of magma generation. The ratio is corrected for decay during subduction, using a simplest model where the [10]Be subducts at the convergence rate to a point beneath the volcanic front, and magma ascent times are short relative to the [10]Be half life. Where a high proportion of the subducted [10]Be is erupted from the arc (e.g., Nicaragua) then most of the sediments must have been subducted to the depths of magma generation. Low values (e.g., Costa Rica, Honshu) require that much of the incoming young sediment be accreted or diluted by subduction erosion. These results are discussed in more detail below, but this brief discussion highlights the way in which the sediment signature recorded in the lavas allows the volcanic arc to serve as a "flow meter" for the volume and lithology of the sediments carried through the seismogenic zone to the depth of magma generation (see also Morris et al. 2002; Valentine and Morris, submitted a,b).

[10]Be and fluid mobility. Quantitative flux balance calculations also require that [10]Be is not leaving the slab to be stored in areas where it cannot be sampled, measured, and included in the flux balance. This assumption may be evaluated through studies of prism sediments, subduction zone metamorphic rocks and experiments. You et al. (1994) showed lower than expected [10]Be concentrations below the décollement at Nankai (ODP Site 808), for which their preferred interpretation was [10]Be fluid mobility. Alternative

interpretations are possible, given that similar offsets in the [10]Be-depth profile are observed at lithologic boundaries at other depths in the column, removed from areas of fluid flow. The magnitude of fluid flow along and below the décollement also has been debated (Taira and Hill 1991). By contrast, the reconnaissance-scale [10]Be-depth profiles from ODP Leg 170 (Sites 1040 and 1043) sampled the sediments immediately above and below the décollement. The subducting sediments (Valentine et al. 1997; Morris et al. 2002) show no deviation from the expected profile, despite strong evidence here for fluid flow along, and just below, the décollement (Kimura et al. 1997; Silver et al. 2000; Kastner et al. 2000). [10]Be analysis of very closely spaced samples in regions of documented fluid flow, together with [9]Be analysis of associated pore fluids, would help evaluate the possibility of [10]Be fluid mobility.

Experimental studies have been conducted on Be partitioning between sediments or igneous/metamorphic minerals, and fluids of varying compositions. At low temperatures (<150° C) and moderate to high pH (>4), Be is strongly adsorbed onto sediment surfaces, with concentrations on the particles 10^5 times that in the associated seawater (Nyffler et al 1984; You et al. 1994, 1996). Accretionary prism fluids have geochemical indicators suggesting that some fraction of the fluids may have originated at regions with temperatures as high at 110-150° (Kimura et al. 1997) and their pH is 7-8. The experimental results suggest that any Be mobility under these conditions should be an insignificant part of the total Be budget. At higher temperatures, Be becomes slightly more mobile, e.g., 10^4 times greater in the particle than the fluid. Hydrothermal fluids reacted with sediments at temperatures of about 300° C carry approximately 0.1 ppb Be (You et al. 1996). Sediment-fluid experiments at 650-700° C begin to show some fluid mobility, with Be in the sediment being 2-4 times that of the associated fluid (Johnson and Plank 1999). Serpentine dehydration experiments (Tatsumi et al. 1986) and studies of Be solubility in equilibrium with mantle minerals (Brenan et al. 1998) suggest that Be is not particularly fluid mobile under mantle conditions.

Mineralogical and geochemical studies of metamorphic assemblages exhumed from the hanging wall of paleo-subduction zones show that white mica is the primary host for Be in the sediment column (e.g., Bebout 1996; Bebout et al 1993, 1999; Grew this volume). Older studies of Be adsorption between seawater and sediment particles suggest that some fraction of adsorbed Be moves into 'unexchangeable' structural sites within the crystals (Nyffler et al. 1984). Bebout et al (1993) reported B, Be and Ba concentrations in subduction assemblage metamorphic rocks thought to have similar protoliths. Water and boron concentrations decrease systematically with increasing grade, while Be and Ba show slight variability about a constant concentration, suggesting no significant Be loss from progressively metamorphosed sediments at conditions up to approximately 40 km depth and about 700° C (see also Grew, this volume).

[10]Be was measured in serpentinite muds recovered from the top of Conical Seamount during ODP Leg 125, to assess the possibility that [10]Be was extracted from the slab at relatively shallow levels (Benton 1997). The seamount is a very large (1 km high by 30-40 km across) serpentine mud volcano located approximately 20 km above the downgoing slab (Fryer et al. 1995). A large number of geochemical tracers in actively venting and pore fluids sampled there suggest that some fraction of the fluid supply derives from the subducting slab (e.g., Haggerty 1991; Haggerty and Fisher 1992; Benton 1997). Processed at Washington University under very low blank conditions (blank [10]Be/[9]Be = 7-9×10^{-16}, < 1000 atom g^{-1}, and analyzed at University of Pennsylvania with a detection limit of 1×10^4 atoms g^{-1}), the serpentinite muds have very low, but measurable [10]Be, in the range 5-7×10^4 atoms g^{-1} (Benton and Morris, unpubl.). [9]Be concentrations were below detection limits (Benton 1997). Be/Nd ratios are rather constant in many

subduction zone lavas (Ryan and Langmuir 1988), but highly variable Nd concentrations in the serpentine muds (e.g., 0.03-2.6 ppm) make it difficult to predict a meaningful ^{9}Be concentration or ^{10}Be/^{9}Be ratio. The ^{10}Be in the serpentinite samples could originate from the downgoing slab, or through very minor near-surface interaction with marine sediments, not currently recognized. The serpentinite mud samples were chosen for initial analysis because of the ease of sample preparation; solid clasts of variably serpentinized harzburgite make a logical next sample set.

In summary, arc lavas sample the downgoing plate, and the chemistry of the lavas may be used to place constraints on the composition of the slab at depth (Morris et al 1990; Plank and Langmuir 1993, 1998; Armstrong 1971). All models using flux balances require the assumption or demonstration of approximately steady-state conditions during the time required for the plate to subduct from the trench to the depths of magma generation. The flux of elements to depth in the subduction zone can be uncertain if they are mobile at shallow levels in the subduction zone (e.g., B, Cs, U, Rb, As) or are contained in sediments that may be scraped off. Set against these uncertainties is the fact that drilling and seismic imaging provide constraints on sediment dynamics only in the upper 2 km and ca. 10-20 km, respectively. Any constraints on sediment transport to the deeper subduction zone must come from the chemistry of fore-arc serpentinites, arc lavas and the deep mantle. An internally consistent model of sediment transport that simultaneously satisfied the results of drilling, imaging, sediment and arc chemistry (e.g., Morris et al. 2002; Valentine and Morris, submitted a,b) gives confidence that this approach using ^{10}Be can be successfully applied.
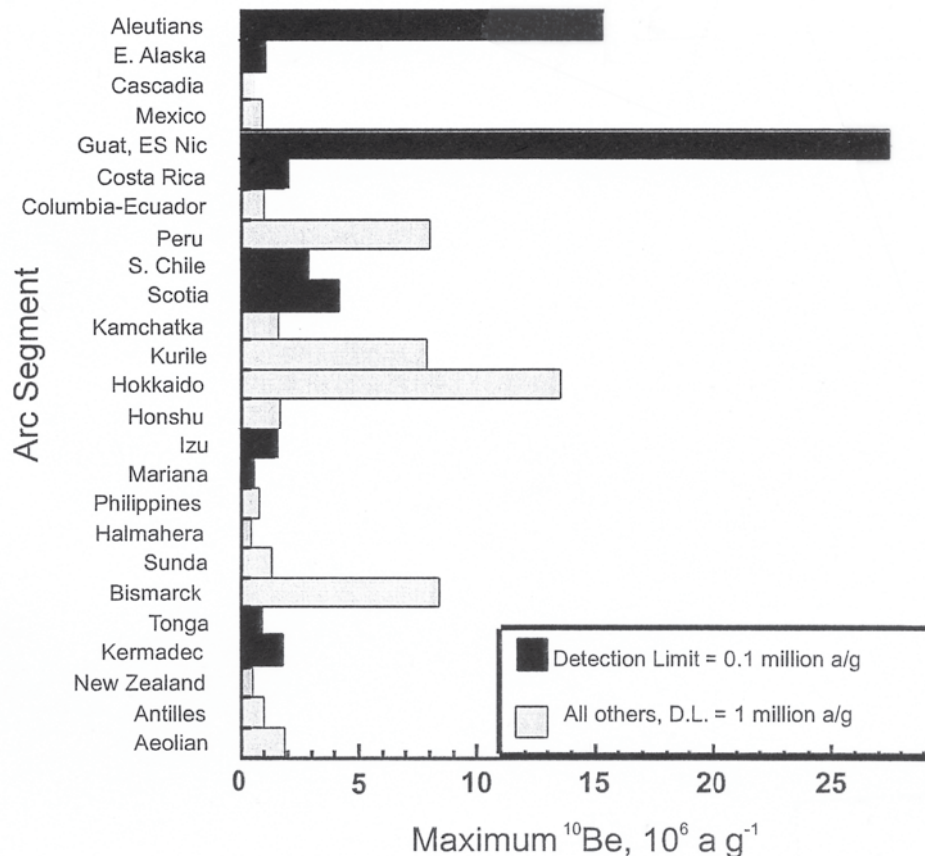
Figure 6. Bar graph showing the maximum ^{10}Be measured in volcanic arcs around the world. The data is taken from Table 2 and references therein. Almost all arcs with high ^{10}Be have a wide range of ^{10}Be values, extending from near background to the maximum value reported.

^{10}Be in volcanic arcs: A global summary

Table 2 and the bar diagram in Figure 6 show the measured concentrations of ^{10}Be in volcanic arc lavas from around the world, in comparison to the detection limits appropriate at the time of measurement. Note that detection limits have improved over time. A detection limit of about 1 million atoms g^{-1} applies to measurements made prior to 1994; more recent work has a detection limit of less than about 0.1 million atoms g^{-1} and exceptionally low-blank work can achieve detection limits of 10^4 atoms g^{-1}. In some cases, the changing detection limit makes a significant difference; note that Marianas samples measured previously were considered barren of ^{10}Be (Tera et al. 1986) while newer measurements show small but real enrichments.

The bulk of the samples shown in Figure 6 are from historic eruptions (1-300 years old). As such, they are too young to have built up *in situ* ^{10}Be through cosmic ray bombardment of the rock or through surface alteration. Mineral separate studies of ^{10}Be and ^{9}Be distribution in volcanic arc rocks (Monaghan et al. 1988; Morris and Tera 1989) showed that the two isotopes were in equilibrium in all phases measured for the 7 historic lavas analyzed. Approximately 20 % of the samples shown are prehistoric, being several hundred years to less than 50 kyr old. These samples are from localities that are geographically critical for testing geodynamic or sediment dynamic models, and for which historic eruptions do not exist. All such samples were leached with 1N HCl in an ultrasonic bath for 1 hr, and both the leachate and the leached sample analyzed. All non-historic samples reported in Figure 6 have negligible amounts of leachable ^{10}Be.

^{10}Be-barren arcs A number of arcs (E. Alaska, Cascadia, Mexico, Honshu, Philippines, Halmahera, Sunda, New Zealand, Lesser Antilles and Aeolian) show no significant ^{10}Be enrichment. The absence of ^{10}Be in these arcs could be due to either ^{10}Be decay in transit from the trench through the mantle to the surface, or to an absence of young sediment recycling in a particular arc.

Convergence rates are low, and subduction times are long for eastern Alaska, Cascadia, and the Lesser Antilles. Because the ^{10}Be clock begins keeping time when the sediment column passes beneath the fore-arc (i.e., once ^{10}Be decay is no longer offset by its deposition), these lavas should contain no subducted ^{10}Be, which would have decayed during subduction. The lavas from these segments do not, in fact, have elevated ^{10}Be, indicating that any sediment/crust assimilation by magmas on their way to the surface did not add ^{10}Be to the lavas (see also George et al., submitted). Most other arcs in Table 2 have rapid enough convergence rates that not all incoming ^{10}Be would decay during subduction to the depths of magma generation.

The expected extent of ^{10}Be decay during transport through the mantle often can be constrained using U-series isotopes. U-series disequilibria isotope measurements show that most arcs include lavas that have excess U. U excesses are seen only in arc lavas. They are generally interpreted to mean that U but not Th was transferred from the slab to the arc mantle wedge and thence to the surface in arc lavas within the last 300 kyr, a short period relative to the ^{10}Be half-life (Gill and Williams 1990; McDermott and Hawkesworth 1991; Hawkesworth et al. 1997; Turner et al 1997; Turner and Hawkesworth 1997, 1998). Lavas from Japan, Kamchatka and Indonesia have U-excesses, indicating that magma ascent is rapid enough that ^{10}Be should not decay away in transit through the mantle.

Arcs such as Japan, Kamchatka, Halmahera, Columbia, and Indonesia show no ^{10}Be enrichment, although other geochemical tracers indicate some sediment subduction and recycling (e.g., Plank and Langmuir 1998; Kersting et al. 1996; Cousens et al. 1994; Edwards et a. 1993; Morris et al. 1983). All sediment columns yet measured outboard of

Table 2. ^{10}Be in volcanic arcs around the world.

Volcanic Arc	Min. ^{10}Be[‡]	Max. ^{10}Be[‡]	D.L.[‡]	Conv. rate[†]	Refs.	Volcanoes analyzed
Aleutians	0.4	15.3	1	7.5	1, 2, 4, 5, 6, 16, 18	Cold Bay, Amak, Shishaldin, Westdahl, Akutan, Makushin, Bogoslof, Okmok, Recheschnoi, Vsveidof, Atka, Kastochi, Seguam, Kanaga, Kiska
E. Alaska	0.1	0.7, 8.4*	0.1	6.4	5, 6, 18	Spurr, Redoubt, Augustine, Trident, Ukinrek, Aniakchak
Cascadia	0.1	0.5	1	3.5	2, 5	Indian Heaven, Mt. St. Helens
Mexico	0.3	0.9	1	7	1, 2	Ceburoco, Cuicuilo, El Chichón
Guatemala, El Salvador, Nicaragua	2.4	27.1	0.1-1	8.3	1 2, 5, 6, 12, 21, 22	Santa Maria, Pacaya, Santa Ana, Izalco, Boqueron, San Miguel, Conchagua, Cosiguina, Telica, Cerro Negro, Asosoca, Momotombo, Nejapa, Masaya, Mombacho, Zapatera, Concepción
Costa Rica	0.8	1.8, 8.4*	0.1	8.8	1, 2, 5, 6, 13, 21, 22	Hacha, Cerro Chopo, Orosi, Miravalles, Arenal, Platenar, Poas, Irazu,
Columbia-Ecuador	0.3	1	1	7	17	Ruiz, Purace, Galeras, Cotopaxi
Peru	0.3	8	1	8.2	2, 4	Chachani, El Misti, Ubinas
C & S. Chile	1.3	2.1	1	8.5	5, 6, 7, 23	San Jose, Chillan, Antuco, Lonquimay, Villarrica, Mocho, Mirador, Osorno, Calbuco, Calburgua, La Barda, Huellemole
Scotia	0.5	4.1	0.1	7.7	24	Bellingshausen, Saunders, Zavaroski, Montague, Candlemass
Kamchatka	0.5	1.6, 3.8[§]	1	8	9	Shiveluch, Klychevskoi, Bezimyanniy, Tolbachik, N. Ichinski, Ichinski, Kizmen, Kangar, Krashennikova, Karimski, Avachinksi, Gorely, Opala, Ksudach
Kurile	1	8	1	8.5	9	Alaid, Parmushir, Chirinkotan, Smt. 2.3, Onekotan, Aekarma, Lovushki, Raikoke, Sarychev, Berg, Smt 7.7, Smt 8.8, Atsonpuri, Lvinaya, Kunashir

Arc	D.L.	^{10}Be		Conv.	Refs.	Volcanoes
Hokkaido	0.5	13.5	1	8.7	2, 3, 15, 20	Rishiri, Tarumai, Usu, Rausu-dake, Komaga-take, E-San, Oshim-Oshima
Honshu	0.2	2.4$	1	10	2, 3, 15, 20	Osorean, Moriyoshi, Kanpu, Iwate, Akitkomatake, Kiroma, Zao, Nasu, Funagata, Fuj
Izu	0.8	1.4	0.1	10	25	Oshima, Miyake-Jima, Tori-shima
Mariana	0.1	1	1	9	2	Iwo-Jima, Uracas, Pagan, Guguan
Mariana	0.2	0.5	0.1	9	2, 14, 26	Asuncion, Uracas, Pagan, Alamagan, Guguan
Philippines	0.8		1	9	2,	Mayon
Halmahera	0.1	0.5	1	9	2	Ibu, Ternate, Makian
Sunda	0.1	0.4	1	7.7	2, 10	Papandjan, Sundoro, Sumbing, Ungaran, Guntur, Galunggung, Cereme, Merbabu, Batur, Ebulobo, Keli-Mutu, Lewotobi
Bismarck	0.5	8.4	1	11	2, 6, 11	Kadovar, Manam, Karkar, Long, Langila, Garove, Makalia, Lolobau, Pago, Bamus, Ulawun, Rabaul
Tonga	0.2	2.2	0.1	<17	24	Niafoua, Tafahi, Fonualei, Late, Metis Shoal, Tofua, Ata
Kermadec	0.4	2.3	0.1	6	24	Raoul, L'Espérance, Valu Fa, Curtis, Macauley, Rumble IV, Clark
New Zealand	0.4	0.5	1	6	18	Tarawera
Antilles		<1	1	4	19	
Aeolian	0.1	1.9$	1	2.5	8, 25	Lipari, Alucudi, Volcano, Stromboli, Vesuvius

‡^{10}Be for arcs and detection limit (D.L.) reported in units of 10^6 atoms g^{-1}

†Convergence rates, in cm yr^{-1}, are from Zhang & Schwartz (1992) and Jarrard (1986)

* refers to values from non-historic lavas with leachable ^{10}Be

$ refers to a single outlier value;

References: 1). Brown et al. (1982); 2) Tera et al. (1986); 3.) Imamura et al. (1984); 4) Monaghan et al. (1988); 5) Morris & Tera (1989); 6) Morris et al. (1990); 7) Sigmarsson et al. (1990); 8) Morris et al. (1993); 9) Tera et al. (1993); 10) Edwards et al. (1993); 11) Gill et al. (1993); 12) Reagan et al. (1994); 13) Herrstrom et al. (1995); 14) Morris (1996); 15) Shimaoka (1999); 16) Ryan (unpubl.); 17) Edwards (unpubl.); 18) George et al. (submitted); 19) Valette-Silver (unpubl.); 20) Shimaoka (in press); 21) Morris et al. (2002); 22) Valentine and Morris (submitted a) 23) Hickey-Vargas et al. (in press); 24) Morris and Tera (2000); 25) Morris (unpubl.); 26) Valentine and Morris (submitted b)

subduction trenches have [10]Be inventories comparable to, or greater than that which is predicted by a model of globally uniform [10]Be production and deposition. In these margins, with moderate-fast convergence rates, these inventories would be high enough to produce [10]Be enrichments in arc lavas if the uppermost part of the sediment column were subducted to the depths of magma generation.

The previous discussion suggests that sediment dynamics is the likeliest explanation for an absence of [10]Be in these arcs. In Honshu, Table 1 shows that less than 1.7% of the subducting [10]Be is erupted in the arc, after correction for [10]Be decay during subduction. A small amount of frontal accretion (Morris et al. 2002) and large amounts of subduction erosion of the Cretaceous accretionary prism (von Huene et al. 1994) would minimize any [10]Be enrichment in the arc. The very low but not zero values for [10]Be in Costa Rican lavas have been attributed to the basal underplating of most, but not all, of the hemi-pelagic sediment section (Valentine et al. 1997; Morris et al. 2002; Valentine and Morris, submitted a,b), perhaps related to the style of graben development on the downgoing plate (Kelly and Driscoll 1998). Subduction erosion and dilution of the incoming [10]Be with old, barren forearc sediment could also explain the low [10]Be in Costa Rica (Vannuchi et al. 2001). Large accretionary prisms outboard of Indonesia, Kamchatka and Halmahera (Von Huene and Scholl 1991; Moore and Silver 1983) suggest that low values in these margins reflect frontal accretion. The absence of [10]Be in Columbian volcanoes still needs an explanation, as this is a non-accretionary margin with a convergence rate fast enough to get [10]Be down and back to the surface. If re-measured with very low detection limits, the Columbia lavas might have just a little [10]Be, rather than being totally barren. Except in cases where the [10]Be inventory in subducting sediments is low (e.g., Marianas) the difference between very low and zero [10]Be concentrations in the arc lavas will not generally change the foregoing interpretations. The differences could, however, allow calculated volumes of sediment accretion and erosion to be better constrained.

[10]Be-rich arcs   Real [10]Be enrichments (See Table 2 and Fig. 6) are seen in a number of volcanic arcs, including the Aleutians, Middle America, Scotia, Kuriles, Izu, Marianas, Bismarck, and Tonga (see references in Table 2). All these margins have convergence rates in excess of 4-7 cm yr^{-1} and are classified as non-accretionary margins (Von Huene and Scholl 1991). U series excesses in these arcs (George et al., submitted; Reagan et al 1994; Elliott et al. 1997; Turner et al. 1997, 2000; Gill et al. 1993; Gill, pers. comm.; Elliott, pers. comm.) indicate that magma ascent times are less than 300 kyr, short with respect to the [10]Be half-life. The lower part of Table 1 shows the results of [10]Be flux modeling. The [10]Be flux out/flux in calculates the amount of [10]Be erupting from the volcanic arc relative to the amount subducted to the depths of magma generation after decay in transit has been taken into account. For the Aleutians, the Guatemala-Nicaragua segment and the Mariana arc, the calculations suggest that 10 to 30% of the subducted [10]Be is recycled in the arc (Zheng et al. 1994; Valentine et al. 1997; Morris et al. 2002; George et al., submitted; Valentine and Morris, submitted a,b).

The fraction of the subducted [10]Be flux returned to the surface in arc volcanism will be a function of the portion of the sediment column subducted to depth, and the efficiency with which Be is extracted from the subducted sediment and fed to the arc ([10]Be recycling efficiency). The estimate of 10-30% [10]Be return flux can be met by 100% sediment subduction and 10-30% [10]Be recycling efficiency; lesser amounts of sediment subduction require greater [10]Be recycling efficiency. A [10]Be recycling efficiency of ~30% is at the high end of the range estimated by arc geochemists (e.g., Plank and Langmuir 1993; 1998). Coupled isotopic variations seen in some arcs (e.g., Reagan et al. 1994) together with the high [10]Be return flux are best satisfied by subduction of >95% of the incoming sediment column at the Aleutian, Mariana and middle Central America arcs.

^{10}Be enrichment in Tonga and the Marianas, where only the top 15-25 m of the incoming sediments are young enough to contain ^{10}Be, requires that virtually the entire section be subducted. Even in the absence of ^{10}Be data for the incoming sediment column, general estimates of this sort can be made about the volumes of subducting sediments.

The results in Tables 1 and 2 and Figure 6 show the highly heterogeneous nature of contemporary sediment subduction. For example, Mexico has no ^{10}Be enrichment in arc lavas, Nicaragua has the highest values yet measured in any arc, and Costa Rica has low but real enrichments of ~1 million atoms g^{-1}. These observations can be explained by >50% sediment accretion off Mexico (Tera et al 1986), complete sediment subduction beneath Guatemala, El Salvador and Nicaragua (Reagan et al. 1994) and no frontal accretion but ca 30% underplating of the incoming section beneath Costa Rica (Morris et al. 2002; Valentine and Morris, submitted a). Kamchatka has no ^{10}Be enrichment, while the adjacent Kurile arc has high ^{10}Be that requires nearly complete subduction of the incoming sediment column. These variations along strike within an arc system point to the complexity of processes that control sediment subduction and accretion, poorly understood at present. They also show that it can be difficult to arrive at a single value for the percentage of sediments (or volume of sediments) recycled within a given arc. That being the case, any global estimate of the amount of sediment subducted annually, a necessary value for models of continental growth through time, will have very large uncertainties.

^{10}Be and magmatic processes

Entering the mantle wedge only from the sedimentary veneer of the downgoing plate, and carrying a clock as its travels through the wedge, ^{10}Be provides some unique constraints on magmatic processes. This section first examines the cross-arc distribution of ^{10}Be in the Kurile, Bismarck and Aleutian arcs, with implications for hydrous mineralogy of the slab and mantle and for mantle melting processes. The following section reviews combined studies of ^{10}Be and U-series isotopes, and the time-scales for subduction modification of the mantle.

^{10}Be in crosarc transects Many convergent margins have volcanoes located behind the main volcanic front, derived from melting of a mantle that was modified above a deeper subduction zone. As such, these rear-arc volcanoes can provide insight into the changing composition of the subduction component between ca. 110-km depth and 200-km depth, with implied constraints on slab surface temperature, mineralogy and the medium (e.g., aqueous supercritical fluid or siliceous melt) that transfers elements from slab to mantle. Rear-arc volcanoes also provide a 'last glimpse'' of the slab before it heads into the deeper mantle, and give some clues as to the composition of the deeply subducted slab.

A number of studies have built upon the initial work on potassium concentration vs. depth (K-h) relationships (Dickinson 1975), examining the changing chemistry of arc lavas with increasing depth to the slab. Several recent studies (e.g., Ryan et al. 1995, 1996; Bebout et al. 1999) have examined the concentration variation of elements such as B, ^{9}Be, Rb, Cs, K, Ba, As, and Sb in cross-arc volcano suites and also in the prograde metamorphic rocks of subduction assemblages. These studies show that the absolute concentrations of elements such as B and Sb are lower in the rear-arc than at the front. This gradient is striking because the generally lower degrees of mantle melting in the rear arc would produce higher concentrations of incompatible elements in rear-arc lavas, if the mantle source composition were the same across the arc. The rear-arc lavas formed above a slab some 180-200-km deep in the Kurile arc have no distinctive subduction enrichment in elements thought to be particularly soluble in hydrous fluids (fluid mobile) such as B, Cs, Rb, and Sb. This is in contrast to lavas from the volcanic front, where high B content

and high B/Be ratios are observed and are correlated with high ^{10}Be/^{9}Be (Morris et al. 1990). These results strongly suggest that the most fluid mobile elements are extracted from the downgoing slab beneath the fore-arc and volcanic front, with little, if any, mobile elements remaining in the slab to feed the rear-most part of the volcanic arc. This picture of progressive distillation of fluid mobile elements from the slab as it subducts is also borne out by B and Li isotopic studies (Ishikawa and Nakamura 1994; Ishikawa and Tera 1997; Nakamura and Moriguti 1998).

^{10}Be follows a different path through the subduction zone, and tells a different story. Figure 7 shows the cross-arc variations in ^{10}Be in the Kurile volcanic arc (Tera et al. 1993; Morris and Tera 2000). ^{10}Be and ^{9}Be concentrations were measured in lavas from five volcanic cross-chains (i.e., paired volcanoes above a slab of increasing depth along approximately the same perpendicular line from the trench). In three of the five cases shown, the rear-arc volcano has ^{10}Be and ^{10}Be/^{9}Be ratios that are comparable, to or higher than, the associated volcanic front locality. The ^{10}Be clock begins keeping time when the sediment column passes beneath the accretionary prism; higher ^{10}Be concentrations in the rear-arc are striking, because the path length from trench to volcano must be longer to the rear arc than to the volcanic front. These high rear-arc ^{10}Be concentrations thus require either a faster transport rate to the rear-arc (i.e., less ^{10}Be decay in transit) or larger sediment Be contribution to the lavas in the rear-arc. The Umnak-Bogoslof cross arc pair in the Aleutians also show ^{10}Be/^{9}Be ratios in the rear arc comparable to the volcanic front, and rear-arc lavas in the Bismarck arc have more ^{10}Be than predicted by assuming constant sediment contribution across the arc (Morris and Tera 1989; Gill et al. 1993). High ^{10}Be concentrations in rear-arc lavas thus appears to be fairly commonplace, rather than an anomalous feature of just one arc.
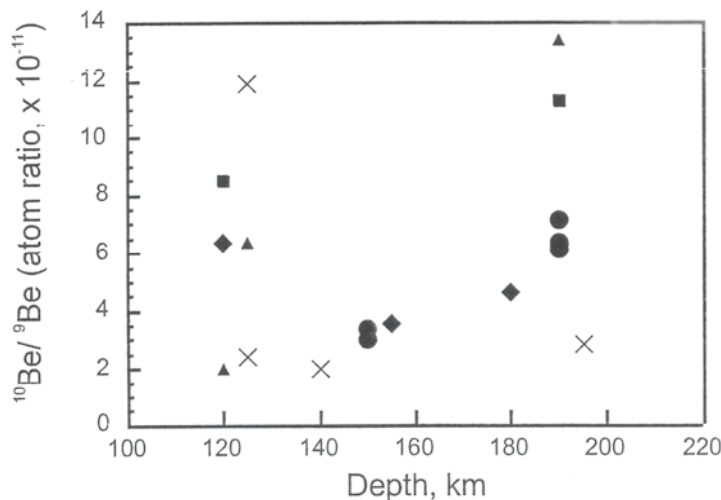
Figure 7. Plot of ^{10}Be/^{9}Be ratios vs. depth for Kurile cross-arc volcanic pairs. Data from Tera et al. (1993). ● = data from Para-mushir and Alaid (50.5-50.8° N latitude). ♦ = Onekotan-Sea-mount 2.3 (49.4-49.7° N). ■ = Aekarma-Chirinkotan (48.9° -49° N). Solid triangles = Lovush-ki-Raikoke (48.1-48.4° N) and **X** = Lvinaya-Seamount 8.8 (44.6-45° N). Noteworthy is that rear-arc volcanoes Alaid, Chirinkotan and Raikoke have measured ^{10}Be/^{9}Be ratios and ^{10}Be concen-trations that are higher than the associated volcanoes at the front, despite longer subduction paths to rear-arc localities.

It is unlikely that the presence of high ^{10}Be in the rear-arc is due to faster transport rates through the mantle. It is conceivable that ^{10}Be transport from the slab to the volcanic front could be slower, if the upward fluid/melt transport were opposing the downward convection of mantle wedge that was approximately coincident with the volcanic front. However, as noted previously, lavas from the Kurile, Bismarck, and Aleutian volcanic front are all characterized by U excesses, suggesting that the transport of slab-derived elements through the mantle to the surface was <300 kyr, a time short relative to the ^{10}Be half-life.

The alternative is that a larger proportion of the Be in the rear-arc mantle is derived

from the ^{10}Be-rich sedimentary veneer of the slab. Several scenarios could satisfy this observation. The first is where a single subduction component is derived from the slab up-dip of the volcanic front and its addition to the mantle creates amphibole and phlogopite (e.g., Davies and Stevenson 1992; Tatsumi and Eggins 1997). Dehydration of mantle amphibole beneath the volcanic front and of mantle phlogopite at ca. 180 km depth would produce 2 volcanic chains, both with ^{10}Be. In the Kuriles, however, volcanoes occur over a slab with a variety of depths (e.g., 120, 130, 140, 150, 160, 180 ad 190 km above the slab), and all lavas erupting over a slab <180-km deep contain ^{10}Be. Neither the distribution of volcanoes nor the presence of ^{10}Be in volcanoes across the entire width of the arc are consistent with this model, where dehydration of just two minerals in the mantle control the slab contribution to arc lavas. In some models, contribution from two separate slab components, a fluid from the altered basaltic crust and a hydrous melt from the subducting sedimentary veneer, is invoked to explain the enrichment in elements such as Th and Ce beneath the volcanic front (e.g., Elliott et al. 1997; Johnson and Plank 1999, Class et al. 2000). In this case, it is difficult to explain the observed correlations in lavas at the volcanic front between elements such as B and U (thought to be fluid mobile) and ^{10}Be, thought to be only sparsely fluid mobile but incompatible during sediment melting. In S. Chilean lavas, strongly correlated enrichments in ^{10}Be, B, U excess and Ra excess (Sigmarsson et al. 1990, 2002) suggest that a single subduction component capable of mobilizing all four elements was involved. If sediment melting beneath the volcanic front is invoked, high ^{10}Be in rear-arc lavas requires that enough ^{10}Be and water be retained in the sediment to allow sediment melting as the slab continues to descend.

Morris and Tera (2000) considered an alternative explanation to be more likely. One possibility is that there is continuous distillation of elements out of the slab as it continues to subduct to higher pressures and temperatures. With increasing pressure and temperature, mineral solubilities in the aqueous supercritical fluid increase and the ability of the fluid to transport a wider spectrum of elements increase (e.g., Ryan et al. 1995). A more specific version of this scenario is where the subduction component beneath the volcanic front is a fluid enriched in mobile elements such as B, Cs, U and only sparsely enriched in ^{10}Be. At greater depths slab surface temperatures are hot enough to allow the sediments to melt, leading to a sediment component that is demonstrably enriched in ^{10}Be, as well as Ba, K, and Th (Ryan et al. 1995). Note that if the latter scenario is correct, it implies that the slab is too cool to allow sediment melting beneath the Kurile, Bismarck or Aleutian volcanic front, but is hot enough by ca. 135 km depth to allow sediment melting.

^{10}Be and U-Series studies. ^{10}Be data can be combined with U-series studies to better investigate the timescales and mechanisms of element transfer from the slab to the mantle. If U but not Th were transferred from the slab to the sub-arc mantle in a single event, then U-series disequilibria isotope characteristics of arc lavas may represent the time since subduction modification of the mantle. Alternative possibilities are that hydrous mantle melting could fractionate U from Th in such a way as to create the U excess, that the excess could result from dynamic melting in the mantle (Spiegelman and Elliott 1993), or that the very young ages seen for some arcs could result from crustal level processes. Because the U-series "ages" have major im plications for geodynamics of the mantle wedge and melt generation/migration (e.g., Gill et al. 1993; Herrstrom et al. 1995; Turner et al. 1997, 2000; Bourdon et al. 1999), its critical to know how they originate.

Combined ^{10}Be and U-series data have been published for lavas from the S. Chile (Sigmarsson et al. 1990, 2002), Bismarck (Gill et al. 1993), Costa Rica (Herrstrom et al.

1995), Nicaragua (Reagan et al. 1994) and Aleutian (George et al. 2000) arc segments. Similar studies are underway for the Tonga (Turner et al. 1997, 2000), Scotia (Leat et al. 2000, Elliott, pers. comm.), Kurile and Kamchatka (J.Gill, pers. comm.), Philippine (Asmerom, pers. comm.) and Mariana (Elliott et al. 1997) arcs. In the case of the Costa Rica, Kamchatka and Mariana arc segments, ^{10}Be concentrations are either negligible, or too low to show meaningful variation with respect to either Th isotopic compositions or U/Th ratios. The Kurile data show no coherent variations with ^{10}Be/^{9}Be ratios (Gill, pers. comm.).

Other suites show co-variation between ^{10}Be and U-series isotopes. The Nicaragua and Bismarck arcs form trends with ca. 90- and 200-ka "ages," respectively (Reagan et al. 1994; Gill et al. 1993). ^{10}Be/^{9}Be ratios of the lavas increase systematically, by a factor of four, as the Th activity ratio and U excess increase. The Aleutian data set (George et al., submitted) define a nearly horizontal array on a U-Th disequilibrium diagram equivalent to an age of <30 ka; there is a general tendency for the highest ^{10}Be concentrations to be in lavas from the oceanic segment with the greater U excesses, but the two data sets are not highly correlated. Tonga lavas form a U-series slope of approximately 60 ka (Turner et al. 1997); there is again a general tendency for highest ^{10}Be/^{9}Be ratios to be seen in lavas with greater U excess, but the data sets are again not highly correlated. The S. Chile data also have a (^{238}U)-(^{230}Th) disequilibrium "age" of <30 ka; the magnitude of the U excess is very well correlated with (^{226}Ra)-(^{230}Th) excess, a characteristic which will decay away within 8 kyr. Both have strong positive correlations with ^{10}Be/^{9}Be ratios and ^{10}Be concentrations (Sigmarsson et al. 1990, 2002).

The results from southern Chile and Nicaragua are particularly striking. The very good correlations with ^{10}Be strongly suggest that the excess U and Ra in southern Chile are a subduction signature rather than a result of dynamic or hydrous melting or crustal contamination. The evidence for correlated transfer from slab to mantle of U, Ra and Be, but not Th, is consistent with a single aqueous fluid derived from the slab rather than a sediment melt or both a melt and a fluid. The straightforward interpretation of the data is that fluid addition and mantle melting occurred within the last 8,000 years (Sigmarsson et al. 2002). If so, several geodynamic consequences follow: (1) fluid fluxing triggered immediate melting of the mantle; (2) fast melt migration pathways were required, likely being channelized through the asthenosphere (rather than via porous flow) (Turner et al 2000) and through fractures in the lithosphere; and (3) the residence time in magma chambers was negligible. An alternative scenario to consider would be one in which the extremely young 8-ka "age" is an artifact. In this case, the processes of extracting a component from the slab, mixing it with the mantle, possible storage and subsequent melting plus magma time in transit to the surface would need to produce strong correlations between elements of different partitioning behaviors and half-lives.

For Nicaragua, ^{10}Be/^{9}Be ratios correlate better with Th isotopic composition than with U excess (Reagan et al.1994). The Nicaragua data set suggests that ^{10}Be, Ba, B, U and Th were added from the slab sometime in the last several million years, possibly in a sediment melt. Another addition of U, perhaps in a fluid, was required sometime in the last several hundred kyr (Reagan et al. 1994).

Where both U and Th may have been added from the slab, the disequilibria systematics cannot be interpreted as a simple age, but with ^{10}Be studies or other geochemical data (e.g., Elliott et al. 1997) the systematics can reveal several episodes of subduction modification of the mantle and provide general timing constraints. The general tendency for high ^{10}Be to go along with greater U excesses does suggest that the U-series characteristics derive from the subducting slab. For arcs with high ^{10}Be, there is often an order of magnitude variation in ^{10}Be/^{9}Be ratios and ^{10}Be concentrations observed

for lavas from a specific arc or arc segment (Table 2 and references therein). For lavas derived by similar degrees of partial melting (e.g., the Aleutians, George et al., submitted), the ^{10}Be concentration range requires varying amounts of sediment addition to the mantle, rather than an approximately constant subduction flux to a variably depleted mantle.

The question of whether or not sediments melt beneath the volcanic arc is extensively debated. The argument hinges around detailed discussion of how elements such as Th, Ce, Be, Ba, and U behave in melts vs. fluids, but the outcome has broad implications for the thermal structure of the downgoing plate. In some arcs, Th addition is interpreted as the result of sediment melting because of its immobility in fluids (e.g., Brenan et al. 1995); U excess is thought to represent the addition of a fluid from the altered oceanic crust, based on multi-element correlations (e.g., Elliott et al. 1997). In S. Chile, the ^{10}Be from the sediment correlates with the U rather than the Th enrichment, requiring that U plus Be, without Th, be mobilized out of the slab. This could be a fluid from the sediment or one from the basaltic crust that also extracts Be from the overlying sediment column; it is unlikely to be a sediment melt. Where Th isotopic composition and ^{10}Be co-vary as in Nicaragua or the Bismarck arc, the data better fit a scenario of sediment melting. The observations of different signatures in the ^{10}Be-U series systematics and the resulting interpretations may indicate that we don't understand well the partitioning of key elements during interactions between fluid, melt, sediment, altered oceanic crust and mantle. More interesting is the possibility that there are real differences in the thermal structure of different subducting plates, such that some are hot enough beneath the arc (ca. 700° C) to permit sediment melting, while others are not.

Future directions

The new capability to measure ^{10}Be at low concentrations (ca. 0.1 million atoms g^{-1}) with very low blanks (ca. 20,000 atoms g^{-1}) opens the door to a large number of new possibilities. In cases where a tectonic, geodynamic or sediment dynamic model can be evaluated from the sediment signature of the arc lavas, re-measurement of some of the low ^{10}Be arc lavas might be useful. Variations along strike (e.g Nicaragua-Costa Rica) can be better evaluated in terms of variations in sediment dynamics, perhaps related to the abundance and depth of grabens on the downgoing plate (e.g., Kelly and Driscoll 1998). Serpentinites in the Mariana fore-arc, thought to reflect extensive fluxing of the shallow mantle by fluids from the slab, now become amenable to study. Low but real ^{10}Be enrichment in young back-arc lavas not overlying the downgoing slab could be used to map transport through the wedge and constrain timescales thereof. In places such as the Chile Ridge spreading center, trace element systematics suggest flow of subduction modified mantle around the slab to the near-trench part of the Ridge; measurable ^{10}Be in the Ridge lavas would confirm such mantle flow and provide a speedometer for flow rates. ^{10}Be enrichment in MORB or OIB lavas could be used to identify recent sediment assimilation, as opposed to ancient sediment subduction. It is probably also worth visiting the question of whether ^{10}Be could be produced in some minerals via nuclear reactions at levels that are now measurable, and could be used as a geochronometer. The latter possibility highlights the need to be cautious in interpreting very low ^{10}Be concentrations in terms of a subduction signature, given that sample alteration, cosmic ray bombardment and possibly nuclear reactions could produce small ^{10}Be enrichments in any tectonic setting.

TECTONIC APPLICATIONS OF *IN SITU* ^{10}BE

Introduction

In this section we review tectonic geology applications of cosmogenic ^{10}Be produced in rock (see Gosse and Phillips 2001, and Bierman et al., this volume, for recent reviews

of other applications of *in situ* [10]Be to surface processes). The contributions of atmospheric [10]Be to understanding subduction zone tectonics have been discussed in the previous section. The *in situ* [10]Be method provides both chronological and denudation information—from landform to orogen spatial s cales over relatively short (generally <1 Myr) timescales. In this context, *in situ* [10]Be complements other dating methods used in Cenozoic tectonics studies, and provides the niche-filling record of rock uplift (as interpreted from stream incision histories, for example) between the timescales of modern GPS geodetics and studies of long term (>4 Myr) orogen-scale exhumation histories using thermochronology (e.g., Ar/Ar, (U-Th)/He, and fission track analyses). Over the past 15 years, the number of tectonic geology applications of the method (Fig. 8) has expanded geometrically.
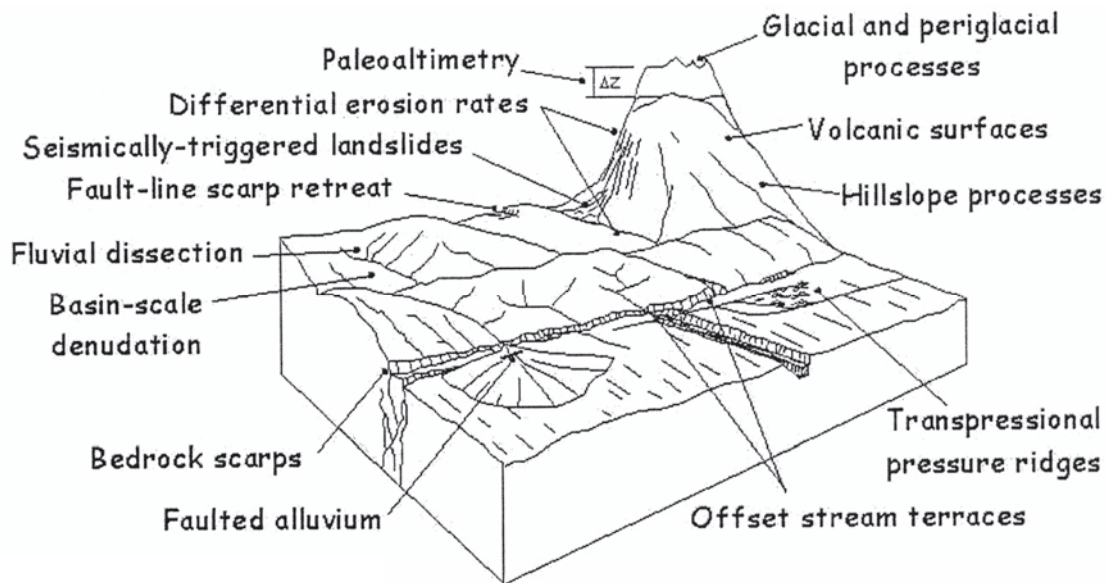
Figure 8. Published and potential applications of *in situ* cosmogenic [10]Be for studying tectonic geology.

For this review, we group the tectonic applications of *in situ* [10]Be under three general 'approaches': (i) those using [10]Be to bracket or directly date the age of a tectonic event such as a seismogenic landslide, fault slip, or volcanic eruption; (ii) those using [10]Be to constrain the incision rate of streams or denudation of entire catchments in tectonically active regions; and (iii) paleoaltimetry. Approach (i) has provided precise estimates of the timing of paleoseismic and volcanic events, their recurrence intervals, and slip rates. The chronology of offset alluvial fan surfaces can assist in showing trends in slip activity and provide timing constraints on fault slip needed for strain partitioning studies. Cosmogenic [10]Be exposure ages have also been used in geological hazard assessments (Gosse et al. 1996; Taylor et al. 1998) to determine the ages of lava and fault motion near Yucca Mountain, Nevada, the proposed U.S. high-level nuclear waste repository. Recognizing that incision and denudation rates calculated with Approach (ii) do not directly provide tectonic uplift rates, the approach provides meaningful data that can be used to understand the rates of orogen evolution in response to rock uplift. Ideally, incision rates are calculated by dating stream straths (erosional surface representing the bedrock floor of ancient streams, cf. Pazzaglia and Brandon 2001) so that the rate of incision into bedrock (not just the alluvial fill) above the modern stream is measured. Likewise, denudation experiments measure the mass flux through an entire drainage, and [10]Be in modern stream sediment has been used to calculate basin-scale denudation rates and relate those rates to rock uplift. Denudation studies provide short-term ($\sim10^4$ yr) accounts

of sediment fluxes and variations in their spatial distributions, which can provide useful information for testing questions of steady state erosion and topographic equilibrium. Incision and denudation rate data can be used in geodynamic studies to evaluate rates and styles of surficial processes at orogen-scales. The use of cosmogenic nuclides in paleoaltimetry (Approach iii) has not yet been accomplished (Gosse and Stone 2001). We outline a basic strategy for this approach, and point out the steps being taken to launch the method.

Exposure chronology of tectonic events

This special volume is dedicated to applications of Be. For this reason we are not reviewing applications of other cosmogenic isotopes, which in some cases may be more useful for dating tectonic events (e.g., in cases where quartz is absent). The principles of interpreting concentrations of ^{10}Be as exposure ages have been discussed earlier in this paper. Applications of *in situ* ^{10}Be to address questions related to tectonic histories are numerous. Chronologies of alluvial fan surfaces have been used to decipher Quaternary paleoseismicity and slip rates (Bierman et al. 1995; Brown et al. 1998a; Granger et al. 1996; Nishiizumi et al. 1993; Siame et al. 1997; Van der Woerd et al. 1998, 2002). To date basaltic lava, ^{10}Be production rates of whole rock samples and olivine have been estimated using nuclear cross sections and comparisons with quartz (Gosse et al. 1996; Nishiizumi et al. 1990). The exposure history of a bedrock surface has mapped the progressive retreat of an early- to mid-Pleistocene fault line scarp to provide an estimate of the timing of the last movement along a fault with low recurrence interval where topographic evidence has been eroded (Taylor et al. 1998). Deformed alluvium has been dated to constrain rates and timing of recent transpression between topographically elusive strike slip segments (Spies et al. 2000; Spies et al. submitted) and above a blind reverse fault (Jackson et al. 2002). By dating raised beaches in the central Arctic, the method has recently been shown to yield emergence curves (Gosse et al. 1998) similar to those based on radiocarbon-dated driftwood. The potential to provide emergence histories for raised shorelines that have been otherwise undatable has global implications for improving boundary conditions for mantle rheology and lithospheric flexure models as well as ice sheet dynamics.

Volcanic surfaces The most direct application of *in situ* cosmogenic ^{10}Be in tectonics is to interpret its concentration in a manner to provide chronological control on tectonic landforms. In this regard, ^{10}Be and other isotopes have been used to determine the age of Quaternary lava flow surfaces and cinder cones. The ^{10}Be method has primarily been restricted to quartz-bearing lithologies. However, the production systematics of ^{10}Be in olivine are similar to those in quartz. Although the mineral chemistries differ, ^{10}Be in both is produced mainly through spallogenic interactions on oxygen, plus smaller contributions from the other elements. Olivine-bearing lavas on Maui were dated (Nishiizumi et al. 1990) by summing production rates based on nuclear cross section estimates for fast neutrons on the four target elements. Recognizing the need for highly precise production rates in olivine, Kong et al. (1999) have begun measuring the production rate of ^{10}Be in basaltic olivines over a narrow Fe/Mg range. Unlike ^{36}Cl, empirically derived production rates of ^{10}Be in whole rock samples have not been determined. In an attempt to date a basalt lava flow surface of Black Cone, in southwestern Nevada, Gosse et al. (1996) with J. Klein of the University of Pennsylvania used a 'whole rock' procedure, necessary because of the absence of olivine phenocrysts. More than 35% of the original sample mass was leached before complete dissolution to remove atmospheric ^{10}Be. Diagnostic textures on the surface of the lava flow suggested that erosion may have been negligible. The lava surface exposure age was 0.88±0.22 Ma (error reflects uncertainty in production rate in addition to analytical errors; production rate calculation according to Nishiizumi et al. 1990) on lava that had been dated at

1.0 ± 0.1 Ma with $^{40}Ar/^{39}Ar$ methods by others (Taylor et al. 1998). The ^{10}Be analysis of about 20 step-leached aliquots from whole rock samples showed that whole rock samples could lose their atmospheric ^{10}Be after 35% leaching. Unfortunately, some samples apparently retained the atmospheric signal even after 90% of the rock was removed by chemical leaching (Klein et al. 1997). In those cases the *in situ* ^{10}Be component could not be isolated and no other whole rock *in situ* ^{10}Be experiments have since been published. Far more exposure chronologies of lavas are derived from cosmogenic ^{36}Cl and ^{3}He (Cerling et al. 1999; Fenton et al. 2001; Kurz et al. 1990; Liccardi et al. 1999; Marti and Craig 1987; Phillips et al. 1996; Sheppard et al. 1995; Zreda et al. 1993) because their production rate systematics in basalts are better established.

Bedrock fault scarps   Exposed bedrock fault scarps afford the opportunity to date the most recent offset and yield information on the timing of multiple rupture events and recurrence frequency. Scarps produced from even high magnitude pure dip slip displacements rarely exceed a few meters height. In the simplest case of a single rupture event, the ^{10}Be concentration measured on the scarp face will record ^{10}Be produced in the subsurface rock prior to faulting, plus the ^{10}Be produced on the exposed scarp since faulting. The pre-faulting concentration can be determined by measuring subsurface profiles in the hanging wall or footwall. In the cases of multiple events on the same scarp, vertical profiles can be sampled along exposed scarp segments and exposure age clusters can be grouped into isochronal zones (Zreda and Noller 1998). The highest exposure zone should appear to be the most weathered and will have the oldest exposure ages. The duration of exposure in each zone provides a means to estimate the recurrence frequency and trends of pre-historic earthquake events. A scarp along the Solitario Canyon fault, a major block bounding fault in the basin and range province of Nevada, was dated by Harrington, Whitney, and Jull (unpubl.) in 1993 using cosmogenic ^{14}C in quartz. They demonstrated that the surface was a pre-Holocene scarp that had been subsequently exhumed (a fault-line scarp). However, due to difficulties in constraining the erosion rates and the component of the measured ^{14}C that was produced when the scarp surface was still underground, no additional paleoseismic information could be extracted. In a subsequent study, Zreda and Noller (1998) sampled spatially separate scarp segments that were interpreted to have been produced during recurrent displacements along the Hebgen Lake fault in Montana. After adjusting for subsurface production prior to rupture, the height vs. age distributions showed a pattern that led them to recognize at least 6 events over a 24 kyr period, with an increasing recurrence frequency.

Fault displacement in unconsolidated sediment   . Direct measurements of ^{10}Be on faults scarps in unconsolidated sediments (alluvial fans, terraces, moraines) has not been attempted because fault scarps are disequilibrium features that are susceptible to high rates of erosion, and are therefore not stable surfaces. Instead, it is possible to bracket the timing of single or multiple slip events by exposure dating surfaces of two or more alluvial fans, moraines, or beaches that were deposited before and after the strain event. The success of alluvium chronologies by Bierman et al. (1995), Brown et al. (1998a), Siame et al. (1997), Van der Woerd et al. (1998, 2002), Zehfuss et al. (2001), and Spies et al. (submitted) attest to the plausibility of surface clast exposure dating of offset alluvial surfaces. Slip rate analyses require highly precise chronologies and a means of distinguishing single event from multiple event histories. In alluvium, both of these quantities are difficult to obtain due to post-offset degradation of the surface.

Two instructive examples of ^{10}Be measured in clasts on the surface of alluvium to constrain slip rates in the Tibet region were published by Brown et al. (1998a) and Van der Woerd et al. (1998). The strategy employed was to determine the ages of fan and terrace surfaces (respectively) to bracket the timing of displacement. Brown et al.

calculated a fault slip rate of 2 mm a^{-1} based on measured heights of faults scarps on three late Pleistocene alluvial fans. In addition to the tectonic implications for shortening across the Tien Shan, they demonstrated that the amount of ^{10}Be inherited from exposure prior to deposition on the alluvial fan was low (corresponding to 2 kyr of exposure, based on modern wash cobbles). Similarly, Van der Woerd et al. established post-glacial slip rates on the Kunlun fault in northeastern Tibet, even from remarkably young (late Holocene) surfaces of fans and moraines (ranging from ca 1.5 to 600 ka). Using combinations of radiocarbon and *in situ* isotopes, they calculated that the slip rates over different periods throughout this duration have been remarkably similar (average 11.5±2 mm a^{-1} over the past 600 kyr). In North America, over 30 ^{26}Al and ^{10}Be exposure ages on large surface boulders in glacial debris flows on fans in Owens Valley were used to calculate a 0.24±0.04 mm a^{-1} slip rate over the past 300 kyr, consistent with rates determined previously (Zehfuss et al. 2001).

Despite these successes, an obstacle to exposure dating of unconsolidated sediment often results from not knowing the amount of ^{10}Be inherited from exposure of the clast at its source locality or during transportation, prior to its final deposition. This inherited component will result in calculated exposure ages that are older than the actual surface being dated (e.g., Trull et al. 1995). There are several ways to isolate and adjust for an inherited nuclide component. Active stream sediment (or sediment in active washes cut through alluvial fans) are too young to acquire measurable ^{10}Be concentrations since deposition, but can have a concentration that reflects ^{10}Be inherited from pre-depositional exposure in the catchment, prior to reworking of older fans, and during transport. The inherited concentration (N_{inh}) measured in the modern sediment can be subtracted from concentrations on older surfaces of fans sourced from the same catchment (Brown et al. 1998a; Spies et al., submitted). However, it is difficult to prove that the amount of inheritance in modern alluvium is the same as the inheritance in sediment deposited previously under different climate and geomophological conditions. A second means of determining the inheritance in single thick alluvial units is by the 'depth-profiling' technique (Anderson et al. 1996; Ayarbe et al. 1998; Repka et al. 1997; Hancock et al. 1999). The premise is that the production of cosmogenic nuclides should decrease exponentially with depth (Eqn. 3). In alluvium with a bulk density of 2 g cm^{-3}, the concentration at 4 m depth is less than 0.5% that at the surface. Assuming that the N_{inh} is constant throughout the aggradational unit, a high concentration at depths greater than 4 m corresponds to the amount of inherited ^{10}Be. The geometry of the concentration vs. depth profile can be modeled to precisely calculate the probable inherited component. In simple cases, a shielded sample at the base of a thick unit could be used to indicate the average inheritance of ^{10}Be in the sediment. However, more is gained from the profile method because the geometry of the concentration vs. depth profile provides information on erosion and burial history of the sediment. The necessity and advantages of using cosmogenic nuclide concentration-depth profiles are described in a number of recent studies (Anderson et al. 1996; Ayarbe et al. 1998; Repka et al. 1997; Hancock et al. 1999).

Some effort has been made to optimize the dating of alluvium. Anderson et al. (1996) proposed a means to minimize the scatter in sample concentrations from the same alluvial landform. Their sampling approach, now widely used (Gosse and Phillips 2001), is to amalgamate a minimum of 40 pebbles of equal quartz mass for surface or subsurface samples. The variance among the inherited concentrations in the amalgamated samples will be smaller than if single cobbles or boulders are sampled. Zentmire et al. (1999) showed that alluvium from once glaciated catchments may not have significant inheritance due to the rejuvenation of the surface by glacial erosion and to glacial shielding of the surface from cosmic radiation. The ^{10}Be concentrations in modern

outwash clasts from the Matanuska Glacier were consistent with the chemical blank, indicating negligible inheritance from previous exposure prior to deposition (Zentmire et al. 1999). Gosse and McDonald (submitted) measured [10]Be concentrations of amalgamated surface samples from two alluvial fans from adjacent tributaries in Fish Lake valley. The catchment of one fan was glaciated during the last glaciation, the other fan had little or no glacial influence. The fan ages were bracketed with radiocarbon (Reheis and Sawyer 1997) and fall around the Pleistocene-Holocene transition. The [10]Be concentrations in samples from the fan with a large glacial influence in its catchment showed a smaller variance and mean age closer to the accepted radiocarbon chronology than the samples from the fan with little or no glacial influence. These observations, together with the lack of significant inheritance in published measurements on alluvium from glaciated catchments (e.g., Bierman et al. 1995; Brown et al. 1998b; Van der Woerd et al. 1998), show that while depth profiles may be necessary in arid regions with non-glaciated catchments, alluvial surfaces from glaciated catchments may not have large inherited concentrations.

Cosmogenic nuclides have also been used to establish the ages of faulting events and of colluvial wedges on the hanging wall of normal faults. The colluvial wedges form as a result of mass wasting off a fault scarp onto the down-dropped block. One of the best examples used [36]Cl (arguably [10]Be would have yielded similar results) to determine the age of colluvial wedges and the timing of recurrent ruptures of alluvium by the Socorro fault scarp, New Mexico (Ayarbe et al. 1998). Depth profiles of [36]Cl concentrations in agglomerate samples (150 pea-sized pebbles) showed rupture trends that are supported by pedological and geomorphological observations along a vertical section through the alluvium cut perpendicular to the fault plane. On the undisturbed footwall alluvium, subsurface concentrations of *in situ* [36]Cl define a depth profile consistent with the depositional age of the alluvium. However, the subsurface samples in the hanging wall section, including within colluvial wedges, show a complicated geometry indicative of more recent sedimentation. Ayarbe et al. (1998) argued that the hanging wall data pointed to a history of erosion of the alluvium fault scarp in a manner consistent with that predicted by simple diffusion modeling, although more data are needed to establish the fault history.

Spies et al. (submitted) have used a combination of detailed soils analyses (including profile development indices), geomorphometry, and cosmogenic nuclides to determine the rupture history of the Carrara Fault, near Yucca Mountain, in the Walker Lane, Nevada (Slemmons 1997; Stamatakos et al. 1997). Transpression along the fault system has produced a ridge of Pleistocene alluvium that has subsequently been cut by combinations of dip-slip and dextral strike slip motions on fault segments. On the southeast end of the feature, drainage density and topography express more active faulting where the ridge is cut by oblique faults that seem to displace Holocene soils. The concentrations of [10]Be in three amalgamated surface samples on the north end are higher (more than 1σ) than the concentrations on the southeast end of the same alluvial unit. Interpreting the concentrations as exposure ages (Fig. 9), the ages fall within the range of soil age determined by profile development indices. Spies et al. attribute the differences in concentration to an increase in erosion associated with the active faulting (roughly 18 cm more erosion would have occurred on the southeast end relative to the less active north end of the ridge.

Seismicity inferred from area affected by land-sliding.   Empirical datasets have been used to correlate the area containing earthquake-triggered landslides and the magnitude of the historical seismic ground acceleration (McCalpin 1996). A logical next step is to

220 +/- 10
220 +/- 10
230 +/- 10

N

0   km   0.5

195 +/- 10
195 +/- 10
205 +/- 10

graben
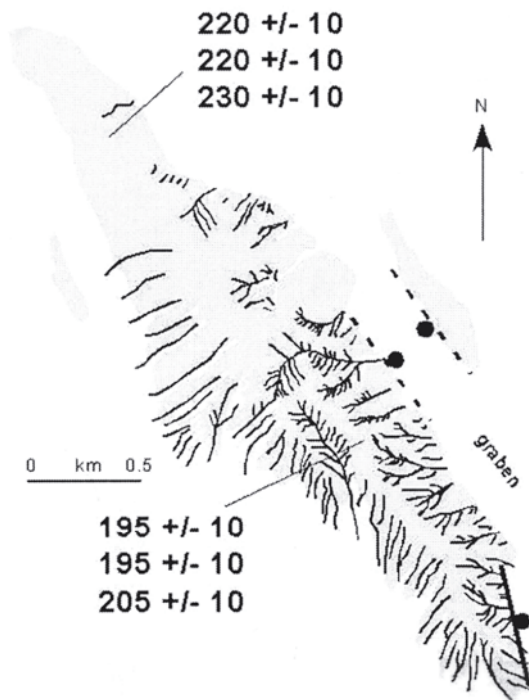
Figure 9. Cosmogenic ^{10}Be exposure ages and stream drainage pattern (to stream order 3) on a transpressional ridge in the Amargosa Valley, Nevada (Spies et al., submitted). Strike slip faults not shown because their position is weakly defined from geophysics. The ridge has an axial drainage divide that averages 16 m above the local valley floor. The ridge has been truncated by oblique slip faults (dashed and solid line) with significant normal slip component (dot represents hanging wall). Uncertainties in age only reflect random error associated with measurement of concentration. ^{10}Be concentration was adjusted for inheritance based on a measurement of modern stream sediment (Spies et al., submitted).

date pre-historic landslides and use the recent empirical datasets to reconstruct paleoseismic history. Measurements of ^{10}Be on the surfaces of boulders on an early Holocene Austrian rock slide yielded internally consistent exposure ages (Kubik et al. 1998) and demonstrated the reliability of the method to date ancient landslides. Hermanns et al. (2001) used ^{21}Ne in quartz in a similar approach, and documented the westward propagation of reverse faulting in the Argentine Puna Plateau. Large >0.3 km^3 landslides were used in all of these studies. In a Colorado Front Range study using smaller landslides, Gosse, Madole, and Klein (unpubl.) found that debris slide boulders can contain inherited concentrations of ^{10}Be that are greater than the concentration produced since the landslide. A difference between the Colorado study and the previous landslide studies is the volume and deformation of the wasted material (e.g., the Austrian and Argentine rock slides were deeper and more pervasively deformed). These results suggest that many measurements may be necessary on debris flows and similar deposits to statistically define inherited samples as outliers.

A related study in western Nevada inferred the minimum time since seismicity of a calculated magnitude occurred (Bell et al. 1998). The local moment paleo-magnitude was estimated by calculating the minimum acceleration required to topple precariously perched boulders in tectonically active areas. ^{36}Cl exposure ages on the boulders were used to estimate the amount of time the boulder may have been perched. Although assumptions regarding the relevance of the exposure ages were made, the data lend support to other paleoseismic inferences based mostly upon trench logs.

Coastal emergence . Paleoshorelines and raised marine terraces dated with *in situ* ^{10}Be can provide constraints to determine (1) the rate of tectonic tilting (Marshall and Anderson 1995) and fault displacement (Perg et al. 2001); (2) the nature of emergence history (constant, exponential, or episodic; Dyke et al. 1991, 1992); differential movement of fault blocks where none was previously recognized (Sissons and Cornish 1982); and (4) physical properties controlling the rheology of the crust, upper mantle, and lower mantle (Peltier 1998).

In a study in progress, Gosse and others collected cobbles and boulders on a

sequence of raised beaches and glacially-plucked bedrock surfaces on an emerging sea cliff face along a Holocene coastline on the east coast of Prince of Wales Island, Central Arctic, Canada (Gosse et al. 1998). Cosmogenic ^{10}Be measurements in boulders were used to show that the distribution of exposure age vs. elevation of shoreline can be fit with a simple exponential curve that is indistinguishable from the regional calibrated radiocarbon-derived sea level curve. The ^{10}Be concentrations were corrected to compensate for the fact that the beaches were not at their present elevation throughout their exposure history (<3%, greatest for the first beaches to emerge due to exponential isostacy). This sensitivity to changes in atmospheric shielding is the basis for the paleoaltimetry approach discussed below. A subtraction of a small component of ^{10}Be produced subaqueously before emergence was also made, which was greatest for the most recent beaches because they spent considerable time in shallow water prior to emergence. In this study these corrections could be based on a published relative sea level curve based on driftwood, but in areas with no radiocarbon chronology, these adjustments will be made iteratively. Measurements of ^{10}Be in cobbles, pebbles, and bedrock cliff surfaces showed more scatter than in the boulders. Geological factors that may have contributed to the scatter in the dates include post-depositional beach sediment movement due to ice push or gelifluction, differential partial shielding due to snow cover, and anthropogenic displacement of quartz clasts. Sensitivity tests for the effects of surface erosion and partial shielding due to snow cover and sea water indicate the combined effects could result in a less than 3% overestimation in exposure age. These results suggest a reasonable reliability of cosmogenic nuclide exposure dating to build emergence curves from Holocene and older emergent shorelines where sufficient high quality radiocarbon datable material is absent. However, the variation about the mean age for a shoreline elevation will be prohibitively large for most tectonic applications unless a sufficient number of samples are dated. The technique will probably be most useful when it is supplemented with radiocarbon dates.

Perg et al. (2001) suggested another approach to dating terraces. In a study to determine the ages of five marine terraces along the active coast of California north of Santa Cruz, ^{10}Be was measured in surface and subsurface amalgamated samples. The exposure ages correspond with Quaternary sea-level high stands, with an implied tectonic uplift rate of 1.1 mm a^{-1} which was higher than previously published rates for the area because the exposure ages were younger than previously estimated. Their approach was used to date sediments that have been bioturbated, but could equally be applicable in areas with other mixing processes (cryoturbation, mass wasting).

Bedrock erosion, stream incision, terrace deformation, and orogen-scale denudation

In the previous section we emphasized uses of ^{10}Be to provide chronometric control on Cenozoic tectonic events. In this section we review applications that interpret the concentration of *in situ* ^{10}Be in terms of an erosion rate, not exposure duration. The recent rejuvenation of interest in landscape modeling may in part be due to the utility of cosmogenic nuclides in providing erosion rate information on scales of outcrops to orogens. In turn, this information can be used to estimate rates of rock uplift and provide surface process information for geodynamic models. Terrestrial cosmogenic nuclides produced *in situ* have really just begun to contribute to orogen-scale investigations. The techniques can provide ages of incised straths (Pazzaglia and Brandon 2001), rates of weathering and erosion on individual bedrock summits and hillslopes, and rates of basin-scale denudation. The availability of a technique that can be used to independently quantify erosion rates on different surfaces is invaluable in areas of spatially variable erosion rates, where isostatic uplift may contribute to net surface uplift of the summits. Cosmogenic ^{10}Be is well suited to such studies because (1) it is radioactive, providing information that stable cosmogenic isotopes cannot, and (2) its half-life is longer than any

other commonly used *in situ* cosmogenic nuclide, so it is useful for averaging over longer time periods. An additional advantage is that a second cosmogenic nuclide, [26]Al, can be measured with [10]Be in virtually all samples containing quartz. In addition to an internal check on the chemical preparation and calculated age, the second nuclide is useful for calculating erosion rates, styles of erosion, and other features of a surface's exposure history.

Determining local bedrock erosion rates with a single isotope. The measurement of [10]Be alone can provide estimates of erosion rates, under certain circumstances. By assuming an erosional equilibrium scenario where erosion is controlling the concentration, and setting exposure duration (*t*) to infinity, erosion rate (ε) can be expressed as (Lal 1991):

$$\varepsilon = \left(\frac{P_{(o)}}{N} - \lambda \right) \mu \qquad (7)$$

where the absorption coefficient $\mu = \Lambda / \rho$. This is useful on surfaces where loss of [10]Be due to erosion is much higher than by decay, or on surfaces known to have been exposed for a long duration. In those cases where it is clear that the concentration has reached erosional steady state, the calculated erosion rate is the average rate. However, even if steady state has not been attained, the single [10]Be measurement will establish the maximum erosion rate permitted by the measured concentration. By making multiple measurements over different surfaces (peaks and depressions) it is possible to calculate the maximum Quaternary erosion rate of a larger area. This approach substantiated geomorphological estimates of the maximum possible erosion rate for Yucca Mountain and surrounding areas (0.3 to 3 mm kyr^{-1}), critical to evaluating the possibility that a high level nuclear waste repository at 200-m depth could be breached within a 100-kyr period (Gosse et al. 1996). A similar approach was used by Burbank et al. (1996) and Leland et al. (1998) to determine maximum erosion rates of strath surfaces in the Himalayas that appeared to be responding more to climate change than to tectonic forces. Notably, the [26]Al/[10]Be ratios they measured plot within the erosional steady state island of a [26]Al/[10]Be vs normalized [10]Be diagram (next section). This indicates that the surfaces probably had simple exposure histories as the authors assumed.

Determining local erosion rates with two cosmogenic nuclides Nishiizumi, Lal, Arnold, Klein, and Middleton first used two isotopes ([26]Al and [10]Be) to determine the exposure history of surfaces of unknown age and unknown erosion rate in the Antarctic Dry Valleys (Nishiizumi et al. 1991; Lal 1991). The strategy is straightforward. A pair of cosmogenic nuclides is measured with at least one being radioactive. The shorter-lived isotope will reach radioactive secular equilibrium before the longer-lived isotope. Therefore the ratio of the two isotopes will decrease over time (upper curve in Fig. 10a). In the case of two radioisotopes, the system reaches a constant ratio when both isotopes are at steady state. If the surface is eroding, the concentration of both isotopes will be proportionally lower because of the decrease in production with depth in the rock. Erosion will cause the radionuclides to reach steady state sooner than in an absence of erosion, and a family of curves describe the ratio of [26]Al/[10]Be for a wide range of gradual and constant erosion rates. The lower curve in Figure 10a connects the ends of these erosion curves. Ignoring uncertainties in the measurement, surfaces with ratios that plot within the area between the two curves have therefore experienced erosion (although in some cases burial of the surface can also explain such ratios). The isotope ratio method can provide estimates of differential bedrock erosion rates by determining multiple local erosion rates over large areas (e.g., Small et al. 1997). The maximum non-glacial erosion rate derived from the cosmogenic [26]Al/[10]Be measurements on bedrock surfaces of flat summit plateaus in eastern Canada, (all older than 25 ka) is 0.7 cm kyr^{-1}, but the

Quaternary long-term average erosion rate is probably less than 0.2 cm kyr^{-1} (Gosse et al. 1995c).

Despite the desire for and implications of this application of *in situ* TCN, very few studies successfully use the method for a number of reasons:
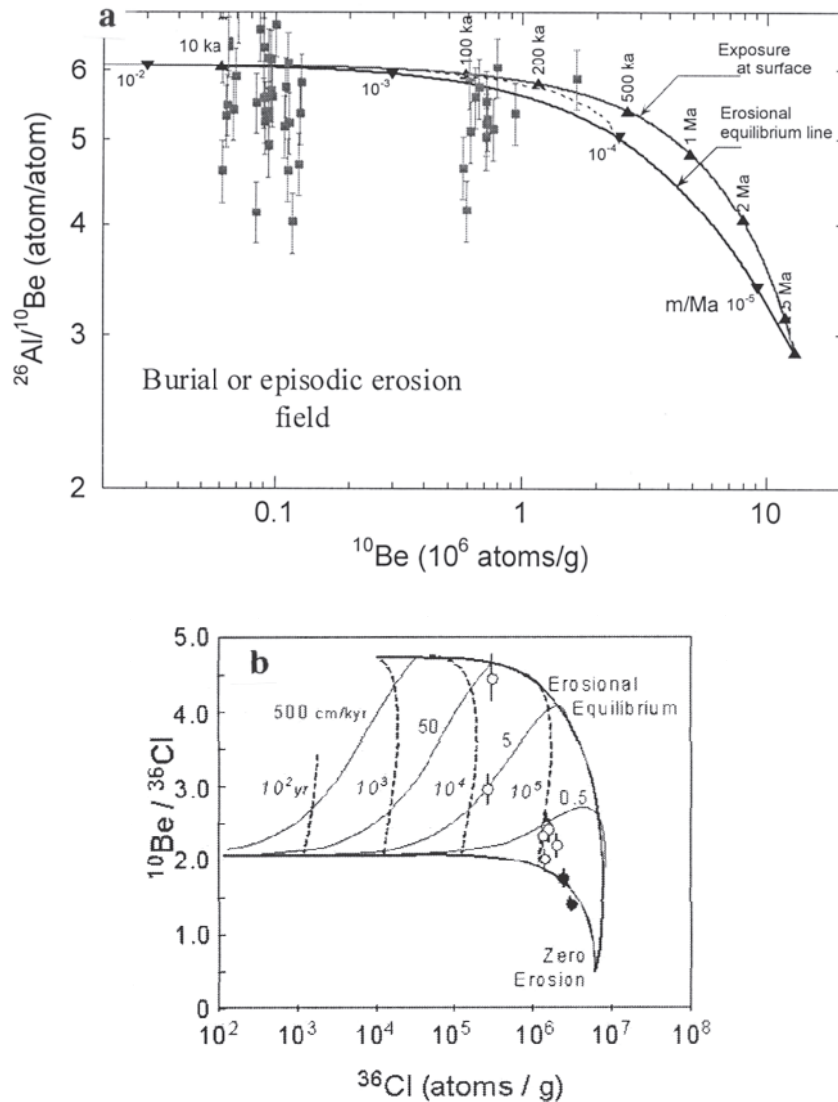
Figure 10. *In situ* isotope ratio plots. (a) ^{26}Al/^{10}Be vs. ^{10}Be (log concentration). The data are from granitic and granodiorite boulders and bedrock in the Wind River Range, Wyoming (Gosse et al. 1995a,b). Upper curve represents the path of a surface that is continuously exposed and not eroded. The area between the curves represents possible paths of surfaces that were eroded at a constant rate during continuous exposure. Samples that plot between the curves or below the lower curve may also have experienced an interruption in their exposure history, such as burial with sufficient shielding to significantly reduce the cosmic ray flux. Episodic erosion, such as glacial plucking, can also yield ratios that fall below the lower curve. (b) Ratio diagram, ^{10}Be/^{36}Cl vs. ^{36}Cl (log concentration, normalized, as in previous figures) for boulder samples from moraines in the Wind River Range, Wyoming (Phillips et al. 1997). The lower curve in Figure 10b corresponds to the upper curve in Figure 10a. The ^{36}Cl isotope is partially produced through thermal neutron capture so the width of the erosion island is greater (relative to the analytical accuracy of the ratio) than a ratio plot for two spallogenic isotopes. Position of samples indicates generally very low erosion rates for boulder surfaces.

(1) The method works well for some surfaces of long exposure duration ($>10^6$ a), but for younger surfaces the analytical uncertainty in the ratio measurement is prohibitively large ($1\sigma \sim 8\%$ or higher were typical until very recently).

(2) The strategy requires that the surface has been eroding at a constant rate, rather than in the episodic pulses more common in mountainous regions.

(3) The isotopic ratio is influenced by partial or complete burial and inheritance from previous exposure events.

(4) If erosion rates are greater than 1 mm kyr^{-1} or the exposure less than 1 Myr, the steady state assumption cannot be tested.

As an example of the approach, Gosse (1994) and Gosse et al. (1995a,b) measured more than 50 ^{26}Al/^{10}Be ratios on bedrock and boulder surfaces throughout the Wind River Range to help determine erosion rates of the Wind River Range granitic gneiss and to determine if the sampled surfaces had complicated (e.g., by burial) exposure histories (Fig. 10a). In an ideal case, the data would be sufficiently precise to define an erosion curve (such as the dashed curve), which would allow simultaneous estimates of erosion and age. The majority of the ratios do not plot within the erosion-equilibrium island, and therefore erosion and exposure age cannot be solved. This was the fate of even recent attempts to determine erosion rates of alpine bedrock summits (Small and Anderson 1998; Small et al. 1997), which prompted some of the criticism by Schaffer (1998). The point here is that even with improvements in the AMS precision, the ^{26}Al/^{10}Be will not provide a meaningful resolution of erosion rates on late Pleistocene surfaces.

However, Liu et al. (1994) showed how a combination of ^{36}Cl and ^{10}Be could be a useful alternative for bedrock erosion rates greater than 1 mm kyr^{-1} and surfaces less than 1 Ma (Fig. 10b). Phillips et al. (1997) used the ^{10}Be/^{36}Cl technique to simultaneously measure rock erosion rates and ages in the Wind River Range. Their average erosion rate on the medium grained foliated granitic gneiss was 0.6 mm kyr^{-1}. One of the powerful advantages of the cosmogenic nuclide method, not unlike U-series dating methods, is that the production ratios of different nuclides are becoming better known, allowing the flexibility of choosing the most appropriate nuclide ratio for the age and erosion rate of the surface of interest.

Denudation history. Denudation is the long-term erosion of the landscape resulting from multiple weathering and erosion processes over a large spatial scale (typically drainage basin to orogen scale). If loss of ^{10}Be from the regolith by erosion exceeds the loss due to radioactive decay (requiring >1 mm kyr^{-1} for a typical regolith), the distribution of quartz is uniform throughout the surface of the basin, and long term sediment storage is minimal, then the denudation rate $\bar{\varepsilon}$ of the basin can be expressed as (Lal 1991; Bierman 1994; Bierman and Steig 1996; Cerling and Craig 1994):

$$\bar{\varepsilon} = \frac{\bar{P}\mu}{\bar{N}} \tag{8}$$

where P is the average production rate for quartz in the basin (weighted according to the basin hypsometric curve, atoms g^{-1} a^{-1}), N is the measured (basin averaged) concentration (atoms g^{-1}), and μ is as defined previously. Investigations using this approach of estimating basin-scale denudation history have attempted to compare the results with independent estimates to evaluate the validity of the above assumptions (Brown et al. 1998b; Granger et al. 1996; Phillips et al. 1998). In the Brown et al. study, differences in the trends in two basin-scale denudation styles were found to be consistent with contrasting debris slide records. Sedimentation and erosion histories based on detailed interpretations of the soils records supported the conclusions of Granger et al. and Phillips et al. Other studies are currently underway to examine the extent to which

(1) temporary storage in valley bottoms in a catchment prior to alluvial fan deposition, and (2) episodic or low erosion rates affect the dating and denudation modeling of sediment in arid regions. Bierman and Steig (1996) proposed a model to interpret concentrations of *in situ* [10]Be in sediment derived from basin. Their calculations show how cosmogenic nuclides can confirm predictions of G.K. Gilbert that landscapes achieve equilibrium states in shorter time periods when erosion rates are higher (a conclusion made by Burbank et al. 1996 based on [10]Be measurements on strath terraces of the Indus River). Comparisons of the time-integrated denudation over the past 10^4 years calculated from [10]Be in stream sediments with records of erosion over different timescales (e.g., decades: Kirchner et al. 2001; or longer (Pazzaglia and Brandon 2001) have been used to infer that erosion rates may be sustained at different timescales and that topographic steady state conditions may be reached in short time periods. The [10]Be catchment denudation method has not yet been used to determine if a region undergoing orogeny has maintained dynamic equilibrium (topographic steady state) over periods beyond a single glacial cycle (Burbank and Anderson 2000).

Brown et al. (1998b) pointed out a useful means of determining the style of weathering and erosion in a basin, and if the style had changed over time. They measured the relative ratio of the [10]Be concentration in fine and coarse alluvial sediment. The ratio increases with an increasing contribution of weathering and erosion processes (e.g., debris slides) that bring coarse material to the surface. This strategy will also be useful in areas subject to periods of intense frost shattering processes, which may increase the overall erosion rate of basins, particularly for basins with a large fraction of their hypsometric curve above the zero degree isotherm. If widely applicable, it may provide a means of relating climate variability to changes in exhumation rates (part of an ongoing dilemma).

Bedrock incision rates   In a hallmark study, Burbank et al. (1996) and Leland et al. (1998) used [10]Be and [26]Al to calculate ages of strath terraces (fluvial erosional surfaces in bedrock) in the Indus River of northern Pakistan. [26]Al and [10]Be ages were sufficiently concordant to establish that erosion and burial effects were negligible after the strath was abandoned. They demonstrated, by measuring [10]Be in modern straths, that there was either a low probability of inheritance or a complicated exposure history that, for instance, would have resulted from the burial of the strath by enough fluvial sediment to shield the surface. They documented that bedrock incision has increased from 1-6 m kyr[-1] to 9-12 m kyr[-1] over a short (15 kyr) time. They could also identify an increase in incision rate downstream toward an active fault. The incision rates can be placed into context with the regional exhumation history determined by thermochronometry, helped to document the coeval maintenance of steady state hill-slopes by mass wasting into the deepening valleys, and has implications for assessing the role of climate on the evolution of mountains in tectonically active regions.

Paleoaltimetry

Paleoaltimetry is the study of the rate and nature of surface elevation change due to a combination of tectonic and isostatic uplift and erosion (i.e., surface uplift, not rock uplift). It differs from studies of the history of exhumed rocks (e.g., thermochronology, and many of the studies cited in the above section). The latter does not necessarily involve any change in the vertical position (elevation) of a topographic surface. Although geodetic analyses are providing data for the very recent history of surface uplift, only cosmogenic nuclides may provide a means of determining pre-historic vertical motion without resorting to models driven by erosion rate. In any case, paleoaltitudes must be measured at many sites over large (>1000 km^2) areas to be useful on an orogen scale (England and Molnar 1990).

The basis of paleoaltimetry studies using cosmogenic nuclides is the dependence of *in situ* production rates on atmospheric depth. Beginning with Hess's balloon missions in 1912 to document the increases in cosmic radiation with altitude, studies have shown how the secondary cosmic neutron and muonic fluxes are attenuated as they penetrate the atmosphere. The cosmic ray flux responsible for the production of ¹⁰Be is predictably attenuated by interactions with atmospheric particles so that production rates at sea level are more than an order of magnitude less than rates at 4 km elevation. Consider a simple example for an uplifted surface of negligible or known erosion rate with an independently known age (or one in which the concentration of cosmogenic radionuclides have reached steady state). The difference between the calculated concentration (for the given exposure duration at its current elevation) and the actual measured concentration can be attributable to the lower time-averaged production rate, reflecting the surface's prior position at lower elevation.

The potential of cosmogenic nuclides in paleoaltimetry was introduced during the inception of the TCN exposure dating technique in 1986 when H. Craig and R.J. Poreda considered the effects of elevation changes of Hawaiian lavas during the production of ³He (Craig and Poreda 1986). To estimate uplift rates, Lal (1991) described how uplift rate ($U = \Delta Z_S / \Delta t$) could be calculated from the TCN concentration, N, in the ideal case of steady state concentration, where an exponential change in production rate as a function of elevation is similar to the change due to erosion:

$$U = \frac{\bar{Z} P_{(o)}}{N_{(o)}} - \bar{Z}(\lambda + \mu\varepsilon) \qquad (9)$$

where $\bar{Z}$ is the mean height (m), and $\lambda + \mu\varepsilon$ is a time term (yr⁻¹) from the effects of decay and constant erosion. The lower limit for uplift that may be constrained using *in situ* TCN paleoaltimetry is a function of the uplift rate and duration of exposure. In the ideal case above, the uplift rate must be greater than the $\bar{Z}\mu\varepsilon$. Deviations from these simple scenarios will require other models to fit the scenario.

Despite the fact that much of the theoretical and experimental foundations are complete, the direct use of cosmogenic nuclides for paleoaltimetry has never been successfully applied for several good reasons. First, finding a surface with independent exposure age and known erosion rate in an area that is useful for paleoaltimetry is no easy feat. Second, the assumption that the surface was never shielded by ice or snow cover is difficult to verify, but crucial, because the effects of small amounts of shielding obscure the slight isotope change due to uplift. Third, the reliability of the atmospheric scaling model is only recently being refined to the necessary level of reliability. Ongoing studies are directed toward understanding the latitudinal change in atmospheric attenuation and to developing a more accurate global atmospheric pressure model. These developments, along with improved precision of AMS and better understanding of production rates (including geomagnetic influences), will accommodate the resolution needed for paleoaltimetry analyses.

With the possible exception of a few ideal instances, future applications of *in situ* TCN paleoaltimetry will need to avoid the influences of unknown erosion and intermittent burial effects. A recent approach is to measure the concentration of the ¹⁰Be in a laterally extensive surface (e.g., a lava or tuff) that is significantly displaced by a fault (M. Caffee, pers. comm.). Sampling of the down-dropped surface must be outside the shielding effects of any colluvial wedge. Because the surfaces are in close proximity, the influence of snow, erosion, and magnetic field effects may be assumed to be constant for both and therefore cancel out. The difference between the TCN concentrations of the two surfaces straddling the fault, with all things equal, should therefore reflect the change

in altitude over time. The next logical step is to model the variability of the uplift rate over the exposure duration. It might become routine to couple the TCN paleoaltimetry with a late Cenozoic thermochronological method that has a low closure temperature ($T_c \sim 70°$ C) such as the (U-Th)/He technique for exhumation histories (House et al. 1998).

Summary

The interpretation of ^{10}Be measurements as exposure ages is non-trivial, so the tectonic community will need to be aware of existing and new strategies to use the isotope for chronology while recognizing the hazards of surface erosion and inheritance. Although measurable progress was made over the past decade in AMS analysis, sample target preparation, and our understanding of ^{10}Be production systematics (Lal 2000b), more technique development is necessary to improve precisions and spawn new applications. Three new tectonic applications of ^{10}Be are currently being developed. In settings with high surface uplift rates and with constrained or negligible erosion rates, *in situ* ^{10}Be and other long-lived or stable isotopes will be used to estimate Late Cenozoic paleoaltimetry. Cosmogenic ^{10}Be will be used to establish a late Quaternary denudation history to compare with low temperature thermochronology exhumation studies for longer durations. The concentrations can also provide information on the relative timing and direction of development of sub-orogen scale tectonic landforms such as propagations of fold and thrust belts.

CONCLUSIONS

The last decade has seen a dramatic increase in the applications of cosmogenic ^{10}Be to studies of the solid Earth. Greatly improved analytical detection limits, better integration of ^{10}Be data with other tracers in carefully designed field programs, and the development of theoretical and analytical methods for using ^{10}Be produced in situ have all had a major impact on the field.

Atmospherically produced ^{10}Be has been used to great effect in studies of Earths' geodynamo and subduction zone processes. Well-correlated variations in geomagnetic paleointensity and ^{10}Be concentrations in marine sediments and ice cores over the last 200 kyr (e.g., SINT-200, SINT-800, NAPIS-75, SINT Be, and cosmogenic nuclide profiles from the GRIP/GISP2 ice cores) show that ^{10}Be can be used as a proxy for geomagnetic field variations, if the analytical program is carefully designed. This suggests that ^{10}Be concentrations in sediment cores can be used to construct a record of geomagnetic field paleointensity variations, even where the paleomagnetic record itself may have been compromised. Further, synchronization of geomagnetic paleointensity features permits the transference of very precise ice core chronologies to lacustrine and deep-sea sediments. Future work can build on this success with studies that use ^{10}Be to test the hypothesis of asymmetric sawtooth variations in the magnetic field, and to further test the suggestion of Milankovitch forcing of the geodynamo.

At convergent margins, the concentrations of ^{10}Be erupting in arc lavas can now be compared with ^{10}Be profiles in the incoming sediment column to quantify the extent of sediment accretion, underplating and erosion beneath the fore-arc as well as sediment subduction to the depths of magma generation. Nearly all of the incoming sediment must be deeply subducted to explain high ^{10}Be in the Aleutian, Central America (except Mexico and Costa Rica), Scotia, Kurile, Izu, Mariana, Bismarck and Tonga volcanic arcs. Rear arc lavas from the Aleutian, Bismarck and Kurile arcs often have as much ^{10}Be as the associated volcano at the front, despite the longer path and greater ^{10}Be decay in transit to the rear arc. The high values in the rear arc require greater sediment Be input behind the front; one explanation is a transition from sediment dehydration beneath the

front to sediment melting beneath the rear-arc. Well-correlated variations in U-series systematics and ^{10}Be for some but not all arcs suggest that the U excess in arc lavas may originate as elements leave the downgoing slab. Where U has been mobilized, but not Th, the time elapsed since element fractionation from the slab appears to be very short (~20 to 30 kyr) for some arcs.

Greatly improved detection limits of ~0.1 million atoms per gram open the door to a range of new work. For example, high ^{10}Be in fore-arc serpentinites would establish the role of the subducting slab in releasing hydrous fluids to the overlying serpentinizing mantle. ^{10}Be could help distinguish between recent and ancient sediment incorporation in contributing to the geochemical characteristics of some OIB suites, and some MORB lavas. It could also be used to track and time any recent mantle flow away from subduction zones.

The cosmogenic nuclides produced in rocks, including ^{10}Be, are now being used extensively in the study of active tectonics. A growing number of studies have successfully provided paleo-seismic constraints, dating times of repeated motions on exposed fault scarps, establishing slip rates from evolution of fault-cut alluvial surfaces, and determining the history of movement on fault-line scarps. With a useful time frame of ~5 ka to ~5 Ma, ^{10}Be provides dates and slip rates in a time window not easily datable otherwise. Combined ^{10}Be and ^{26}Al dating in principle allows erosion rates and exposure ages to be determined simultaneously, an approach suitable for long exposure histories. Where concordance between the two isotopes indicates negligible erosion, exposure ages can be used to provide uplift and incision rates.

As refinements in production rate scaling, AMS, and sampling strategies continue, studies employing *in situ* ^{10}Be measurements will have the accuracy and precision required to resolve higher frequency tectonic events. As the (U-Th)/He thermochronological method develops concurrently (e.g., House et al. 2000), there is a great potential for the pairing of these methods to provide complementary insight into late Cenozoic low temperature tectonic evolution of orogens. When coupled with detailed soils stratigraphy, geomorphological evidence, and supporting chronologies, ^{10}Be and other cosmogenic nuclides will begin to provide more insights into spatial variations of denudation rates and styles, contribute to paleoseismic databases, extend records of the timing and slip rates of Quaternary faults for examining strain partitioning among multiple faults, and to determine whether orogens have been evolving under sustained topographic equilibrium or erosional steady state conditions.

REFERENCES

Acton GD, Okada M, Clement BM, Lund SP, Williams T (2002) Paleomagnetic overprints in ocean sediment cores and their relationship to shear deformation caused by piston coring. J Geophys Res 107(B4):3-1 to 3-15

Aldahan A, Possnert G (1998) A high-resolution [10]Be profile from deep sea sediment covering the past 70 ka: Indication for globally synchronized environmental events. Quat Geochron 17:1023-1032

Aldahan A, Possnert G (2000) The [10]Be marine record of the last 3.5 Ma. Nucl Inst Methods Phys Res B 172:513-517

Aldahan AA, Possnert G, Gard G (1994) [10]Be in two sediment cores from the north Atlantic and chronological implications for the late Quaternary. N Jahrb Geol Palä ont Monats H7:418-433

Aldahan AA, Ning S, Possnert G, Backman J, Boström K (1997) [10]Be records from sediments of the Arctic Ocean covering the past 350 ka. Marine Geol 144:147-162

Aldahan A, Possnert G, Johnsen SJ, Clausen HB, Isaksson E, Karlen W, Hansson M (1998) Sixty year [10]Be record from Greenland and Antarctica. Proc Indian Acad Sci 107:139-147

Aldahan A, Possnert G, Peck J, King J, Colman S (1999) Linking the [10]Be continental record of Lake Baikal to marine and ice archives of the last 50 ka: Implication for the global dust-aerosol input. Geophys Res Lett 26:2885-2888

Anderson RF, Bacon MP, Brewer PG (1983a) Removal of [230]Th and [231]Pa at ocean margins. Earth Planet Sci Lett 66:73-90

Anderson RF, Bacon MP. Brewer PG (1983b) Removal of [230]Th and [231]Pa from the open ocean. Earth Planet Sci Lett 62:7-23

Anderson RF, Lao Y, Broecker WS, Trumbore SE, Hofmann HJ, Wölfli W (1990) Boundary scavenging in the Pacific Ocean: a comparison of [10]Be and [231]Pa. Earth Planet Sci Lett 96:287-304

Anderson RS, Repka JL, Dick GS (1996) Explicit treatment of inheritance in dating depositional surfaces using *in situ* [10]Be and [26]Al. Geology 24:47-51

Armstrong, RL (1971) Isotopic and chemical constraints on models of magma genesis in volcanic arcs, Earth Planet. Sci. Lett 12:137-142

Ayarbe JP, Phillips FM, Harrison JBJ, Elmore D, Sharma D (1998) Application of cosmogenic nuclides to fault-scarp chronology: preliminary results from the Socorro Canyon fault. Soil, water, and earthquakes around Socorro, New Mexico. *In* Harrison JBJ (ed) 1998 Rocky Mountain Cell 'Friends of the Pleistocene' Guide, p 39

Bacon MP (1984) Glacial to interglacial changes in carbonate and clay sedimentation in the Atlantic estimated from thorium-230 measurements. Isotope Geosci 2:97-111

Bacon MP, Rosholt JN (1982) Accumulation rates of [230]Th and [231]Pa and some transition metals on the Bermuda Rise. Geochim Cosmochim Acta 46:651-666

Bard E (1998) Geochemical and geophysical implications of the radiocarbon calibration. Geochim Cosmochim Acta 62:2025-2038

Bard E, Raisbeck GM, Yiou F, Jouzel J (1997) Solar modulation of cosmogenic nuclide production over the last millennium: comparison between ^{14}C and [10]Be records. Earth Planet Sci Lett 150:453-462

Bassinot FC, Labeyrie KL, Lancelot Y, Quidelleur X, Shackleton NJ, Vincent E (1994) The astronomical theory of climate and the age of the Brunhes-Matuyama magnetic reversal. Earth Planet Sci Lett 126:91-108

Baumgartner S, Beer J, Wagner G, Kubik P, Suter M, Raisbeck GM, Yiou F (1997a) [10]Be and dust. Nucl Instr Meth Phys Res B. 123:296-301

Baumgartner S, Beer J, Suter M, Diitrich-Hannen B, Synal H-A, Kubik PW, Hammer C, Johnsen S (1997b) Chlorine-36 fallout in the Summit Greenland Ice Core Project ice core. J Geophys Res 102: 26659-26662

Baumgartner S, Beer J, Masarik J, Wagner G, Meynadier L, Synal H-A (1998) Geomagnetic modulation of the [36]Cl flux in the GRIP ice core, Greenland. Science 279:1330-1332

Bebout, GE (1996) Volatile transfer and recycling at convergent margins: Mass balance and insights from high-P/T metamorphic rocks. *In* Bebout G, Scholl D, Kirby S, Platt J (eds) Subduction: Top to Bottom. Am Geophys Union Monogr 96:179-194

Bebout, GE, Ryan JG, Leeman WP (1993) B-Be systematics in subduction related metamorphic rocks: characterization of the subduction component. Geochim Cosmochim Acta 57:2227-2238

Bebout GE, Ryan JG, Leeman WP, Bebout A (1999) Fractionation of trace elements by subduction-zone metamorphism-effect of convergent margin thermal evolution. Earth Planet Sci Lett 171:63-78

Beer J, André e M, Oeschger H, Stauffer B (1983) Temporal [10]Be variations in ice. Radiocarbon 25:269-278

Beer J, André e M, Oeschger H, Siegenthaler U, Bonani G, Hofmann H, Morenzoni E, Nessi M, Suter M, Wölfli W, Finkel R, Langway, Jr. C (1984) The Camp Century [10]Be record: implications for long-term variations of the geomagnetic dipole moment. Nucl Instr Phys Meth B5:380-384

Beer J, Siengenthaler U, Bonani G, Finkel RC, Oeschger H, Suter M, Wölfi W (1988) Information on past solar activity and geomagnetism from ^{10}Be in the Camp Century ice core. Nature 331:675-679

Beer J, Blinov A, Bonani G, Finkel RC, Hofmann HJ, Lehmann B, Oeschger H, Sigg A, Schwander J, Staffelbach T, Stauffer BR, Suter M, Wölfli W (1990) Use of ^{10}Be in polar ice to trace the 11-year cycle of solar activity. Nature 347:164-166

Beer J, Bonani GS, Dittrich B, Heller F, Kubik PW, Tungsheng L, Chengde S, Suter M (1992) ^{10}Be and magnetic susceptibility in Chinese loess. Geophys Res Lett 20:57-60

Bell JW, Brune JN, Liu T, Zreda M, Yount JC (1998) Dating precariously balanced rocks in seismically active parts of California and Nevada. Geology 26:495-498

Benton L (1997) Origin and Evolution of Serpentine Seamount Fluids, Mariana and Izu-Bonin Forearcs: Implications for the recycling of subducted material. PhD dissertation, University of Tulsa, Tulsa, Oklahoma

Bhattacharyya A, Mitra B (1997) Changes in cosmic ray cut-off rigidities due to secular variations of the geomagnetic field. Ann Geophysicae 15:734-739

Bierman PR (1994) Using *in situ* produced cosmogenic isotopes to estimate rates of landscape evolution: A review from the geomorphic perspective. J Geophys Res 99:13885-13896

Bierman PR, Steig EJ (1996) Estimating rates of denudation using cosmogenic isotope abundances in sediment. Earth Surf Proc Landforms 21:125-139

Bierman PR, Gillespie AR, Caffee MW (1995) Cosmogenic ages for earthquake recurrence intervals and debris flow fan deposition, Owens Valley, California. Science 270:447-450

Bourdon B, Turner S, Allegre C (1999) Melting dynamics beneath the Tonga-Kermadec island arc inferred from ^{231}Pa-^{235}U systematics. Science 286:2491-2493

Brachfeld S, SK Banerjee (2000) A new high-resolution geomagnetic paleointensity record for the North American Holocene: A comparison of sedimentary and absolute intensity data. J Geophys Res B 105:821-834

Brassart JE, Tric E, Valet JP, Herrero-Bervera E (1997) Absolute paleointensity between 60 and 400 ka from the Kohala Mountain (Hawaii). Earth Planet Sci Lett 148:141-156

Brenan JM, Shaw HF, Ryerson FJ, Phinney DL (1995) Mineral-aqueous fluid partitioning of trace elements at 900° C and 2.0 GPa: Constraints on the trace element geochemistry of mantle and deep crustal fluids. Geochim Cosmochim Acta 59:3331-3350

Brenan JM, Ryerson FJ, Shaw H (1998) The role of aqueous fluids in the slab-to-mantle transfer of boron, beryllium and lithium during subduction: Experiments and models. Geochim Cosmochim Acta 62:3337-3347

Brook EJ, Brown ET, Kurz MD, Ackert RP, Raisbeck GM, Yiou F (1995a) Constraints on erosion and uplift rates of Pliocene glacial deposits in the Transantarctic Mountains using *in situ*-produced ^{10}Be and ^{26}Al. Geology 23:1063-1066

Brook EJ, Kurz MD, Ackert RP, Raisbeck GM, Yiou F (1995b) Cosmogenic nuclide exposure ages and glacial history of late Quaternary Ross Sea drift in McMurdo Sound, Antarctica. Earth Planet Sci Lett 131:41-56

Brown L, Klein J, Middleton R, Sacks IS, Tera F (1982) ^{10}Be in island arc volcanoes and implications for subduction. Nature 299:718-720

Brown ET, Bourles DL, Colin F, Raisbeck GM, Yiou F, and Desgarceaux S (1995) Evidence for muon-induced *in situ* production of ^{10}Be in near-surface rocks from the Congo. Geophys Res Lett 22:703-706

Brown ET, Bourles DL, Burchfiel BC, Oidong D, Jun L, Molnar P, Raisbeck GM, Yiou F (1998a) Estimation of slip rates in the southern Tien Shan using cosmic ray exposure dates of abandoned alluvial fans. Geol Soc Am Bull 110:377-386

Brown ET, Stallard RF, Larsen MC, Bourles DL, Raisbeck GM, Yiou F (1998b) Determination of predevelopment denudation rates of an agricultural watershed (Cayaguas River, Puerto Rico) using *in situ*-produced ^{10}Be in river-borne quartz. Earth Planet Sci Lett 160:723-728

Burbank DW, Anderson RS (2000) Tectonic Geomorphology: Blackwell Scientific, Oxford, UK, 270 p

Burbank DW, Leland J, Fielding E, Anderson RS, Brozovic N, Reid MR, Duncan C (1996) Bedrock incision, rock uplift and threshold hillslopes in the northwestern Himalayas. Nature 379:505-510

Castagnoli G, Lal D (1980) Solar modulation effects in terrestrial production of carbon-14. Radiocarbon 11:133

Cerling TE, Craig H (1994) Geomorphology and *in-situ* cosmogenic isotopes. Ann Rev Earth Planet Sci 22:273-31

Cerling TE, Webb RH, Poreda RJ, Rigby AD, Melis TS (1999) Cosmogenic ^{3}He ages and frequency of late Holocene debris flows from Prospect Canyon, Grand Canyon, USA. Geomorphology 27:93-111

Channell JET, Kleiven HF (2000) Geomagnetic palaeointensity and astrochronological ages for the Matuyama-Brunhes boundary and boundaries of the Jaramillo subchron: palaeomagnetic and oxygen isotope records from ODP Site 983. Phil Trans R Soc Lond A 358:1027-1047

Channell JET, Hodell DA, Lehman B (1997) Relative geomagnetic paleointensity and ^{18}O at ODP Site 983 (Gardar Drift, North Atlantic) since 350 ka. Earth Planet Sci Lett 153:103-118

Channell JET, Hodell DA, McManus J, Lehman B (1998) Orbital modulation of the Earth's magnetic field intensity. Nature 394:464-468

Channell JET, Stoner JS, Hodell DA, Charles CD (2000) Geomagnetic paleointensity for the last 100 kyr from the sub-Antarctic South Atlantic: a tool for interhemispheric correlation. Earth Planet Sci Lett 175:145-160

Chase Z, Anderson RF, Fleisher MQ, Kubik PW (in press) Scavenging of ^{230}Th, ^{231}Pa and ^{10}Be in the Southern Ocean (SW Pacific sector): The importance of particle flux and advection. Deep-Sea Res II

Chengde S, Beer J, Bonani G, Liu T, Oeschger H, Suter M, Wölfli W (1992) ^{10}Be in Chinese loess. Earth Planet Sci Lett 109:169-177

Cini Castagnoli G, Albrecht A, Beer J, Bonino G, Shen CH, Callergari E, Taricco C, Dittrcih-Hannen B, Kubik P, Suter M, Zhu GM (1995) Evidence for enhanced ^{10}Be deposition in Mediterranean sediments 35 Kyr BP. Geophys Res Lett 22:707-710

Cini Castagnoli G, Bonino G, Della Monica P, Procopio S, Taricco C (1998) On the solar origin of the 200 yr Suess wiggles: evidence from thermoluminescence in sea sediments. Il Nuovo Cimento 21 C:237-241

Class C, Miller DM, Goldstein, SL, Langmuir CH (2000) Distinguishing melt and fluid components in Umnak volcanics, Aleutian arc. Geochem Geophys Geosystems 1, paper #1999GC000010

Cousens BL, Allan JF, Gorton M P (1994) Subduction-modified pelagic sediments as the enriched component in back-arc basalts from the Japan Sea; Ocean Drilling Program sites 797-794. Contrib Mineral Petrol 117:421-434

Craig H, Poreda R (1986) Cosmogenic ^{3}He in terrestrial rocks: the summit lavas of Maui. Proc Natl Acad Sci (USA) 83:1970-1974

Damon PE, Sonett CP (1991) Solar and terrestrial components of the atmospheric C-14 variation spectrum. *In* Sonett CP, Giampapa MS, Mathews MS (eds) The Sun in Time. The University of Arizona, Tucson, p 360-388

Damon PE, Cheng S, Linick T (1989) Fine and hyperfine structure in the spectrum of secular variations of atmospheric ^{14}C. Radiocarbon 31:704-718

Davies JH, Steventson DJ (1992) Physical model of source region of subduction zone volcanics. J Geophys Res 97:2037-2070

Dickinson WR (1975) Potash-depth (K-h) relations in continental margin and intra-oceanic magmatic arcs. Geology 3:53-56

Dyke AS, Morris TF, Green DEC (1991) Postglacial tectonic and sea level history of the central Canadian Arctic. Geol Surv Can Bull 397:56

Dyke AS, Morris TF, Green DEC, England J (1992) Quaternary Geology of Prince of Wales Island, Arctic Canada. Geol Surv Can Mem 433:142

Eddy JA (1976) The Maunder minimum. Science 192:1189-1201

Edwards CMH, Morris JD, Thirlwall MF (1993) Separating mantle from slab signatures in arc lavas using B/Be and radiogenic isotope systematics. Nature 362:530-533

Elliot T, Plank T, Zindler A, White W, Bourdon B (1997) Element transport from slab to volcanic front at the Mariana arc. J Geophys Res 102:14991-15019

Elsasser WM, Ney EP, Wenkker JR (1956) Cosmic ray intensity and geomagnetism. Nature 178:1226

England P, Molnar P (1990) Surface uplift, uplift of rocks, and exhumation of rocks. Geology 18: 1173-1177

Fenton CR, Webb RH, Pearthree PA, Cerling TE, Poreda RJ (2001) Displacement rates on the Toroweap and Hurricane faults; implications for Quaternary down-cutting in the Grand Canyon, Arizona. Geology 29:1035-1038

Finkel RC, Nishiizumi N (1997) Beryllium-10 concentrations in the Greenland Ice Sheet Project 2 ice core. J Geophys Res 102:26699-26706

Finkel R, Suter M (1993) AMS in the Earth Sciences: Technique and applications. Adv Analyt Geochem 1: 1-114

Frank M (2000) Comparison of cosmogenic radionuclide production and geomagnetic field intensity over the last 200,000 years. Phil Trans R Soc Lond A 358:1089-1107

Frank M, Eckhardt J-D, Eisenhauer A, Kubik PW, Dittrich-Hannen B, Segl M, Mangini A (1994) Beryllium-10, thorium-230, and protactinium-231 in Galapagos microplate sediments: Implications of hydrothermal activity and paleoproductivity changes during the last 100,000 years. Paleoceanography 9:559-578

Frank M, Eisenhauer A, Bonn WJ, Walter P, Grobe H, Kubik PW, Dittrich-Hannen B, Mangini A (1995) Sediment redistribution versus paleoproductivity change: Weddell Sea margin sediment stratigraphy

and biogenic particle flux of the last 250,000 years deduced from ${}^{230}Th_{ex}$, ${}^{10}Be$ and biogenic barium profiles. Earth Planet Sci Lett 136:559-573

Frank M, Schwarz B, Baumann S, Kubik PW, Suter M, Mangini A (1997) A 200 kyr record of cosmogenic radionuclide production rate and geomagnetic field intensity from ${}^{10}Be$ in globally stacked deep-sea sediments. Earth Planet Sci Lett 149:121-129

Frank M, Gersonde R, Mangini A (1999) Sediment redistribution, ${}^{230}Th_{ex}$ - normalization and implications for the reconstruction of particle flux and export paleoproductivity. *In* Fischer G, Wefer G (eds) Use of Proxies in Paleoceanography: Examples from the South Atlantic. Springer-Verlag, Berlin–Heidelberg, p 409-426

Frank M, Gersonde R, van der Loeff MR, Bohrmann G, Nürnberg CC, Kubik PW, Suter M, Mangini A (2000) Similar glacial and interglacial export bioproductivity in the Atlantic sector of the Southern Ocean: Multiproxy evidence and implications for glacial atmospheric CO_2. Paleoceanography 15: 642-658

Fryer P, Mottl M, Johnson L, Haggerty J, Phipps S, Maekawa H (1995) "Serpentine bodies in the forearcs of Western Pacific convergent margins: origin and associated fluids." *In* Taylor B, Natland J (eds) Active Margins and Marginal Basins of the Western Pacific. Washington, DC, Am Geophys Union, p 259-279

Fuller M, Hastedt M, Herr B (1998) Coring-induced magnetization of recovered sediment. Proc Ocean Drill Prog Sci Res 157:47-56

George R, Turner S, Nye C, Hawkesworth C (2000) Along-arc U-Th-Ra disequilibria in the Aleutians: Rapid timescales of fluid transfer. V M Goldschmidt 2000 J Conf Abstr 5:436

George R, Turner S, Hawkesworth CJ, Morris J, Nye C, Ryan JG, Zheng SH (submitted) Melting processes and fluid and sediment transport rates along the Alaska-Aleutian arc from an integrated U-Th-Ra-Be isotope study. J Geophys Res

Gill JB, Williams RN (1990) The isotope and U-series studies of subduction-related volcanic rocks. Geochim Cosmochim Acta 54:1427-1442

Gill JB, Morris JD, Johnson RW (1993) Timescale for producing the geochemical signature of island arc magmas: U-Th-Po and Be-B systematics in recent Papua New Guinea lavas. Geochim Cosmochim Acta 57:4269-4283

Gillespie AR, Bierman P (1995) Precision of terrestrial exposure ages and erosion rates estimated from analysis of cosmogenic isotopes produced *in situ*. J Geophys Res 100:24637-24649

Gosse, JC (1994) Alpine glacial history reconstruction: 1. Application of the cosmogenic ${}^{10}Be$ exposure age method to determine the glacial chronology of the Wind River Mountains, Wyoming, USA; 2. Relative dating of Quaternary deposits in the Rio Atuel Valley, Mendoza, Argentina. PhD dissertation, Lehigh University, Bethlehem, Pennsylvania

Gosse JC, McDonald E (submitted) Variation of inheritance in alluvium as a function of catchment glaciation: Implication for glacial erosion and exposure age dating. Radiocarbon

Gosse JC, Phillips FM (2001) Terrestrial cosmogenic nuclides: theory and applications. Quat Sci Rev 20:1475-1560

Gosse JC, Stone JO (2001) Terrestrial cosmogenic nuclide methods passing milestones toward palaeo-altimetry. EOS Trans Am Geophys Union 82-7:82,86,89

Gosse JC, Evenson EB, Klein J, Lawn B, Middleton R (1995a) Precise cosmogenic ${}^{10}Be$ measurements in western North America: Support for a global Younger Dryas cooling event. Geology 23:877-880

Gosse JC, Klein J, Evenson EB, Lawn B, Middleton R (1995b) Beryllium-10 dating of the duration and retreat of the last Pinedale glacial sequence. Science 268:1329-1333

Gosse JC, Grant DR, Klein J, Lawn B (1995c) Cosmogenic ${}^{10}Be$ and ${}^{26}Al$ constraints on weathering zone genesis, ice cap basal conditions, and Long Range Mountain (Newfoundland) glacial history. CANQUA-CGRG Conf Abstr, Memorial University of Newfoundland, St. Johns, Canada, p 19

Gosse JC, Harrington CD, Whitney JW (1996) Applications of *in situ* cosmogenic nuclides in the geologic site characterization of Yucca Mountain, Nevada. Materials Res Soc Symp Proc 412:799-806

Gosse JC, Hecht G, Mehring N, Klein J, Lawn B, Dyke A (1998) Comparison of radiocarbon and *in situ*-cosmogenic nuclide-derived postglacial emergence curves for Prescott Island, Central Canadian Arctic. Geol Soc Am Abstr Progr 30(7):A-298

Gosse JC, Dyke AS, Klein J (in prep.) Crustal emergence curve for central Arctic based on terrestrial cosmogenic nuclide chronology of a sea cliff and raised beaches. Geophys Res Lett

Granger DE, Muzikar PF (2001) Dating sediment burial with *in situ*-produced cosmogenic nuclides: theory, techniques, and limitations. Earth Planet Sci Lett 188:269-281

Granger DE, Kirchner JW, Finkel R (1996) Spatially averaged long-term erosion rates measured from in-situ produced cosmogenic nuclides in alluvial sediment. J Geology 104:249-257

Gu ZY, Caffee MW, Chen MY, Guo ZT, Lal D, Liu TS, Southon J (1996) Five million year ${}^{10}Be$ record in Chinese loess and red clay: climate and weathering relationships. Earth Planet Sci Lett 144:273-287

Guyodo Y, Valet J-P (1996) Relative variations in geomagnetic intensity from sedimentary records: the past 200 thousand years. Earth Planet Sci Lett 143:23-36

Guyodo Y, Valet J-P (1999) Global changes in intensity in the Earth's magnetic field during the past 800 kyr. Nature 399:249-252

Guyodo Y, Gaillot P, Channell JET (2000) Wavelet analysis of relative geomagnetic paleointensity at ODP Site 983. Earth Planet Sci Lett 184:109-183

Guyodo Y, Acton GD, Brachfeld S, Channell JET (2001) A sedimentary paleomagnetic record of the Matuyama chron from the western Antarctic margin (ODP Site 1101). Earth Planet Sci Lett 191:61-74

Haggerty JA (1991) Evidence from fluid seeps atop serpentine seamounts in the Mariana Forearc: Clues for emplacement of the seamounts and their relationship to forearc tectonics. Marine Geol 102:293-301

Haggerty JA, Fisher JB (1992) Short-chain organic acids in interstitial waters from Mariana and Bonin forearc serpentines. *In* Fryer P, Pearce JA, Stokking LB et al. (eds) Proc Ocean Drilling Program Sci Results 125:387-395

Hancock GS, Anderson RS, Chadwick OA, Finkel RC (1999) Dating fluvial terraces with ^{10}Be and ^{26}Al profiles: application to the Wind River, Wyoming. Geomorphology 27:41-60

Haubold HJ, Beer J (1992) Solar activity cycles revealed by time series analysis of argon-37, sunspot-number, and beryllium-10 records. Proc IUGG, Vienna, Solar-Terrestrial Varia Glob Chan, p 11-34

Hawkesworth CJ, Turner SP, McDermott F, Peate DW, van Calsterern P (1997) U-Th isotopes in arc magmas: implications for element transfer from the subducted crust. Science 276:551-555

Heisinger B, Niedermayer M, Hartmann JF, Korschinek G, Nolte E, Morteani G, Neumaier S, Petitjean C, Kubik P, Synal A, Ivy-Ochs S (1997) In-situ production of radionuclides at great depths. Nucl Instr Meth Physics Res B123:341-346

Henken-Meillies WU, Beer J, Heller F, Hsu KJ, Shen C (1990) ^{10}Be and ^{9}Be in South Atlantic DSDP Site 519: relation to geomagnetic reversals and to sediment composition. Earth Planet Sci Lett 98:267-276

Hermanns RL, Niedermann S, Garcia AV, Gomez JS, Strecker MR (2001) Neotectonics and catastrophic failure of mountain fronts in the southern intra-Andean Puna Plateau, Argentina. Geology 29:619-623

Herrstrom EA, Reagan MK, Morris JD (1995) Variations in lava composition associated with flow of asthenosphere beneath southern Central America. Geology 23:617-620

Hickey-Vargas R, Murong S, Lopez-Escobar L, Roa HM, Morris J, Reagan R, Ryan J (in press) Multiple subduction components in the mantle wedge: Evidence from eruptive centers in the Central SVZ, Chile. Chem Geol

House MA, Wernicke BP, Farley KA (1998) Dating topography of the Sierra Nevada, California, using apatite (U-Th)/ He ages. Nature 396:66-69

House MA, Farley KA, Stockli DF (2000) Helium chronometry of apatite and titanite using Nd-YAG laser heating. Earth Planet Sci Lett 183:365-368

Imamura M, Hashimoto Y, Yoshida K, Yamane I, Yamashita, Inoue T, Tanaka S, Nagai H, Honda M, Kobayashi K, Takaoka, Ohba Y (1984) Tandem accelerator mass spectrometry of ^{10}Be/^{9}Be with internal beam monitor methods. Nucl Inst Meth B6:211-216

Imbrie J, Imbrie JZ (1980) Modelling the climate response to orbital variations. Science 207:942-953

Imbrie J, Hays JD, Martinson DG, McIntyre A, Mix AC, Jorley JJ, Pisias NG, Prell WL, Shackleton NJ (1984) The orbital theory of Pleistocene climate: Support from a revised chronology of the marine d^{18}O record. *In* Berger AL et al. (eds) Milankovitch and Climate, Part 1. NATO ASI Ser 126. Reidel, Dordrecht, The Netherlands, p 269-305

Ishikawa T, Nakamura E (1994) Origin of the slab component inferred in arc lavas from across-arc variation of Band Pb isotopes. Nature 370:205-208

Ishikawa T, Tera F (1997) Source composition and distribution of the fluid in the Kurile mantle wedges: Constraints from across-arc variations of B/Nb and B isotopes. Earth Planet Sci Lett 152:123-138

Ivy-Ochs S, Schluchter C, Kubik PW, Synal H-A, Beer J, Kerschner H (1998) The exposure age of Egesen moraine at Julier Pass, Switzerland, measured with the cosmogenic radionuclides ^{10}Be, ^{26}Al, and ^{36}Cl. Eclogae Geologica Helvetica 89:1049-1063

Jackson J, Ritz JF, Siame L, et al. (2002) Fault growth and landscape development rates in Otago, New Zealand, using *in situ* cosmogenic Be-10. Earth Planet Sci Lett 195:85-193

Jarrard RD (1986) Relations among subduction parameters. Rev Geophys 24:217-284

Johnson M, Plank T (1999) Dehydration and melting experiments constrain the fate of subductd sediments. Geochem Geophy Geosystems (G3)1, #14

Juárez MT, Tauxe L, Gee JS, Pick T (1998) The intensity of the Earth's magnetic field over the past 160 million years. Nature 394:878-881

Karlin R (1990) Magnetic mineral diagenesis in marine sediments from the Oregon continental margin. J Geophys Res 95:4405-4419

Kastner M, Morris J, Chan LH, Saether, O, Luckge, A (2000) Three distinct fluid systems at the Costa Rica Subduction Zone: Chemistry, hydrology, and fluxes. V M Goldschmidt 2000 J Conf Abstr 5:572

Keller EA, Gurrola L, Tierney TE (1999) Geomorphic criteria to determine direction of lateral propagation of reverse faulting and folding. Geology 27:515-518

Kelly RK, Driscoll NW (1998) Structural controls on Be-10 occurrences in arc lavas. EOS Trans Am Geophys Union 79:45

Kent DV (1973) Post depositional remanent magnetization in deep-sea sediment. Nature 246:32-34

Kent DV, Opdyke ND (1977) Paleomagnetic field intensity variation recorded in a Brunhes epoch deep-sea sediment core. Nature 266:156-159

Kersting AB, Arculus RJ, Gust D (1996) Lithospheric contributions to arc magmatism; isotope variations along strike in volcanoes of Honshu, Japan. Science 272:1464-1468

Kimura G, Silver EA, Blum P, et al. (1997) Proceeding of the Ocean Drilling Program. *In* Initial Reports 170. College Station, Texas, p 458

Kirchner JW, Finkel RC, Riebe CS, Granger DE, Clayton JL, Megahan WF, (2001) Episodic mountain erosion inferred from sediment yields over 10-year and 10,000-year timescales. Geology 29: 591-594.

Kissel C, Laj C, Labeyrie L, Dokken T, Voelker A, Blamart D (1999) Rapid climatic variations during marine isotopic stage 3: magnetic analysis of sediments from nordic seas and North Atlantic. Earth Planet Sci Lett 171:489-502

Klein J, Lawn B, Gosse J, Harrington C (1997) Can terrestrial cosmogenic Be-10 be measured in whole rock samples to decipher surface exposure histories. Geol Soc Am Abstr Progr 29:A-346

Kobayashi K, Kitazawa K, Kanaya T, Sakai T (1971) Magnetic and micropaleontological study of deep sea sediments from the western equatorial Pacific. Deep-Sea Res 18:1045-1062

Kocharov GE (1990) Investigation of astrophysical and geophysical problems by AMS: Successes achieved and prospects. Nucl Instr Meth B52:583-587

Kok YS (1999) Climatic influence in NRM and ^{10}Be-derived geomagnetic paleointensity data. Earth Planet Sci Lett 166:105-119

Kok YS, Tauxe L (1996a) Saw-toothed pattern of relative paleointensity records and cumulative viscous remanence. Earth Planet Sci Lett 137: 95-99

Kok YS, Tauxe L (1996b) Saw-toothed pattern of sedimentary paleointensity records explained by cumulative viscous remanence. Earth Planet Sci Lett 144:E9-E14

Kok YS, Tauxe L (1999) A relative geomagnetic paleointensity stack from Ontong-Java plateau sediments for the Matuyama. J Geophys Res 104:25401-25413

Kok YS, Ynsen I (2002) Reply to comment by J-P Valet and L Meynadier on "A relative geomagnetic paleointensity stack from Ontong-Java plateau sediments for the Matuyama." J Geophys Res 107(B3):3-1-2

Kong P, Nishiizumi K, Finkel RC, Caffee MW (1999) *In situ*-produced cosmogenic ^{10}Be and ^{26}Al in olivine. EOS Trans Am Geophys Union 80:F1166

Kubik PW, Ivy-Ochs S, Masarik J, Frank M, Schlüchter C (1998) ^{10}Be and ^{26}Al production rates deduced from an instantaneous event within the dendro-calibration curve, the landslide of Köfels, Ötz Valley, Austria. Earth Planet Sci Lett 161:231-241

Kurz MD, Colodner D, Trull TW, Moore RB, O'Brien K (1990) Cosmic ray exposure dating with *in situ*-produced cosmogenic ^{3}He: results from young Hawaiian lava flows. Earth Planet Sci Lett 97:177-189

Laj C, Kissel C (1999) Geomagnetic field intensity at Hawaii for the last 420 kyr from the Hawaii Scientific Drilling Project core, Big Island, Hawaii. J Geophys Res 104:15317-15338

Laj C, Kissel K, Garnier F (1996) Relative geomagnetic field intensity and reversals for the last 1.8 My from a central equatorial Pacific core. Geophys Res Lett 23:3393-3396

Laj C, Raïs A, Surmont J, Gillot PY, Guillou H, Kissel C, Zanella E (1997) Changes of the geomagnetic field vector obtained from lava sequences on the island of Volcano (Aeolian Islands, Sicily). Phys Earth Planet Inter 99:161-177

Laj C, Kissel C, Mazaud A, Channell JET, Beer J (2000) North Atlantic palaeointensity stack since 75 ka (NAPIS-75) and the duration of the Laschamp event. Phil Trans R Soc Lond A 358:1009-1025

Laj C, Kissel C, Scao V, Beer J, Thomas DM, Guillou H, Muscheler R, Wagner G (2002) Geomagnetic intensity and inclination variations at Hawaii for the past 98 kyr from core SOH-4 (Big Island): a new study and a comparison with existing contemporary data. Phys Earth Planet Inter 129:205-243

Lal D (1988) *In situ*-produced cosmogenic isotopes in terrestrial rocks. Ann Rev Earth Planet Sci 16: 355-388

Lal D (1991) Cosmic ray labeling of erosion surfaces: *in situ* nuclide production rates and erosion rates. Earth Planet Sci Lett 104:424-439

Lal D (1996) On cosmic-ray exposure ages of terrestrial rocks: a suggestion. Radiocarbon 37:889-898

Lal D (2000a) Cosmogenic ^{10}Be: A critical view on its widespread dominion in geosciences. Proc Indian Acad Sci (Earth Planet Sci) 109:181-186

Lal D (2000b) Cosmogenic nuclide production rate systematics in terrestrial materials: present knowledge, needs, and future actions for improvement. Nucl Inst Methods Phys Research B 172:772-781

Lal D, Peters B (1967) Cosmic ray produced radioactivity on the Earth. *In* Encyclopedia of Physics, vol 46(2). Springer-Verlag, New York, p 581-588

Lao Y, Anderson RF, Broecker WS, Trumbore SE, Hofmann HJ, Wolfli W (1992) Transport and burial rates of particulate fluxes of ^{10}Be and ^{231}Pa in the Pacific ocean during the Holocene period. Earth Planet Sci Lett 113:173-189

Lao Y, Anderson RF, Broecker WS, Hofmann HJ, Wolfli W (1993) Particulate fluxes of ^{230}Th, ^{231}Pa, and ^{10}Be in the northeastern Pacific ocean. Geochim Cosmochim Acta 57:205-217

Leat PT, Livermore RA, Millar, IL (2000) Magma supply in back-arc spreading centre segment E2, East Scotia Ridge. J Petrology 41:845-866

Leland J, Reid MR, Burbank DW, Finkel R, Caffee M (1998) Incision and differential bedrock uplift along the Indus River near Nanga Parbat, Pakistan Himalaya, from ^{10}Be and ^{26}Al exposure age dating of bedrock straths. Earth Planet Sci Lett 154:3-107

Leslie BW, Hammond DE, Berelson WE, Lund SP (1990) Diagenesis in anoxic sediments from the California continental borderland and its influence on iron, sulfur, and magnetite behavior. J Geophys Res 95:4453-4470

Liccardi JM, Kurz MD, Clark PU, Brook EJ (1999) Calibration of cosmogenic 3He production rates from Holocene lava flows in Oregon, USA, and effects of the Earth's magnetic field. Earth Planet Sci Lett 172:261-271

Liu B, Phillips FM, Fabryka-Martin JT, Fowler MM, Stone WD (1994) Cosmogenic 36Cl accumulation in unstable landforms I: Effects of the thermal neutron distribution. Water Resources Res 30:3115-3125

Lund SP, Schwartz M (1999) Environmental factors affecting geomagnetic field palaeointensity estimates from sediments. *In* Maher BA, Thompson T (eds) Quaternary Climates, Environments and Magnetism. Cambridge University Press, Cambridge, UK, p 323-311

Malkus WVR (1968) Precession as the cause of geomagnetism. Science 160:250-264

Marshall JS, Anderson RS (1995) Quaternary uplift and seismic cycle deformation, Península de Nicoya, Costa Rica. Geol Soc Am Bull 107:463-473

Marti K, Craig H (1987) Cosmic-ray produced neon and helium in the summit lavas of Maui. Nature 325:335-337

Martinson DG, Pisias NG, Hays JD, Imbrie J, Moore TC, Shackleton NJ (1987) Age dating and the orbital theory of the ice ages: Development of a high-resolution 0 to 300,000-year chronostratigraphy. Quat Res 27:1-29

Masarik J, Beer J (1999) Simulation of particle fluxes and cosmogenic nuclide production in the Earth's atmosphere. J Geophys Res 104:12099-12112

Masarik J, Frank M, Schaffer JM, Wieler R (2001) Correction of *in situ* cosmogenic nuclide production rates for geomagnetic field intensity variations during the past 800,000 years. Geochim Cosmochim Acta 65:2995-3003

Mazaud A (1996) 'Sawtooth" variation in magnetic in tensity profiles and delayed remanence acquisition in deep sea cores. Earth Planet Sci Lett 139:379-386

Mazaud A, Laj C, Bender M (1994) A geomagnetic chronology for Antarctic ice accumulation. Geophys Res Lett 21:337-340

McCalpin JP (1996) Paleoseismology. Academic Press, San Diego, 588 p

McDermott F, Hawkesworth C J (1991) Th, Pb and Sr isotope variations in young island arc volcanics and ocean sediments. Earth Planet Sci Lett 104:1-15

McFadden PL, Merrill RT (1993) Inhibition and geomagnetic field reversals. J Geophys Res 98:6189-6199

McFadden PL, Merrill RT (1997) Sawtooth paleointensity and reversals of the geomagnetic field. Phys Earth Planet Inter 103:247-252

McHargue LR, Damon PE (1991) The global beryllium-10 cycle. Rev Geophys 29:141-158

McHargue LR, Damon PE, Douglas J (1995) Enhanced cosmic-ray production of ^{10}Be coincident with the Mono Lake and Laschamp geomagnetic excursions. Geophys Res Lett 22:659-662

McHargue LR, Donahue D, Damon PE, Sonett CP, Biddulph D, Burr G (2000) Geomagnetic modulation of the late Pleistocene cosmic-ray flux as determined by ^{10}Be from Blake Outer Ridge marine sediment. Nucl Instr Methods Phys Res B 172:555-561

Merrill RT, McElhinny MW, McFadden PL (1996) The magnetic field of the Earth. In: Paleomagnetism, the core, and the deep mantle. Academic Press, San Diego, p 531

Meynadier L, Valet J-P (1996) Post-depositional realignment of magnetic grains and asymmetrical saw-tooth patterns of magnetization intensity. Earth Planet Sci Lett 140:123-132

Meynadier L, Valet J-P, Weeks R, Shackleton NJ, Hagee VL (1992) Relative geomagnetic paleointensity of the field during the past 140 ka. Earth Planet Sci Lett 114:39-57

Meynadier L, Valet J-P, Bassinot FC, Shackelton NJ, Guyodo Y (1994) Asymmetrical saw-tooth pattern of the geomagnetic field intensity from equatorial sediments in the Pacific and Indian Oceans. Earth Planet Sci Lett 126:109-127

Meynadier L, Valet J-P, Guyodo Y, Richter C (1998) Saw-toothed variations of relative paleointensity and cumulative viscous remanence: testing the records and the model. J Geophys Res 103:7095-7105

Milankovtich M (1941) Kanon der Erdbestrahlung und seine Andwendung auf das Eiszeitenproblem. Belgrade: Königlich Serbische Akademie. Published in English as Canon of Insolation and the Ice-Age Problem (1969). Translation by Israel Program for Scientific Translations, U S Department of Commerce, and U S National Science Foundation, Washington, DC

Monaghan MC, Krishnaswami S, Turekian KK (1985/86) The global-average production rate of ¹⁰Be. Earth Planet Sci Lett 76:279-287

Monaghan MC, Klein J, Measures C (1988) The origin of ¹⁰Be in island-arc volcanic rocks. Earth Planet Sci Lett 89:288-298

Moore GF, Silver EA (1983) Collision processes in the northern Molucca Sea. *In* Hayes D (ed) The Tectonic and Geologic Evolution of Southeast Asian Seas and Islands: Part 2. Am Geophys Union Monogr 27:360-372

Morris J (1991) Applications of cosmogenic ¹⁰Be to problems in the Earth sciences. Ann Rev Earth Planet Sci 19:313-350

Morris JD (1996). The subducted component in Mariana Island arc lavas: Constraints from Pb and Be isotopes and light element systematics. Izu-Bonin-Mariana Workshop, August 1996, Japan. RJ Stern, M Arima, convenors

Morris J, Tera F (1989) ¹⁰Be and ⁹Be in mineral separates and whole rocks from volcanic arcs: Implications for sediment subduction. Geochim Cosmochim Acta 53:3197-3206

Morris JD, Tera F (2000) Beryllium isotope systematics of volcanic arc cross-chains. V M Goldschmidt 2000 J Conf Abstr 5:720

Morris JD, Jezek PA, Hart SR, Gill J (1983) The Halmahera island arc, Molucca Sea collision zone, Indonesia: A geochemical survey. *In* Hayes DE (ed) The Tectonics and Geologic Evolution of Southeast Asian Seas and Islands. Am Geophys Union Monogr 27:373-387

Morris JD, Leeman WP, Tera F (1990) The subducted component in island arc lavas: constraints from Be isotopes and B-Be systematics. Nature 344:31-36

Morris J, Ryan J, Leeman WP (1993) Be isotope and B-Be investigations of the historic eruptions of Mt. Vesuvius. J. Volcanol Geotherm Res 58:345-358

Morris J, Valentine R, Harrison T (2002) ¹⁰Be imaging of sediment accretion, subduction and erosion, NE Japan and Costa Rica. Geology 30:59-62

Nagy E, Valet J -P (1993) New advances for paleomagnetic studies of sediment cores using U-channels. Geophys Res Lett 20:671-674

Nakamura E, Moriguti T (1998) Across-arc variation of Li isotopes in lavas and implications for crust/mantle recycling at subduction zones. Earth Planet Sci Lett 163:167-174

Ning S, Aldahan AA, Haiping Y, Possnert G, Königsson L-K (1994) ¹⁰Be in continental sediments from North China: Probing into the last 5.4 MA. Quat Geochron 13:127-136

Ninkovich D, Opdyke ND, Heezeh BC, Foster JH (1966) Paleomagnetic stratigraphy, rates of deposition and tephrachronology in North Pacific deep-sea sediments. Earth Planet Sci Lett 1:476-492

Nishiizumi K, Klein J, Middleton R, Craig H (1990) Cosmogenic ¹⁰Be, ²⁶Al, and ³He in olivine from Maui lavas. Earth Planet Sci Lett 98:263-266

Nishiizumi, KC, Kohl P, Arnold JR, Klein J, Fink D, Middleton R (1991) Cosmic ray produced ¹⁰Be and ²⁶Al in Antarctic rocks: exposure and erosion history: Earth Planet Sci Lett 104:440-454

Nishiizumi K, Kohl CP, Arnold JR, Dorn R, Klein J, Fink D, Middleton R, Lal D (1993) Role of *in situ* cosmogenic nuclides ¹⁰Be and ²⁶Al in the study of diverse geomorphic processes. Earth Surf Proc Land 18:407-425

Nyffler UP, Li Y-H, Santschi PH (1984) A kinetic approach to describe trace-element distribution between particles and solution in natural aquatic systems. Geochim Cosmochim Acta 48:1513-1522

O'Brien K (1979) Secular variations in the production of cosmogenic isotopes in the Earth's atmosphere. J Geophys Res 84:423-431

Opdyke ND, Kent DV, Lowrie W (1973) Details of magnetic polarity transitions recorded in a high deposition rate deep-sea core. Earth Planet Sci Lett 20:315-324

Paillard DL, Labeyrie L, Yiou P (1996) Macintosh program performs time-series analysis. EOS Trans Am Geophys Union 77:379

Pazzaglia F, Brandon M (2001) A fluvial record of long-term steady-state uplift and erosion across the Cascadia Forearc High, Western Washington State. Am J Sci 301:385-431

Peck JA, King JW, Colman SM, Kravchinsky VA (1996) An 84-kyr record from the sediments of Lake Baikal, Siberia. J Geophys Res 101(B5):11365-11385

Peltier WR (1998) Postglacial variations in the level of the sea: implications for climate dynamics and solid-Earth geophysics. Rev Geophys 36:603-689

Perg, LA, Anderson RS, Finkel RC (2001) Young ages of the Santa Cruz marine terraces determined using ^{10}Be and ^{26}Al. Geology 29(10):879-882

Peters B (1955) Radioactive beryllium in the atmosphere and on the earth. Proc Indian Acad Sci 41:67-71

Petit JR (and 18 others) (1999) Climate and atmospheric history of the past 420,000 years from the Vostok ice core, Antarctica. Nature 399:420-436

Phillips FM, Zreda MG, Elmore D, Sharma P (1996) A reevaluation of cosmogenic ^{36}Cl production rates in terrestrial rocks. Geophys Res Lett 23:949-952

Phillips FM, Zreda MG, Gosse JC, Klein J, Evenson EB, Hall RD, Chadwick OA, Sharma P (1997) Cosmogenic ^{36}Cl and ^{10}Be ages of Quaternary glacial and fluvial deposits of the Wind River Range, Wyoming. Geol Soc Am Bull 109:1453-1463

Phillips WM, McDonald EV, Reneau SL, Poths J (1998) Dating soils and alluvium with cosmogenic ^{21}Ne depth profiles: case studies from the Pajarito Plateau, New Mexico, USA. Earth Planet Sci Lett 160:209-223

Plank T, Langmuir CH (1993) Tracing trace elements from sediment input to volcanic output at subduction zones. Nature 362:739-743

Plank T, Langmuir CH (1998) The chemical composition of subducting sediment and its consequences for the crust and mantle. Chem Geol 145: 325-394

Plank T, Balzer V, Carr M (submitted) Nicaraguan volcanoes record paleoceanographic changes accompanying closure of the Panama Gateway. Science

Raï s A, Laj C, Surmont J, Gillot PY, Guillou H (1996) Geomagnetic field intensity between 70,000 and 130,000 years B.P. from a volcanic sequence on La Ré union, Indian Ocean. Earth Planet Sci Lett 140:173-189

Raisbeck GM, Yiou F, Fruneau M, Loiseaux JM, Lieuvin M, Ravel JC (1981a) Cosmogenic ^{10}Be/^{7}Be as a probe of atmospheric transport process. Geophys Res Lett 8:1015-1018

Raisbeck GM, Yiou F, Fruneau M, Loiseaux JM, Lieuvin M, Ravel JC, Lorius C (1981b) Cosmogenic ^{10}Be concentrations in Antarctic ice during the past 30,000 years. Nature 292:825-826

Raisbeck GM, Yiou F, Zhou SZ (1994) Paleointensity Puzzle. Nature 371:207-208

Raisbeck GM, Yiou F, Bourles D (1985) Evidence for an increase in cosmogenic ^{10}Be during a geomagnetic reversal. Nature 315:315-317

Raisbeck GM, Yiou F, Bourles D, Lorius C, Jouzel J, Barkov NI (1987) Evidence for two intervals of enhanced ^{10}Be deposition in Antarctic ice during the last glacial period. Nature 326:273-277

Rea D, Ruff LJ (1996) Composition and mass flux of sediment entering the world's subduction zones: Impolications for global sediment budgets, great earthquakes and volcanism. Earth Planet Sci Lett 140:1-12

Reagan MK, Morris JD, Herrstrom EA, Murrell MT (1994) Uranium series and beryllium isotope evidence for an extended history of subduction modification of the mantle beneath Nicaragua. Geochim Cosmochim Acta 58:4199-4212

Reheis MC, Sawyer TL (1997) Late Cenozoic history and slip rates of the Fish Lake Valley, Emigrant Peak, and Deep Springs fault zones, Nevada and California. Geol Soc Am Bull 109:280-299

Repka JL, Anderson RS, Finkel RC (1997) Cosmogenic dating of fluvial terraces, Fremont River, Utah. Earth Planet Sci Lett 152:59-73

Reymer A, Schubert G (1984) Phanerozoic addition rates to the continental crust and crustal growth. Tectonics 3:63-77

Robinson C, Raisbeck GM, Yiou F, Lehman B, Laj C (1995) The relationship between ^{10}Be and geomagnetic field strength records in central North Atlantic sediments during the last 80 ka. Earth Planet Sci Lett 136:551-557

Rochester MG, Jacobs JA, Smytie DE, Chong KF (1975) Can precession power the geomagnetic dynamo? Geophys J R Astron Soc 43:661-678

Ryan JG, Langmuir CH (1988) Beryllium sysematics in young volcanic rocks: implications for ^{10}Be. Geochim Cosmochim Acta 52:237-244

Ryan JG, Morris J, Tera F, Leeman WP, Tsvetkov A (1995) Cross-arc geochemical variations in the Kurile arc as a function of slab depth. Science 270:625-627

Ryan J, Morris J, Bebout G, Leeman W (1996) Describing chemical fluxes in subduction zones: Insights from "depth-profiling" studies of arc and forearc rocks. *In* Bebout G, Scholl D, Kirby S, Platt J (eds) Subduction Top to Bottom. Am Geophys Union Monogr 96:263-268

Sagnotti L, Macrí P, Camerlenghi A, Rebessco M (2001) Antarctic environmental magnetism of Antarctic Late Pleistocene sediments and interhemispheric correlation of climatic events. Earth Planet Sci Lett 192:65-80

Schaffer J (1998) Comment to Small, E. E. and Anderson, R.S.: Pleistocene relief production in Laramide Mountain Ranges, western U.S. Geology 26:121-123

Schwartz M, Lund SP, Johnson TC (1996) Environmental factors as complicating influences in the recovery of quantitative geomagnetic field paleointensity estimates from sediments. Geophys Res Lett 23:2693-2696

Shea MA, Smart DF (1992) Recent and historical solar proton events. Radiocarbon 34:255-262

Sheppard MK, Arvidson RE, Caffee M, Finkel R, Harris L (1995) Cosmogenic exposure ages of basalt flows: Lunar Crater volcanic field, Nevada. Geology 23:21-24

Shimaoka AK (1999) Be Isotopic Ratios in Island-Arc Volcanic Rocks from the North-East Japan: Implications for Incorporation of Oceanic Sediments into Island-Arc Magma. PhD dissertation, The University of Tokyo

Shimaoka AK, Imamura M, Kaneoka I (in press) Investigation of acid leaching conditions for obtaining the primary ^{10}Be signatures in volcanic materials. Chem Geol

Siame LL, Bourlés DL, Sébrier M, Bellier O, Castano JC, Araujo M, Perez M, Raisbeck GM, Yiou F (1997) Cosmogenic dating ranging from 20 to 700 ka of a series of alluvial fan surfaces affected by the El Tigre fault, Argentina. Geology 25:975-978

Siegenthaler U, Heimann M, Oeschger H (1980) ^{14}C variations caused by changes in the global carbon cycle. Radiocarbon 22:177-191

Sigmarsson O, Condomines M, Morris JD, Harmon RS (1990) Uranium and ^{10}Be enrichments by fluids in Andean arc magmas. Nature 346:163-165

Sigmarsson O, Chmeleff J, Morris J, Lopez-Escobar L (2002) Rapid magma transfer from slab derived ^{226}Ra-^{230}Th disequilibria in lavas from southern Chile. Earth Planet Sci Lett 196:189-196

Silver EA, Kastner M, Fisher A, Morris J, McIntosh K, Saffer D (2000) Fluid flow paths in the Middle America Trench and Costa Rica margin. Geology 28:679-682

Sissons JB, Cornish R (1982) Differential glacio-isostatic uplift of crustal blocks at Glen Roy, Scotland. Quat Res 18:268-288

Slemmons DB (1997) Carrara Fault, in southern Nevada from paleoseismic, geologic and geophysical evidence: implications to the earthquake hazards and tectonics near Yucca Mountain, Nevada. EOS Trans Am Geophys Union 78:F453

Small E, Anderson RS (1998) Pleistocene relief production in Laramide mountain ranges, western United States. Geology 26:123-126

Small EE, Anderson RS, Repka JL, Finkel R (1997) Erosion rates of alpine bedrock summit surfaces deduced from *in situ* ^{10}Be and ^{26}Al. Earth Planet Sci Lett 150:413-425

Somayajulu BLK (1977) Analysis of causes for the beryllium-10 variations in deep sea sediments. Geochim Cosmochim Acta 41:909-913

Sonett CP, Seuss HE (1984) Correlation of bristlecone pine ring widths with atmospheric ^{14}C variations: A sun-climate relation. Nature 307:141-143

Sonett CP, Morfill GE, Jokipii RR (1987) Interstellar shock waves and ^{10}Be from ice cores. Nature 330:458-460

Spiegelman M, Elliott T, (1993) Consequences of melt transport for uranium series disequilibrium in young lavas. Earth Planet Sci Lett 118:1-20

Spies CS, Whitney JW, Gosse J, Slemmons DB, Caffee M (2000) Terrestrial cosmogenic nuclide dating of deformed alluvium along the Carrara Fault in the northern Amargosa Desert, Nye County, Nevada. Geol Soc Am Abstr Progr 32(7):A-166

Spies CS, Whitney JW, Gosse J, Slemmons DB, Caffee M (submitted) Tectonic geomorphology and evolution of an active Walker Lane transpressional ridge feature. Geomorphology

Stamatakos J, Connor CB, Hill BE, Lane Magsino S, Ferrill DA (1997) The Carrara Fault in southwestern Nevada revealed from detailed gravity and magnetic results: implications for seismicity, volcanism, and tectonics near Yucca Mountain, Nevada. EOS Trans Am Geophys Union 78:F453

Steig EJ, Polissar PJ, Stuiver M, Grootes PM, Finkel, RC (1996) Large amplitude solar modulation cycles of ^{10}Be in Antarctica: implications for atmospheric mixing processes and interpretation of the ice core record. Geophys Res Lett 23:523-526

Steig EJ, Morse DL, Waddington ED, Polissar, PJ (1998) Using the sunspot cycles to date ice cores. Geophys Res Lett 25:163-166

Steig EJ, Morse DL, Waddington ED, Stuiver M, Grootes PM, Mayewski PA, Twickler MS, Whtilow SI (2000) Wisconsin and Holocene climate history from an ice core at Taylor Dome, western Ross embayment, Antarctica. Geografiska Annaler 82A:213-235

Stone JO (1999) A consistent Be-10 production rate in quartz—muons and altitude scaling. AMS-8 Proc Abstr Vol, Vienna, Austria

Stone JO (2000) Air pressure and cosmogenic isotope production. J Geophys Res B105 10:23753-23759

Stoner JS, Channell JET, Hillaire-Marcel C (1998) A 200 ka geomagnetic chronostratigraphy for the Labrador Sea: Indirect correlation of the sediment record to SPECMAP. Earth Planet Sci Lett 159: 165-181

Stoner JS, Channell JET, Hillaire-Marcel C, Kissel C (2000) Geomagnetic paleointensity and environmental record from Labrador Sea core MD95-2024: global marine sediment and ice core chronostratigraphy for the last 110 kyr. Earth Planet Sci Lett 183:161-177

Stoner JS, Laj C, Channell JET, Kissel C (2002) South Atlantic and North Atlantic geomagnetic paleointensity stacks (0-80 ka): implications for inter-hemispheric correlation. Quat Sci Rev 21: 1141-1151

Størmer C (1955) On the trajectories of electric particles in the field of a magnetic dipole with applications to the theory of cosmic radiation. Astrophysica Norvegica 1:115-167

Stuiver M (1961) Variations in radiocarbon concentration and sunspot activity. J Geophys Res 66:273-276

Stuiver M, Braziunas TF (1989) Atmospheric ^{14}C and century-scale solar oscillations. Nature 338:405-408

Stuiver M, Braziunas TF (1993) Sun, ocean, climate and atmospheric $^{14}CO_2$, an evaluation of causal and spectral relationships. The Holocene 3:289-305

Stuiver M, Quay P (1980) Changes in atmospheric carbon-14 attributed to a variable sun. Science 207: 11-19

Suess HE, Linick TW (1990) The ^{14}C record in bristlecone pine wood of the past 8000 years based on the dendrochronology of the late C.W. Ferguson. Phil Trans R Soc London A 330:403-412

Taira A, Hill I (1991) Proc. Ocean Drilling Program, Initial Reports 131. College Station, Texas

Tanaka S, Inoue T (1979) ^{10}Be dating of North Pacific sediment cores up to 2.5 million years B.P. Earth Planet Sci Lett 49:34-38

Tarduno JA, Wilkison SL (1996) Non-steady state magnetic mineral reduction, chemical lock-in and delayed remanence acquisition in pelagic sediments. Earth Planet Sci Lett 144:315-326

Tatsumi Y, Eggins S (1997) Subduction Zone Magmatism. Blackwell Science, Oxford, UK, 211 p

Tatsumi Y, Hamilton DL, Nesbitt RW (1986) Chemical characteristics of fluid phase released from a subducted lithosphere and origin of arc magmas: evidence from high-pressure experiments and natural rocks. J Volcanol Geothermal Res 29:293-309

Tauxe L (1993) Sedimentary records of relative paleointensity and the geomagnetic field: theory and practice. Rev Geophys 31:319-354

Tauxe L, Wu G (1990) Normalized remanence in sediments of the western equatorial Pacific: Relative paleointensity of the geomagnetic field? J Geophys Res 95:12337-12350

Tauxe L, LaBrecque JL, Dodson R, Fuller M (1983) U-channels—a new technique for paleomagnetic analysis of hydraulic piston cores. EOS Trans Am Geophys Union 64:219

Taylor EM, plus 12 others (1998) Quaternary Geology of the Yucca Mountain Area, Southern Nevada. *In* 'Friends of the Pleistocene' Pacific Cell, 1998 Ann Mtg, p 223

Tera F, Brown L, Morris J, Sacks IS, Klein J, Middleton R (1986) Sediment incorporation in island-arc magmas: inferences from ^{10}Be. Geochim Cosmochim Acta 50 :535-550

Tera F, Morris J D, Ryan J, Leeman WP, Tsvetkov A (1993) Significance of ^{10}Be/^{9}Be-B correlation in lavas of the Kurile-Kamchatka Arc. EOS Trans Am Geophys Union 74:674

Thompson LG, Peel DA, Mosley-Thompson E, Mulvaney R, Dai J, Lin PN, Davis ME, Raymond CF (1994) Climate since AD 1510 on Dyer Plateau, Antarctic Peninsula: Evidence for recent climate change. Ann Glaciol 20:420-426

Thompson LG, Mosley-Thompson E, Henderson KA (2000a) Ice core palaeoclimate records in tropical South America since the Last Glacial Maximum. J Quat Sci 15:377-394

Thompson LG, Yao T, Mosley-Thompson E, Davis ME, Henderson KA, Lin PN (2000b) A high resolution millennial record of the South Asian monsoon from Himalayan ice cores. Science 289:1916-1919

Tric E, Valet J-P, Tucholka P, Paterne M, Labeyrie L, Guichard F, Tauxe L, Fontugne M (1992) Paleointensity of the geomagnetic field during he last 80,000 years. J Geophys Res 97:9337-9351

Tric E, Valet J-P, Gillot PY, Lemeur I (1994) Absolute paleointensities between 60 and 160 kyrs B.P. from Mount Etna, Sicily. Phys Earth Planet Inter 85:113-129

Trull TW, Brown T, Marty B, Raisbeck GM, Yiou F (1995) Cosmogenic ^{10}Be and ^{3}He accumulation in Pleistocene beach terraces in Death Valley, California, USA: Implications for cosmic-ray exposure dating of young surfaces in hot climates. Chem Geol 119:191-207

Turner S, Hawkesworth C (1997) Constraints on flux rates and mantle dynamics beneath island arcs from Tonga-Kermadec lava geochemistry. Nature 389:568-573

Turner S, Hawkesworth C (1998) Using geochemistry to map mantle flow beneath the Lau Basin: Geology 26:1019-1022

Turner S, Hawkesworth C, Rogers N, Barlett J, Worthington T, Hergt J, Pearce J, Smith I (1997) ^{238}U-^{230}Th disequilibria, magma petrogenesis and flux rates beneath the depleted Tonga-Kermadec island arc. Geochim Cosmochim Acta 61:4855-4884

Turner S, Bourdon B, Hawkesworth C, Evans P (2000) ^{226}Ra-^{230}Th evidence for multiple dehydration events, rapid melt ascent and the time scales of differentiation beneath the Tonga-Kermadec island arc. Earth Planet Sci Lett 179:581-593

Valentine R, Morris J, Duncan D (1997) Sediment subduction, accretion, underplating, and arc volcanism along the margin of Costa Rica: Constraints from Ba, Zn, Ni and ^{10}Be concentrations. EOS Trans Am Geophys Union 78:673

Valentine R, Morris J (submitted a) Sediment accretion, erosion and subduction along the Costa Rica convergent margin: Constraints from geochemical imaging using ^{10}Be. J Geophys Res

Valentine R, Morris J (submitted b) ^{10}Be estimates of sediment subduction in the Izu-Mariana volcanic arc system. Geochem Geophys Geosystems

Valet J-P, Meynadier L (1993) Geomagnetic field intensity and reversals during the past four million years. Nature 366:234-238

Valet J-P, Meynadier L (2001) Comment on "A relative geomagnetic paleointensity stack from Ontong-Java plateau sediments for the Matuyama" by YS Kok and L Tauxe, J Geophys Res 106:11013-11015

Valet J-P, Herrero-Bervera E, Lockwood JP, Meynadier L, Tric E (1998) Absolute paleointensity from Hawaiian lavas younger than 35 ka. Earth Planet Sci Lett 161:19-32

Van der Woerd J, Ryerson FJ, Tapponnier P, Gaudemer Y, Finkel R, Meriaux AS, Caffee M, Guaguang Z, Qunlu H (1998) Holocene left-slip rate determined by cosmogenic surface dating on the Xidatan segment of the Kunlun fault (Qinghai, China). Geology 26:695-698

Van Der Woerd J, Tapponnier P, Ryerson FJ, et al. (2002) Uniform postglacial slip-rate along the central 600 km of the Kunlun Fault (Tibet), from Al-26, Be-10 and C-14 dating of riser offsets, and climatic origin of the regional morphology. Geophys J Intl 148:356-388

Vannuchi P, Scholl DW, Meschede M, McDougall-Reid K (2001) Tectonic erosion and consequent collapse of the Pacific margin of Costa Rica: Combined implications from ODP Leg 170, seismic offshore data and regional geology of the Nicoya Peninsula. Tectonics 20:649-688

Verosub KL, Herrero-Bervera E, Roberts AP (1996) Relative geomagnetic paleointensity across the Jaramillo subchron and the Matuyama/Brunhes boundary. Geophys Res Lett 23:467-470

Voelker A, Sarnthein M, Grootes PM, Erlenkeuser H, Laj C, Mazaud A, Nadeeau MJ, Schleicher M (1998) Correlation of marine ^{14}C ages from the Nordic Sea with GISP2 isotope record: implication for ^{14}C calibration beyond 25 ka BP. Radiocarbon 40:517-534

Vogt S, Herzog GF, Reedy RC (1990) Cosmogenic nuclides in extraterrestrial materials. Rev Geophys 28:253-275

von Huene R, Scholl DW (1991) Observations at convergent margins concerning sediment subduction, subduction erosion and the growth of continental crust. Rev Geophys 29: 279-316

von Huene R, Klaeschen D, Cropp B, Miller J (1994) Tectonic structure across the accretionary and erosional parts of the Japan Trench Margin: J Geophys Res 99:22349-22361

Wagner G, Masarik J, Beer J, Baumgartner S, Imboden D, Kubik PW, Synal H-A, Suter M (2000a) Reconstruction of the geomagnetic field between 20 and 60 kyr BP from cosmogenic radionuclides in the GRIP ice core. Nucl Instr Meth Phys Rev B 172:597-604

Wagner G, Beer J, Laj C, Kissel C, Masarik J, Muscheler R, Synal H-A (2000b) Chlorine-36 evidence for the Mono Lake event in the Summit GRIP ice core. Earth Planet Sci Lett 181:1-6

Wagner G, Beer J, Masarik R, Muscheler R, Kubik PW, Mende W, Laj C, Raisbeck GM, Yiou F (2001) Presence of the solar de Vries cycle (205 yr) during the last ice age. Geophys Res Lett 28:303-306

Weeks R, Laj C, Endignoux L, Fuller M, Roberts A, Manganne R, Blanchard E, Goree W (1993) Improvements in long-core measurement techniques: applications in palaeomagnetism and palaeoceanography. Geophys J Intl 114:651-662

Williams T, Thouveny TN, Creer KM (1998) A normalised intensity record from Lac du Bouchet: geomagnetic palaeointensity for the last 300 kyr. Earth Planet Sci Lett 156:33-46

Yamazaki T (1999) Relative paleointensity of the geomagnetic field during Brunhes Chron recorded in North Pacific deep-sea sediment cores: orbital influence? Earth Planet Sci Lett 169:23-35

Yamazaki T, Oda H (2002) Orbital influence on Earth's magnetic field: 100,000-year periodicity in inclination. Nature 295:2435-2438

Yamazaki T, Ioka N, Eguchi N (1995) Relative paleointensity of the geomagnetic field during the Brunhes chron. Earth Planet Sci Lett 136:525-540

Yiou F, Raisbeck GM (1972) Half-life of ^{10}Be. Phys Rev Lett 29:372-375

Yiou F, Raisbeck GM, Bourles D, Lorius C, Barkov NI (1985) ^{10}Be in ice at Vostok Antarctica during the last climatic cycle. Nature 316:616-617

Yiou F, Raisbeck GM, Baumgartner S, Beer J, Hammer C, Johnsen S, Jouzel J, Kubik, PW, Lestringuez J, Stié venard M, Suter M, Yiou P (1997) Beryllium-10 in the Greenland Ice Core Project ice core at Summit, Greenland. J Geophys Res 102:26783-26794

You C-F, Morris JD, Geiskes JM, Rosenbauer R, Zheng SH, Xu X, Ku TL, Bischoff JL (1994) Mobilization of beryllium in the sedimentary column at convergent margins. Geochim Cosmochim Acta 58:4887-4897

You C-F, Castillo P, Geiskes JM, Chan LC, Spivack AF (1996) Earth Planet Sci Lett 140:41-52

Zehfuss PH, Bierman PR, Gillespie AR, Burke RM, Caffee MW (2001) Slip rates on the Fish Springs fault, Owens Valley, California, deduced from cosmogenic ^{10}Be and ^{26}Al and soil development on fan surfaces. Geol Soc Am Bull 113:241-255

Zentmire KN, Gosse JC, Baker C, McDonald E, Wells S (1999) The problem of inheritance when dating alluvial fans and terraces with TCN: Insight from the Matanuska Glacier. Geol Soc Am Abstr Progr 31(5):A81

Zhang Z, Schwartz S (1992) Depth distribution of moment release in underthrusting earthquakes at subduction zones. J Geophys Res 97:537-544

Zheng S, Morris J, Tera F, Klein J, Middleton R (1994) Beryllium isotopic investigation of sedimentary columns outboard of subduction zones. ICOG 1994 Abstr 8:366

Zreda M, Noller JS (1998) Ages of prehistoric earthquakes revealed by cosmogenic chlorine-36 in a bedrock fault scarp at Hebgen Lake. Science 292:1097-1099

Zreda MG, Phillips FM, Kubik PW, Sharma P, Elmore D (1993) Cosmogenic ^{36}Cl dating of a young basaltic eruption complex, Lathrop Wells, Nevada. Geology 21:57-60